Universiteit Utrecht

ediment
ufter', the

wiebe Kramer

April 2010

Universiteit Utrecht

ıt transport
ɛtherlands

Wiebe Kramer

Leeuwarden
March 2010

MSc Thesis
2nd version

Supervisors
Prof. Dr. P. Hoekstra
Dr. M. Van der Vegt

Department of Physical Geography
Faculty of Geosciences
Utrecht University

PREFACE

In September and October 2008 a field research program was executed in ‘the Slufter’, the Netherlands, to further develop our understanding of the dynamic behavior of small coastal inlets. This survey is launched by the Utrecht University and is part of a long-term project. Three interrelated studies were carried out on morphodynamics, tide- and wave driven sediment transport mechanisms and fluxes in and around the Slufter tidal inlet.

This thesis provides a process-based approach primarily focused on tidal-driven sediment transport processes in the main channel of the Slufter. Fellow student Ralf Klein Breteler examined the wave-driven cross- and longshore sediment transport patterns in the breaker zone and in the Slufter system when completely inundated under storm conditions. Stijn van Puijvelde discussed the morphological development of the Slufter through application of both field measurements and historical data, constructed a hypsometric curve and discussed the interaction between the Slufters morphology and hydrology.

Many persons have contributed to the establishment of this thesis. First, my special thanks go to Ralf and Stijn for their balanced, serene attitude and meaningful contribution to discussions and physical labor which brought this research to a good end. Next, I like to thank my supervisors: dr. Maarten van der Vegt and prof. dr Piet Hoekstra. Additionally, I am grateful for the support given by the technical staff of Utrecht University: Chris Roosendaal, Henk Markies and Marcel van Maarseveen and Roy Frings who assisted with dune-tracking methods.

Finally I would like to thank the ones that gave me the most personal support: my girlfriend in particular and my family.

TABLE OF CONTENT

LIST OF FIGURES

LIST OF TABLES

LIST OF PICTURES

ABSTRACT

Small tidal inlets along sandy coasts are important features which hold a great variety of flora and fauna. National park 'de Slufter' at Texel, the Netherlands, is a small tidal inlet. Its natural dynamics and ecological values must be maintained in future. Taking into consideration that the Slufter is a temporal phenomenon, the stability of the Slufter is therefore an important issue.

Incidentally, Rijkswaterstaat relocates the down drift migration channel to the south, but generally the natural dynamics in the Slufter have free play. For future management planning and maintenance strategies we have to expand our knowledge on the dynamic behavior of small tidal inlets. Contradictory to the relative long physical appearance of the Slufter (150 years), many tidal inlet models predict a short-term closure of the Slufter. This raises questions to coastal engineers. Therefore Utrecht University has launched a series of fieldworks at the Slufer.

This research is a qualitative assessment on the tidal hydrodynamics and sediment transport at the Slufter. The goal is to identify the sediment transport trends (import or export) during the neap-spring cycle, based on measurements and sediment transport models. Net import or export patterns are important for the stability of the inlet. The main research question reads as follows:
What is the influence of tides on the import and export of sediment in the Slufters main channel.

In order to answer the research question field measurements were carried out in and around the mouth of the Slufter, in September and October 2008. Results show that during non-flooding conditions (water levels < 1.1 m + N.A.P.), tides are the fundamental transport mechanisms for water and sediment at the Slufter. During spring tide, tidal interaction with the Slufters' basin hypsometry enhances flow asymmetry which becomes ebb dominant. Measured fluxes are quite equal for both inflow and outflow stages, but calculated sediment fluxes clearly indicate an export of sediment during spring tidal conditions. This difference can partly attributed to high measured suspended sediment concentrations during flood.

During neap tide, both computed and measured sediment fluxes indicate an import of sediment. The flood dominance is a direct result of the external tide, which emerges in longer ebb durations resulting in higher maximum landward directed flow velocities. During spring tide, tidal interaction with the Slufters' basin hypsometry enhances flow asymmetry which becomes ebb dominant. Measured and calculated fluxes clearly indicate an export of sediment during spring tidal conditions. Tidal flow asymmetry in the Slufter is mainly controlled by the geometry of the inletsbasin, rather than a differentiation between duration of the ebb and flood currents.

During storm conditions the total basin of the Slufter is inundated, and both current field and suspended sediment concentration (SSC) greatly differ from calm condition. During these flooding conditions (HW > 1.1 m + N.A.P.), import of water mainly occurs over the beach flat, whereas export mainly occurs through the relative narrow tidal channel. During storms sediment fluxes in the main

channel are significantly larger than during non-flooding conditions. A residual circulation flow pattern has been identified during the storm. Dominant transport in the Slufers main channel during a storm event is seaward directed. The effect of waves on sediment transport is mainly restricted to the offshore zone, where sediment entrainment is enhances due to wave dynamics.

1 INTRODUCTION

1.1 Problem setting

Small tidal inlets along sandy coasts in the Netherlands are of great importance on ecology and coastal defense. The intertidal marshes in small tidal inlets hold a great diversity of flora and fauna often enclosed by a scenic landscape. In addition, the dune rows surrounding small inlets are part of a natural coastal defense preventing the hinterland from flooding. Hence, conservation of these natural dynamic systems is widely cherished.

A small tidal inlet is a dynamic system including complex interactions between a-biotic and biotic components. Both components and interactions are guided by feed-back mechanisms. The fundamental driving processes are a-biotic (motion of water- and sediments) and dictated by offshore dynamic processes and conditions (tidal motion, waves and currents). Transport of water and sediments lead to a continuous adaption of morphology, vegetation and fauna. Understanding of the processes that drive water and sediments in small inlets on different spatial and temporal scales is therefore important for both ecologists and coastal engineers.

Small inlets in the Netherlands are generally known as slufters. The name is derived from the national park located on Texel, one of the West Frisian barrier islands in the Netherlands. Slufters are brackish or salt dune valleys connected by the sea by an opening in the foredunes, receiving seawater through an inlet channel. At least once a year the total basin of slufters inundates. Due to limited previous fieldwork on slufters, knowledge is scarce and mainly based on studies performed on larger scale tidal inlets. Hence, dynamics of small natural openings in particular are still poorly understood.

The stability of slufters is an important issue. Slufters are temporary phenomena; they are considered as a stage along a coast which is transforming from an accretion coast to an erosion coast and vice versa. Several stability relationships have been derived for these large systems (Escoffier, 1940; Bruun and Gerritsen, 1960; Van de Kreeke, 1985). These theories predict a closure of the inlet; nonetheless the existence of the Slufter on Texel lasts for over one-and-a-half century and seems to prove otherwise. Artificially excavated inlets are highly subjected to accretion, while natural slufters appear to be able to exist in the presence of a significant longshore drift. This raises questions for scientists.

To develop further insight into the dynamics of small tidal inlets the University of Utrecht has launched a series of field campaigns in the Slufter on Texel. The first series of fieldworks (2008) had a explorative character. The ambition was to gain a first large data-set on morphodynamics, hydrodynamics and sediment concentration characteristics in and around the tidal main channel in order to get a step closer to the understanding of the Slufters dynamic behavior. The main aim of this research is to study the tide-induced processes that are responsible for the import and export of sediments.

1.2 Theoretical Background

1.2.1 Tidal Inlets and Slufters

Due to the complex interaction of wind, waves, tides and currents, tidal inlets are among the most dynamic coastal features. Tidal inlets generally have a short, narrow channel connecting the ocean (or sea) in between two barrier islands with a tidal basin or lagoon. Others are completely surrounded by land, acting as a branched system connected to sea. Scale of inlets may differ from small inlets in the order of one kilometer to ten kilometers, where water surface levels may rise and fall uniformly in response to the forcing ocean tide, to larger systems (>10 km) where non-uniform tidal fluctuations occur (van Rijn, 1994).

Better understanding of the hydrodynamics and morphodynamics of slufters can be achieved by applying the knowledge of small tidal inlets. However, considering the Slufters unique morphological behavior, a distinction should be made between the two systems. Therefore it is of considerable value to study the essential (dis)similarities of small tidal inlets, slufters and slufter-like areas, in particular in relation to hydraulic and sediment transport processes and conditions.

Slufter-like areas are systems that can be considered as vegetated sandy flat areas in coastal zones without satisfying to the explicit condition that the system receives seawater on a daily basis. The basins elevation and tidal amplitude are two main characteristics to make a distinction between slufters and slufter-like areas (Arens et al., 2005).

The fundamental distinction between slufters and tidal inlets comprises the systems dimensions. Storage volume of the Slufters basin is limited in comparison to the large systems. For average or neap tide conditions, water flow remains restricted to the tidal creeks. According to Reneerkens (2003) tidal prism of the Slufter comprises 150000 m^3, Durieux (2005) estimates a volume of $4.3e^5$ m^3. In spite of these differences, the tidal prism of the Slufter is clearly a factor 2500-6000 smaller than the Texel inlet (10^9 m^3). One may expect that this difference in scale also results in a different dynamic behavior of the hydrodynamics and sediment transport processes. Due to the Slufters small basin length in comparison to the tidal wave length it is expected that the modification of the tidal wave inside Slufters is limited.

A second distinguishing factor is the basin hypsometry of Slufters, defined as the vertical distribution of basin surface area. Basin hypsometry controls the rate of inundation in the intertidal zone (Boon & Byrne, 1981). Areas with rather low marshes are prone to inundation, while tidal inlets similar to the Slufter at Texel consisting of a basin with relative high shoals, may only be flooded during spring tides or due to storm surges. The hypsometry of a tidal basin governs the tidal prism and has a profound effect on the hydrodynamics in the channel. (paragraph 1.2.2).

1.2.2 Tidal asymmetry and ebb/flood dominance

The asymmetry of the tide is one of the controlling factors for the residual sediment transport and hence the morphological development in estuaries and tidal basins (Wang et al., 2002). Tidal asymmetry usually emerges in a differentiation between duration of the ebb and flood currents. Also tidal asymmetry results in different ebb and flood peak velocities, whereby discrepancy between ebb and flood currents increases with tidal asymmetry. For this thesis, asymmetry is defined in terms of channel tidal velocity asymmetry, since channel tidal velocity $u(t)$ is considered to be a driving force for sediment transport within the system.

The tides, at any location, are in fact a summation of a finite set of sinusoids which are controlled by both moons and suns gravity. The dominant tidal constituent at the North Sea and the coast of Texel is M_2. The Slufter experiences a semi-diurnal tidal regime implying that it receives and discharges water twice a day. Semi-diurnal tides are expected when amplitudes for M_2, S_2, and N_2 are large compared to the amplitudes for K_1 and O_1. Distortion of the tide occurs during its propagation from deep water into shallow inlet systems. As a result, higher harmonics ("overtides") are produced, with M_4 as the most important constituent. A simple expression of distorted vertical tide, relative to mean sea level in tidal lagoon is expressed as follows.

$$h(t) = M_2 \cos \omega t + M_4 \cos(2\omega t - f) \qquad [1\text{-}1]$$

Where ω is the M_2 tidal frequency, t is time (hours) and f is the relative phase between M_2 and M_4. The non-linear response to tidal forcing is expressed in amplitude growth of high frequency M_2 overtides (M_4 and M_6). In fact, the determinant tidal constituents in shallow inlets are M_2 and its first harmonic, M_4. The difference between rise and fall duration, ΔD ($T_{rise} - T_{fall}$), is zero when M_2 and M_4 are in phase (0°) and (180°), while reaching maximum and minimum values when f is respectively 90° and 270° (fig 1-1)(Boon and Byrne, 1980).

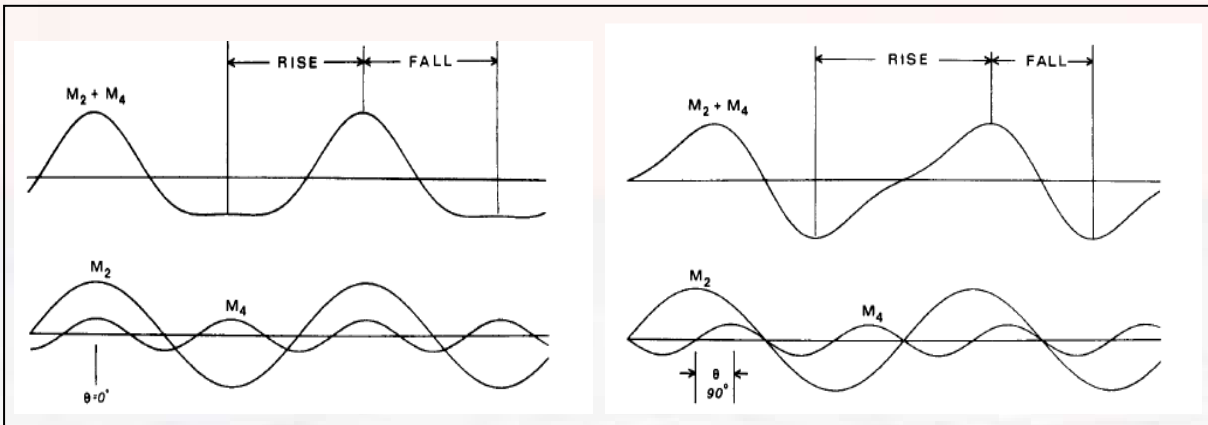

Figure 1-1 Combination of principal lunar semidiurnal constituent, M_2, with its first harmonic, M_4. **A)** Rise and fall durations are equal for given a phase displacement of 0°. Curve distortion is positive symmetric with respect to maxima and minima. **B)** Rise duration exceeds fall duration given a phase displacement of 90°. Curve distortion is positive antisymmetric with respect to maxima and minima (Boon and Byrne, 1980).

Considering the Slufters small dimension it is expected that non-linear distortion, due to bottom friction, inside the Slufter is practically negligible. The basin length is much smaller than the tidal wave length. Therefore the basin responds equally and simultaneously and the water surface in the basin will fluctuate as a horizontal plane (van Rijn, 1993). Tidal asymmetry in the Slufter can be the result of one- or a combination of the following mechanisms:

External asymmetry
The Slufter is connected to the North Sea, which can be considered as a shallow basin. In relatively shallow water the top of a wave can propagate faster than the through, since the propagation speed of waves is related to the water depth. Therefore the ebb phase has a longer duration than the flood phase. The tidal wave is already strongly deformed when it enters the Slufter (Dronkers, 1986).

Truncation
When depths in relatively small inlets are less than the mean tide amplitude, truncation of the lower part of the ocean tide can significantly shorten the rising tide and lengthen the falling tide duration (Lincoln and FitzGerald, 1988). Since wave celerity and depth are positively related, the top of the wave travels faster than the through, causing deformation. A similar effect of truncation is reached in the presence of a natural morphological threshold. When offshore waterlevel exceeds the height of the threshold, the basin will be filled rapidly resulting in short and strong flood currents. On the other hand the return flow is extended in time and characterized by decreased current velocities.

Basin hypsometry
Tidal distortion can arise due to the interaction with geometry of the basin. According to Boon and Byrne (1981), and FitzGerald and Nummedal (1983) asymmetry of an ebb-dominant form may be produced, when the inlet surface area increases with tidal elevation. In inlet systems with open bays (no tidal flats) or high elevated marshes, a flood dominant tidal asymmetry may be more likely to occur (Mota Oliveria 1970; Seelig and Sorenson 1978; and Speer and Aubrey 1985).

A physical argument for this effect can be made considering the inlet continuity equation (Keulegan, 1967):

$$u(t) = \frac{A_b}{A_c}\frac{dh_b(t)}{dt} \qquad [1\text{-}1]$$

where $u(t)$ is the channel velocity, $h(t)$ denotes the bay tide, A_b is the basin wet surface and A_c is the cross-sectional area. Assume the same volume of water entering and leaving the inlet and uniform levels in the basin. If A_b increases with the rising tide at higher speed as A_c, then the rate of rise (dh/dt) decreases, while the rate of fall increases over time. This means there is a longer rise time and faster fall time, indicating ebb velocity peak larger than flood velocity peak and a resulting ebb dominance.

In a series of three papers, Speer, Aubrey and Friedrichs (1985, 1985 and 1988) identified the two parameters, *a/h* and v_s/v_c as being key indicators of ebb/flood dominance in a tidal inlet system, where *a/h* is the ratio between amplitude of the tidal range and the mean depth, v_s/v_c represents the ratio of volume of intertidal storage against the volume of channels. Conclusions were done based on real observations, analytical theory and numerical modeling. Parameter *a/h* is found to be most responsible for a asymmetric tides in flood dominant inlets while the parameter v_s/v_c is mostly responsible for asymmetric tides in ebb dominant systems. Under the hypothesis that morphological equilibrium equates to a uniform tide, Dronkers (1986) derived an asymmetry ratio based on certain tidal basin form parameters:

$$\gamma = \left(\frac{h+a}{h-a}\right)^2 \frac{S_{lw}}{S_{hw}} \qquad [1\text{-}2]$$

Where γ is the Dronkers parameter, h is the mean hydraulic depth in the channels, a denotes the tidal amplitude, S_{lw} is the total basins surface water at low water and S_{hw} is the total basins surface water at high water. A value of γ equal to one suggests a uniform tide, with values greater or smaller than one indicating respectively flood- or ebb-dominance; h is the averaged depth of the channels or mean hydraulic depth and is given approximately by $h=a+V_{lw}/S_{lw}$; a, the tidal amplitude, V_{lw} is the volume of water in the tidal basin during low water.

The above mentioned relationships suggest that flow patterns in inlets are strongly controlled by the basin morphology. Tidal inlets which channels are wide, deep and whose intertidal flats are low, generally below mean sea level, experience flood tide dominance. Generally net accumulation of suspended sediment takes place so that deposition occurs in the tidal basin (Fortunato and Oliveira, 2003). Because most of this deposition will take place on the intertidal flats of the channel these will rise relatively rapidly in the tidal frame so that the channel cross section changes from its initial wide deep rectangular configuration to a central ‘slot’ channel within high bounding mudflats and marshes (Fortunato and Oliveira, 2003). Due to the large area of high elevated shoals and marshes, the channels mean depth will decrease as the flood enters the inlet. Therefore the crest of the flood tide propagates less rapidly than the trough of the ebb and an ebb-dominance is originated. Consequently, these inlets becomes net exporters of sediment. This type of asymmetry is particularly related to the finer fraction of sediment (suspended load).

As stated earlier, the Slufters geometry is a distinguishing factor as the vast majority of the tidal basins surface is situated above mean water level. This can be clearly seen in figure 1-2 which represents a 3D-topograpic representation of a large part of the Slufters basin. The picture is obtained by merging AHN images with field data (van Puijvelde, 2009). Blue parts are deepest and basically continuously filled with water. Green parts represent the salt marshes that are situated above MWL and inundated during spring tide and/or surges. Yellow parts are only flooded during severe storms and/or spring tide. Brown dots denote the positions of measurement instruments. Based upon this 3D-image of the Slufters basin an hypsometric curve is obtained representing total wet surface in the study area with

varying water level. Also the basins storage capacity with varying water level is attained which basically reflects the tidal prism of the Slufter (figure 1-2).

As can be seen in figure 1-2 B and C, the Slufter has a very large surface area elevated between 1.0 and 1.5 m +NAP. This results in a rapid increase of the wet surface area and water volume during storm surges.

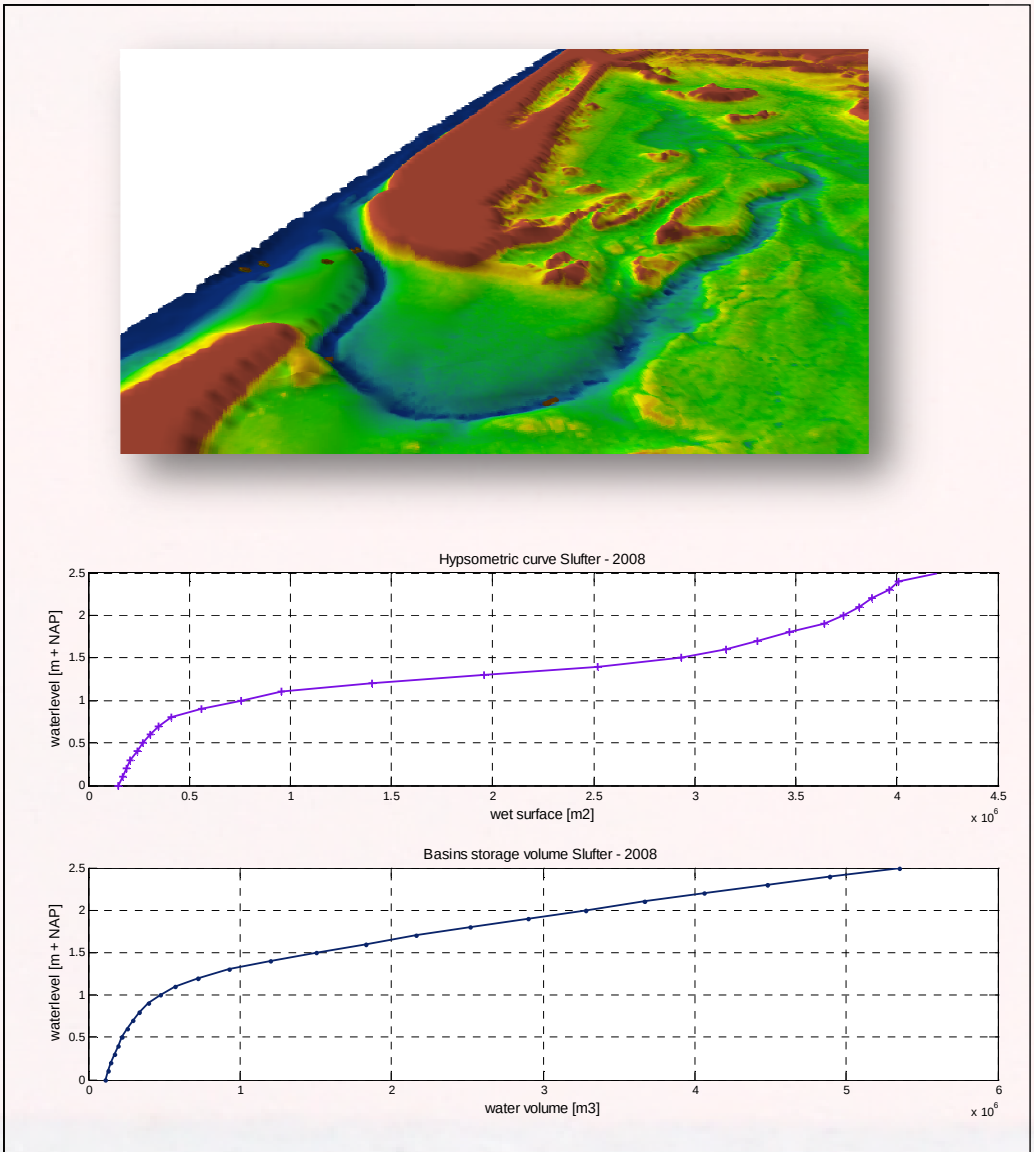

Figure 1-2 A) Modified 3D-topographic representation of the Slufter basin. Field data of survey leveling is merged to the Algemeen Hoogtebestand Nederland (AHN) Brown dots indicate locations of measurement instruments. **B**): Hypsometric curve of the Slufter with varying water level. **C**): Basins storage volume with varying waterlevel (van Puijvelde, 2009).

1.2.3 Tidal asymmetry and sediment transport

Marine sediments are transported by either currents, driven by tides, wind or waves or by waves, or most often a combination of both mechanisms (Soulsby, 1997). The movement of sands basically occurs by the basic processes of entrainment, transportation and deposition. Due to the current and/or

waves, friction is exerted enhancing turbulent diffusion stirring up sediment particles into suspension (Soulsby, 1997). This is known as entrainment. The initiation of motion of sediments occurs when bottom shear stress is larger than a critical value.

Transport of sediments can occur in two ways. First, in response to friction, grains may move through hopping and rolling remaining relatively close to the bed. This mode is known as *bed load transport* q_b and is generally the dominant mode of transport for slow flows (van Rijn, 1993). Bed load transport occurs if the friction velocity is larger than its critical value but smaller than the sediment settling velocity w_s ($u_{*crit} < u_* < w_s$) (de Swart and Zimmerman, 2009). Secondly, *suspended load transport* comprises the generally finer particles which are entrained by relative strong currents and/or waves. Suspended load transport occurs if the friction velocity is higher than the settling velocity ($u_* > w_s$) (de Swart and Zimmerman, 2009).

Bed load transport respond instantaneously to a reverse flow direction (van Maren et al., 2004), whereas a settling time delay causes a lag before suspended material reaches equilibrium with local current conditions. Bed load transport and deposition of coarse sediment is directly related to the maximum current velocities during ebb and flood and this transport is found to be proportional to the local velocity to the third power (van Maren et al., 2004). Also this mode of transport occurs immediately above the bed and is supported by intergranular collisions rather than fluid turbulence (Wilson, 1966 in Camenen & Larson, 2003). The deposition rate highly depends on the settling velocity of particles which is determined by the sediment characteristics. This implies that various kinds of sediments behave differently in terms of transport properties.

The inequality of the period of flood and ebb and the difference between the maximum current velocities occurring during flood and ebb are extremely important for sediment transport of both fine and coarse material.

Maximum flow asymmetry

Tidal asymmetry generally emerges in a difference in flood- and ebb phase duration. An unequal duration of flood and ebb phase causes a difference between maximum flow velocities during the rise and the fall of the tide. In a closed embayment, flow velocities during the shortest time span are generally the highest. Flood-dominance emerges when the duration of the ebb phase exceeds the duration of the flood phase leading to stronger flood currents. Maximum asymmetry mainly applies to the coarser material (Nichols and Boon, 1991).

Time flow asymmetry

Variation in flow velocity is proven to be the controlling factor for the suspended load transport. Transport and deposition of fine sediments depend mainly on the velocity variations (du/dt) around low and high water slack (Dronkers, 1986). Dronkers suggest that flood or ebb dominance as a result of maximum flow asymmetry does not necessarily lead to deposition or erosion of the intertidal flats. Instead, flow asymmetry and in particular the length of high water slack duration

as compared to the low water slack, appear to control the net sediment budget of the intertidal areas.

Settling lag and scour lag

Lag effects can emerge in a residual transport even without the effect of tidal asymmetry. Settling lag is referred to as the finite time taken by a fine-grained sediment particle to respond to changing current direction and velocity (Pritchard, 2005). As a result of a settling lag, a particle that settles on the falling tide reaches the bed some distance from the point at which settling commenced (Hoitink et al., 2003). The spatial and temporal asymmetries in currents can lead to a net sediment flux averaged over a tidal cycle. Settling lag may be enhanced by scour lag, when the threshold shear stress for erosion delays the re-entrainment of sediment into suspension (Pritchard, 2005 and Swarts & Zimmerman, 2009). A combination of settling lag and scour lag results in a landward transport of suspended sediment (Van Straaten & Kuenen, 1957).

Advection

Advection is another mechanism which can cause a residual transport of suspended material without the necessity of tidal asymmetry. The term advection refers to the sediment transport from one region to another. Advective residual suspended sediment transport is the sediment mass which is transported by means of ebb and flood currents through a cross section, in this case the mouth of the Slufter. Advection can produce a number of concentration peaks during the flood tide linked to the high concentration of sediments in the high-energetic breaker zone. Due to the effect of advection, import of fine sediment is favored.

1.2.4 Stability of tidal inlets

Tidal inlets are subject to changes in hydraulics and sediment supply. Feed-back mechanisms between hydraulics and sediment transport with local morphology lead to a continuous adaption of all parameters within the system in order to maintain or reach an equilibrium state. Hence, the concept of stability demonstrates the systems adaptation to distortions. Basically, inlets face a balance between tidal driven residual sediment transport in the mouth and wave-driven longshore drifts (Bruun, 1978). Human interference is an additional parameter which may strongly affect the stability of inlets. Unstable inlets tend to fill up and eventually disappear, whereas stable inlets tend to continue to exist.

Size of the inlet and its sustainable character are controlled by the relative strength of opposite mechanisms; currents in the throat keep the inlet open and longshore drift tend to close the inlet. Escoffier (1940) introduced the closure curve (figure 1-3), which approaches the stability of tidal inlets based on a concept of equilibrium. Escoffier (1940) proposes that when flow velocities in the inlet drop below equilibrium velocity deposition occurs. The two intersections of the closure curve with equilibrium velocity represent an unstable (A_{c1}) and stable root (A_{c2}). As the entrance cross-sectional area is enlarged beyond the value A_{c2}, the ebb tidal transport decreases. As a result, the cross-sectional area will decrease and return to the equilibrium value A_{c2}. A reduction in cross sectional area from

value A_{c2} will take the mean flow velocities to a higher value than the annual mean flux; the inlet will scour and return to the equilibrium cross-sectional area. Assume an unstable inlet given a cross-sectional value A_{c1}, increase of A_{c1} eventually leads to A_{c2}, whereas decrease of A_{c2} leads to further increase of bottom friction; the system will then disappear.

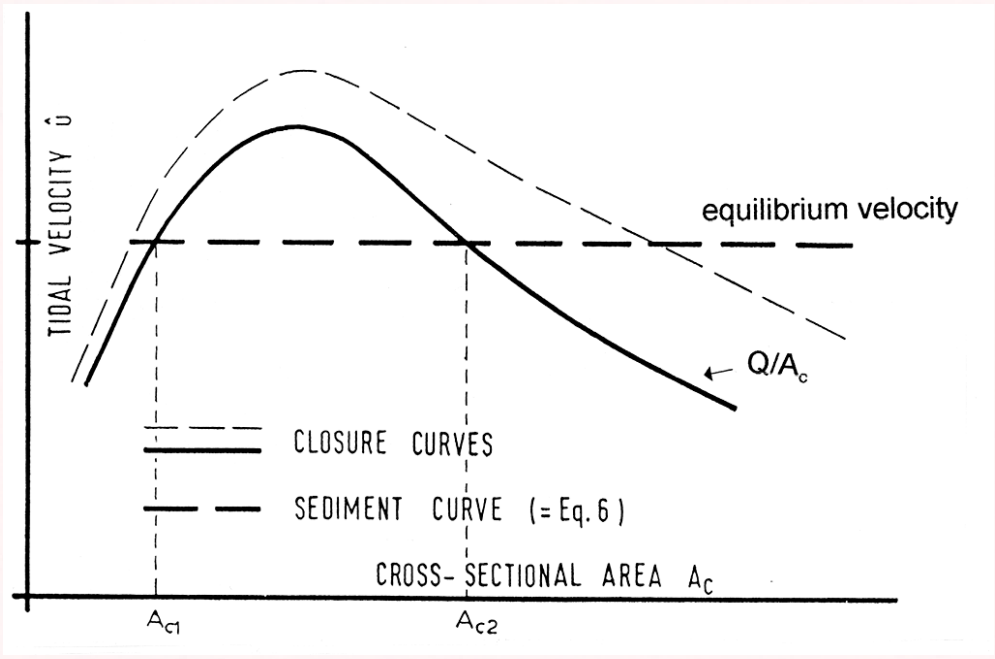

Figure 1-3 Closure curve of tidal inlets, showing a stable- and unstable cross-sectional area determined by an equilibrium velocity which is equal to the annual mean flux. The concept is developed by Escoffier (1940) in: van de Kreeke (1984).

1.2.5 Summary theoretical background

Slufters in general are small tidal inlets with specific properties in comparison to other inlets. The most distinctive factor is its basin hypsometry which is expressed by high elevated shoals. Tidal inlets experience a feedback relationship between their morphology and the current velocities generated inside them. Tidal asymmetry in a tidal inlet is most commonly a result of one or a combination of the following factors:

- Offshore tide
- Bottom friction
- Basin hypsometry

Flow asymmetry consequently affects net sediment transport patterns in a tidal inlet which can either be expressed in a ebb- or flood dominance. It is found that ebb/flood dominance in inlets are strongly controlled by the basin morphology. Tidal inlets with high elevated shoals tend to be ebb dominant, while inlets with deep, wide channels and which intertidal flats are low a flood dominant tidal asymmetry may be more likely to occur. This can emerge in a maximum flow asymmetry and/or time flow asymmetry which determine the dominant sediment transport direction. Other mechanisms as lag-effects and advection also affect residual suspended sediment transport. Sediment can be either transported as bed-load, which is the dominant mode for slow flows(<1 m/s), or suspended load which is expected to be dominant mode of transport when flow velocities are high (>1 m/s). A net import or export of sediment is important for the stability of small tidal inlets.

1.3 Research Area

The Slufter is a small tidal inlet located on the North Sea side of the barrier island, Texel (figure 1-4). Its total basin area comprises approximately 400 Ha mostly consisting of salt marshes and with multiple creeks. The main meandering channel has a strong dynamic character i.e. the mouth can change position within a single tidal cycle. The net annual northward movement is approximately 100 m (Durieux, 2004). To prevent dune erosion, Rijkswaterstaat closely monitors the behavior of the main channel and intervenes when the main channel reaches the northern dune front by relocating the channel to the south. In recent years this occurs basically each 5 years. Main cause of the rapid channel migration is the substantial longshore drift as a result of the wave climate and coastal orientation. Furthermore, regular sand nourishments take place since 1990 up-drift of the Slufter along the Texel coast (Durieux, 2004), delivering an additional sand supply.

Figure 1-4 Study area: the Slufter. Inset left-bottom: the Netherlands, left-top: Texel, Frisian barrier island (Google Earth image, 2008).

Due to its small tidal prism and dynamical morphological character near the mouth the Slufter can best be characterized as a small wave-dominated inlet. Subject to a significant longshore drift and relatively small stream power in the main channel the Slufter is prone to accumulation. A distinguishing factor of the Slufter in comparison to most other inlets is the basin geometry or hypsometry such that under normal tides, most parts of the Slufter are elevated above mean high water (MWL) (Reneerkens, 2003). Only tidal creeks are partly flooded whereas large parts of the basin are only inundated under spring tide and/or storm surges (Basisrapport Zandige Kust (1995) in Durieux, 2005).

As the Slufter is situated along the North Sea basin it experiences a semi-diurnal tidal regime where average tidal range is approximately 1.65 m. Astronomical tidal forcing can lift water levels up to 0.9 m + NAP, but water levels can reach much higher values due to the additional effect of wind-stress and pressure systems that comes with meteorological depressions. Annual return frequencies decrease with increasing fierceness, but high floods where water levels reach 1.95 m +NAP occur 5 times a year on average (table 1-1).

Winds generally blow from the west to south-west generating waves with a mean significant wave height of 1.3 m. The most severe storms in the Netherlands strike the coast from north-west; moderate storms commonly blow from the (south)-west. Taking the coastal orientation of Texel into consideration, north-western storm will approach the Slufter almost perpendicular. Negative surges (set-down) are experienced during offshore winds resulting in a lowering of the mean water level.

	Return frequency (n/year)	Water level Slufter (m + NAP)
Average flood	296 60	80 120
Average high flood	18 6	150 180
High floods	5 1	195 240
Low storm surge	0.5 0.2	255 280
Average storm surge	0.1 0.02	300 340
High storm surge	0.01 0.002	355 390

Table 1-1 Return frequency table of flooding events regard to water levels in the Slufter (RIKZ, 1998 ; in: Durieux , 2004)

1.3.1 Historical background

A continuous struggle between nature and man, particularly in the northern part of Texel, unfolded in numerous projects to increase land surface in the period 1629-1925. In this period Texel was subjected to significant geomorphological changes. Dikes were built to reduce the threat of the sea and in 1830 the Zanddijk was completed, connecting the Eijerlandsche Duinen with the rest of Texel at the Slufterbollen. In 1855 a second dike, De Lange Dam, was finished running parallel and westerly to the Zanddijk (fig 1-5). De Lange Dam did not survive as in 1858 a severe storm breached the dike at three locations creating three Slufters (De Muy, De Kleine Slufter and De Grote Slufter). Immediate efforts were made to re-establish the coastline leading to the closure of the Muy in 1860 and De Grote Slufter. However, people were less successful in closing De Kleine Slufter. The latter constantly created an opening with the sea and in 1925 a final attempt was made which again resulted in a failure. (Durieux, 2004).

t of the Slufter-area.
ıns are included.
ɔrg, 1961; in Durieux,

From this moment the Zanddijk was reinforced, the natural opening in the sea remained undisturbed and De Kleine Slufter became known as "De Slufter". Under the strict condition that the Slufters presence does not induce coastal erosion, it now exists for more than 150 years.

The last few decades, large morphological changes are limited to the Slufters mouth under the direct influence

of waves and currents. Also, Rijkswaterstaat regularly relocates the channel thereby effecting the morphology of the Slufters mouth.

1.4 Previous Research on Slufters

Former studies in de Slufter and slufter-like areas were performed in the 'Verdronken Zwarte Polder Slufter' at Zeeuws-Vlaanderen, the Netherlands, 't Zwin' between the coast of the Netherlands and Belgium, and in the present research area: 'De Slufter' on Texel.

The Slufter

- In 2002 Boersema and Reneerkens from Utrecht University carried out a fieldwork. Particular emphasis laid on the evolution and development of the Slufters main channel. Reneerkens found hydrodynamic flood dominance when HW remains below 0.9 m + N.A.P. whereas ebb dominance was found above this level.
- Durieux (2004) from Delft University performed a desk-study on the stability of the Slufters main channel with 1-D modeling approach using Sobek. Durieux concludes that the Slufters channel is very unstable. The Slufter channel is generally ebb-dominant leading to a net accumulation of sediment in proximity of the mouth which is unfavourable for the stability of the Slufter. However, due to frequent storms the system remains open. During storms high flow velocities in the channel will develop and associated sediment transport fluxes will also be significant. Durieux also states that due to the continuously channel migration, the length will increase in absence of human interference. A lengthening of the channel will increase ebb dominance and reduce stability.

't Zwin

- Doomen and Beijk from Utrecht University did fieldwork in 't Zwin in 2001 and studied mutual interaction between channel morphology and hydrodynamics / sediment transport patterns in relation to the stability of 't Zwin. Results showed a net tidally averaged sediment import in 't Zwin. This conclusion is supported by the depositional trend of the system.

De Verdronken Zwarte Polder

- Van Helvert, Zantinge and Zuiderwijck from Utrecht University did fieldwork in 2006 studying tidal asymmetry, influences of waves/ tides on sediment transport and waves – induced sediment transport patterns in the breaker zone. This fieldwork was carried out in good detail using modern equipment. Conclusions were that De Verdonken Zwarte Polder did not show flood dominance caused by the tidal asymmetry.

1.5 Research Objectives

The central objective of the research project 2008 on the Slufter, Texel is to deliver a contribution to the scientific understanding on the role of tidal- and wave-induced processes on the sediment transport patterns and morphologic development of the Slufter.

The research on the Slufter 2008 is subdivided into three interrelated subjects. Ralf Klein Breteler (2009) carried out a process based approach of wave-driven influence on cross- and longshore sediment transport patterns in the breaker zone and in the Slufter system when completely inundated under storm conditions. Stijn van Puijvelde studied the tidal deformation, constructed a hypsometric curve and the studied morphologic development of the system (historically and during the fieldwork period). Van Puijvelde also studied the relation between hydrodynamics and morphology of the Slufter.

The main objective of this thesis is to analyze the influence of tidal driven processes on sediment import and export patterns in the Slufters main channel under different tidal- and weather conditions. A distinction is made between neap- and spring tidal conditions under calm, non-flooding conditions. As for the flooding conditions, analyses are based on results measured at two locations (main channel and beach flat, table1-2) No further subdivision is made between neap and spring tidal conditions due to the overruling processes that occur during flooding conditions.

Non-flooding conditions				**Flooding conditions**			
Main channel				**Main channel**		**Beach flat**	
Neap tide		**Spring tide**					
flood	ebb	flood	ebb	flood	ebb	flood	ebb

Table 1-2 General research structure

1.6 Research Questions and Outline

Main research question

- What is the influence of tides on the import and export of sediment in the Slufters main channel?

Sub questions

- Does the tidal current field contribute to a net, tidally-averaged, transport of sediment in or out of the tidal inlet.

- What is the (quantitative) role of storm events for the import/export of sediment in the main tidal channel? What is the contribution of tidal asymmetries and incoming waves?

- What is the dominant mode of sand transport: bed-load or suspended load and how does this vary with offshore hydrodynamic conditions?

Thesis outline

- Chapter 2 presents the methodology and equipment applied for the realization of this research. A description is given of the data set that is collected by the instruments used in the fieldwork.
- Chapter 3 describes the hydrodynamic conditions at the Slufter inlet. It starts with an analysis of tide induced hydrodynamics for low-energetic, *non flooding* conditions in the main channel. A distinction is made between neap- and spring tidal conditions. Next, the hydrodynamics during high-energetic, *flooding* conditions are described. Here a distinction is made between the Slufters main channel and the inundated adjacent beach flat.
- In chapter 4 sediment transport in the Slufters main channel and beach flat are analyzes for the same conditions as in chapter 3. This is done based on sediment concentration measurements, dune migration measurements and sediment transport models.
- Chapter 5 discusses the results and presents conclusions of the research.

2 METHODS AND EQUIPMENT

This chapter presents the methodology and equipment applied for the realization of this research. Field data is obtained by applying instruments that require thoughtful approaches in the field. Results were elaborated carefully, demanding employment of specific techniques. Data acquisition and technical computing is done with MATLAB 2007b allowing one to cope with large amount of data. A part of data acquisition is done with Excel 2007.

2.1 Instrumentation

During the field work hydraulic processes and sediment dynamics in the Slufters main channel were continuously monitored through an fixed measuring frame anchored in the centre of the channel. The measuring frame, or mainframe, has recorded data in great detail. The mainframe was equipped with 2 pressure sensors, 3 EMF-instruments that measure flow velocities, 8 OBS-sensors measuring sediment concentration and 1 ripple profiler which measured ripple shape and migration (Picture 2-1). The latter is not used for analysis in this research. The configuration of the mainframe is composed of two separate measuring modules: the “Truc Vert” measuring module (a), which is an advanced instrumentation package, equipped with modern hardware and software and was recently applied for a study along the south-west coast of France by dr. Gerben Ruessink. In addition, due to the numerous instruments part of the data were controlled and sent to miniframe 16 (b).

Picture 2-1 A) Main instrument frame, positioned in the centre of the Slufters main channel. The three installed cylinders are respectively ‘Truc Vert- and Tripod miniframe 16 measuring modules and one battery storage cylinder. Photograph was taken at September 23, 2008 11:18 during very low water conditions. B) Main deployment of instruments in the main channel during the installation phase. The dish-shaped devices are EMF-sensors, while long dark instruments represens the OBS-devices. Photograph was taken at September 8, 2008 14:36.

To obtain a good impression of vertical flow and concentration distribution in the main channel, three EMF-sensors were installed logarithmically at respectively 15, 25 and 65 cm from bottom level.

Sediment concentrations were measured with a smaller vertical resolution (table 2-2). The pressure sensor was placed 28.5 cm from bottom and constantly remained submerged (table 2-2).

Pressure Sensor	EMF	OBS
		105 cm
	65 cm	65 cm
		45 cm
28.5 cm		27 cm
	25 cm	24 cm
		21 cm
		18 cm
	15 cm	15 cm

Table 2-2 Schematic overview of the instrument relative and absolute position from the bottom.

Two other miniframes were used at other locations in the fields. These miniframes are very mobile and were part of the fieldwork positioned in the breaker zone, upstream of the main channel and for one week on the beach flat (fig 2-1 and table 2-2). The miniframes were equipped with a single EMF and three OBS-sensors.

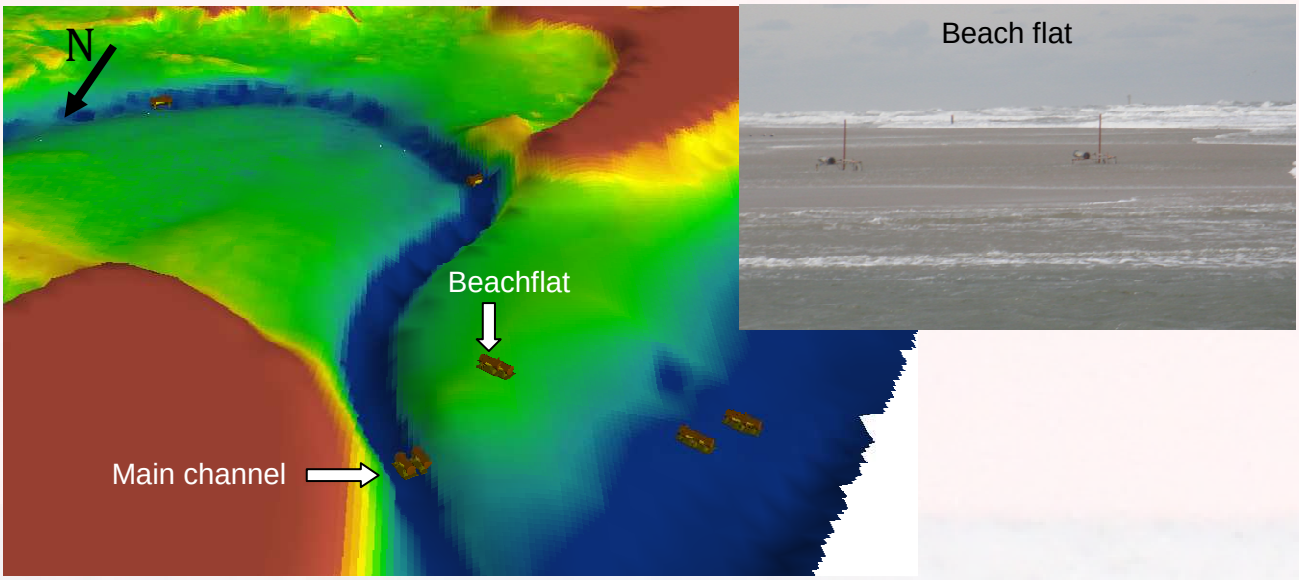

Figure 2-1 3-D representation of study area with designated measurement locations. To the top-right: picture of miniframe 14 and 15 at the beach flat at September 30, 2008 15:55. Blue color indicates low elevated areas, red color indicates high elevated areas.

Breaker Zone	Upstream	Beach flat
09/09- 20/09		
	21/09 – 30/09	
		01/10 – 07/10
07-10-17/10		

Table 2-2 Periods of measurements miniframe 14 and 15 with location

2.1.1 Measuring protocol

Between September 11 and October 16, 2008 measurements were done in the Slufter-channel. Data loses have occurred between 04/10 – 10/10 when the instruments at the main instrument frame were buried in sand as a result of channel migration (paragraph 2-6).
The "Truc Vert" module measured with a frequency of 4 Hz, with no blanks interval in 30 minutes burst length. The miniframes initially measured at 2 Hz frequency in 17 out of 30 minutes burst-modes. On 24/09 the software program was replaced because the original program did not function well and measured continuously at 2 Hz speed. The program was replaced by a 4 Hz program in order to better measure wave orbital motions.

Data was transferred from the data logger on the frames towards a laptop. During this data transfer no measurements could be carried outData storage capacity of all miniframes is limited (6 MB) and requires downloading of data every 6 days, whereas Truc Vert is able to store data continuously for over a month. Due to slow data transfer rate (1 MB/hour) of the miniframe and vulnerability of computers in the field favorable weather and tidal conditions were desired. During rough weather conditions with high water levels no data could be transferred between data logger and computer. For exact fieldwork program and measuring periods a referral is made to Appendix D.

2.1.2 Electromagnetic Flow Meter

Electromagnetic Flow Meters (EMF) are used to measure instantaneous flow velocities. The basis of the instrument comprises the motion of water particles which behave as moving electrical conductors. "When currents move through the EMF generated magnetic field, an electromotive force is induced which is directly proportional to the speed of the current and at right angles to both the magnetic field and the direction of the current (Faraday's law of electromagnetic induction)" (Grasmeijer, 2005). Measured velocity components X and Y at the mainframe represent flow in longitudinal and lateral direction. Positive values in X-direction indicate flood directed currents. As for the Y-vector, positive values point to northern directed flows in this case.

2.1.3 Pressure sensors

The pressure (Keller) sensor measures pressure exerted on it by the overlying water and air. In the course of the fieldwork air pressure is continuously monitored and its effect is afterwards subtracted from the pressure signal leaving the water pressure which can be expressed as water depth using water density. From water pressure water level fluctuations can be obtained i.e. tidal fluctuation and/or waves.

2.1.4 OBS

The Optical Backscatter Sensor (OBS) was used to measure suspended sediment concentration (SSC) in the water column. OBS emits an infra-red signal which is reflected by sediment particles where the amount of backscatter is a measure for the quantity of sediment in the water. Limitation of this instrument is that it can only be calibrated for one particular grain size distribution. Problems occur when grain size distribution contain either clay and sand particles or all kinds of other items e.g. water plants and air bubbles, that can cause reflection. This diminishes the reliability of the measurement results in the Slufter.

2.1.5 DGPS

The Slufters geomorphology was measured by DGPS (Differential Global Positioning System). DGPS is an enhanced version of GPS technique and accurately determines of X-, Y- and Z- coordinates. GPS-location is based on its relative position to at least three satellites and additional use of a fixed base station on the ground (picture 2-2) that corrects for the satellite signal which strongly diminishes the chance of errors and particularly improves the vertical performance in contrast to regular GPS. Leveling is done with a mobile rover that was continuously connected with the fixed base location through radio signals. Accuracy of millimeters in horizontal and centimeters in vertical direction is achieved.

Picture 2-2 Base station of DGPS with the radio station at the left side and receiver at the right side.

2.2 Calibration

To convert digital signals to physical values data calibration is applied to each of the instruments. Calibration values for both the pressure sensors and EMF-instruments can be directly obtained from the instrumentation manual whereas OBS-calibration requires laboratory treatment.

To convert voltage signals into vectors U_x and U_y the following calibration formulas are used:

$$U_x = \frac{EMF_x - Off_x}{\alpha_x reg_x} \qquad [3\text{-}1]$$

$$U_y = \frac{EMF_y - Off_y}{\alpha_y reg_y} \qquad [3\text{-}2]$$

where U_x denotes the velocity component in longitudinal direction (in m/s) where positive values indicate flood directed currents. U_y is the lateral velocity (in m/s). EMF_x and EMF_y are measured signals of the EMF sensors (mV), Off_x and Off_y are offset values of the EMF, α_x and α_y are the transfer factors of the EMF. Finally reg_x and reg_y represent the regression coefficients.

Conversion of the measured signal of the Keller pressure sensor to water pressure signal (mbar) is done with formula 3-3:

$$p_w = \frac{reg_{pr}}{\alpha_{pr}} press + C_{pr} - p_{air} \qquad [3\text{-}3]$$

where p_w is the water pressure above the sensor in millibars, reg_p stands for the regression coefficient, α_{pr} is the transfer factor, *press* is the measured signal of the Keller sensor in millivolts, C_{pr} is the intercept and p_{air} denotes the barometric pressure. This instrument is accurate to ca. 0.25% of the measured value and has a linear calibration curve with a correlation coefficient > 0.99. The instrument offset is determined in the laboratory prior to deployment and taken into account by the calibration curve (Grasmeijer, 2005). Subsequently water pressure can be converted to actual water depth with the following formula:

$$h_w = \frac{g}{\rho_w} p_w + h_{sens} \qquad [3\text{-}4]$$

where h_w is water depth (m), g is gravitational acceleration (9.81 m/s^2), ρ_w is water pressure (mbar) and h_{sens} is depth of Keller pressure sensor from bottom.

Calibration values for OBS-instruments required laboratory procedures and are obtained individually for each instrument. Sediment samples were collected at every measuring site. Calibration was done in a circulation tank using a sand sample from one particular measuring site. The sensor output was correlated with the sediment concentration through a second order polynomial (equation 3-5) over the range from 0 to 30 kg m^{-3} ($R^2 > 0.99$). Measured signal (mV) is converted to SSC(g/L or kg/m^3) through:

$$C = \alpha + \beta OBS + \gamma OBS^2 \qquad [3\text{-}5]$$

where C is the SSC in g/L or kg/m^3, α is the intercept, OBS is the measured signal in mV, β and γ are respectively regression coefficient 1 and 2.

2.3 Data Validation

Following calibration, data is examined on validity. In this procedure data series are inspected on inconsistencies. Errors in data series can occur due to numerous reasons: the presence of bubbles, sea weed etc in the water column , silting-up of the instruments or when instruments stand clear of water. For reliable results it is stated that at least 5 cm of water must be on top of the instruments. Therefore results will be only considered when this condition is met. To detect and delete errors, MATLAB—programming is used.

Velocity data and concentration data in particular have shown significant spikes, varying from condition to condition. Data series is subjected to two criteria which both have to hold to qualify for de-spiking. Detected and deleted values are substituted by a new point obtained as averaged from the previous two and next two values i.e. $n_{altered}=(n\text{-}2 + n\text{-}1 + n\text{+}1 + n\text{+}2)/4$. Criteria read as follows:

1. A derivative criterium dV/V: for large deviations in successive date series.
2. An absolute criterium: to avoid data loss at near-zero values.

The weight of both criteria is determined dependent on the signals reliability from visual inspection and interpretation. Particular the OBS-instruments have shown results that had to be critically examined. Cases can be such that immediate exclusion of data from analysis is inevitable.

Generally dV/V for OBS-data was set at 0.01 for results at the beach flat. Results measured in the main frame generally showed more inconsistencies whereby dV/V here was set at stricter criteria: 0.01-0.005.

As stated in paragraph 2.1 flow velocities have been measured at 15, 25 and 65 cm above bed level. It is expected that the flow velocities increase with depth (EMF65 > EMF25 > EMF15) in such a way that the vertical flow profile is logarithmically shaped (fig 2-3A). However on many occasions the topmost EMF (65 cm + bedlevel) measured smaller absolute flow velocities in comparison to the other instruments (EMF65 < EMF 25 >EMF15) as can been seen in figure 2-2.

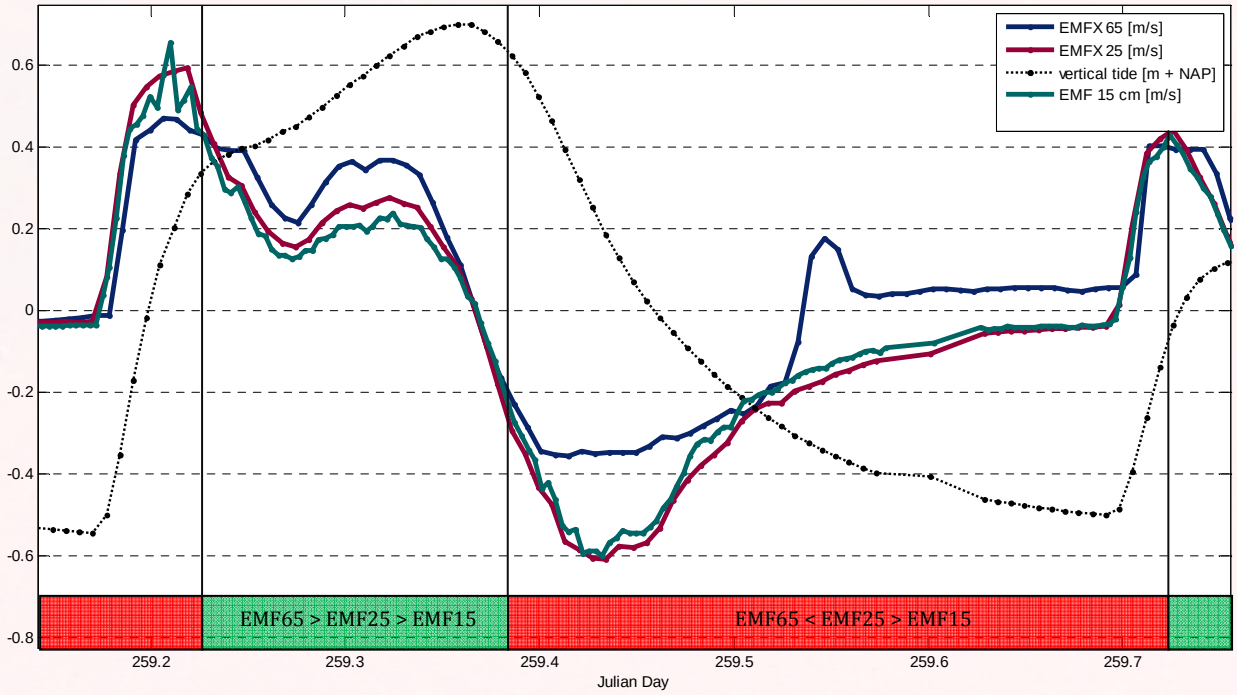

Figure 2-2 Flow distribution for different EMF-sensors at respectively 15, 25 and 65 cm above bed level

The fact that EMF65 has often recorded lower values compared to EMF15 and EMF25 can be attributed to several reasons:

- A minimum water height of ca. 20 cm above each of the instrument is required to obtain useful data. Since the relative position of EMF65 is 0.45 m – N.A.P., the requirements do not satisfy when water levels drop below 0.25 m – N.A.P.
- The presence of a second friction layer at the water surface may lead to a decline of the flow velocities in the near water surface region. The additional friction layer can be caused by winds and wave dynamics, which are most intensified when waves propagate in opposite direction to the flow.
- The vertical flow distribution at low current speeds during tidal slack periods, easily deviates from a logarithmic shape.
- Malfunctioning of the EMF65 sensor.

For this research, calculations of the mean flow velocity, through depth-integrated velocity profiles are merely based on flow data which are reliable and meet the theoretical order of flow magnitudes (EMF65 > EMF25 > EMF15). When these requirements do not meet, EMF65 data is excluded for analysis.

2.4 Water and Sediment transport calculations

To be able to cope with the large amount of data, data series are 5 minutes averaged. A sediment flux is computed by time-averaging the products of the instantaneous suspended sediment concentration, $c(x,z,t_i)$ and the instantaneous flow velocity, $v(x,z,t_i)$

$$F(x,z,t_i) = \frac{1}{N}\sum_{i=1}^{N} c(x,z,t_i)v(x,z,t_i) \qquad [3\text{-}6]$$

where $F(x,c)$ is the sediment flux, expressed as the rate per unit area at position (x) and height (z) in the vertical. Instantaneous velocity profiles are obtained using flow velocities on three levels allowing one to establish a profile with logarithmic shape that can be expressed with the formula:

$$U(z) = \frac{U_*}{\kappa}\ln(\frac{z}{z_0}) \qquad [3\text{-}7]$$

Where $U(z)$ is depth-dependent flow velocity, U_* is friction velocity, κ indicates the von Karman's constant (=0.40) and z_o denotes the bed roughness height. Plotting a logarithmically converted U gives simple output a and b following the equation 3-8. Velocity profiles are constructed by linear regression of $ln(z)$ and z:

$$y = ax + b \qquad [3\text{-}8]$$

Where a represents $\frac{U_*}{\kappa}$ and b is $\frac{U_*}{\kappa}\ln(z_0)$, a and b are subsequently plotted in a logarithmic profile, assuming increasing flow velocities with depth. Due to relative high values in the near-bottom zone, an additional fourth constant is set at depth 0.05 m + z with velocity 0.01 m/s, to optimize the logarithmic fit.

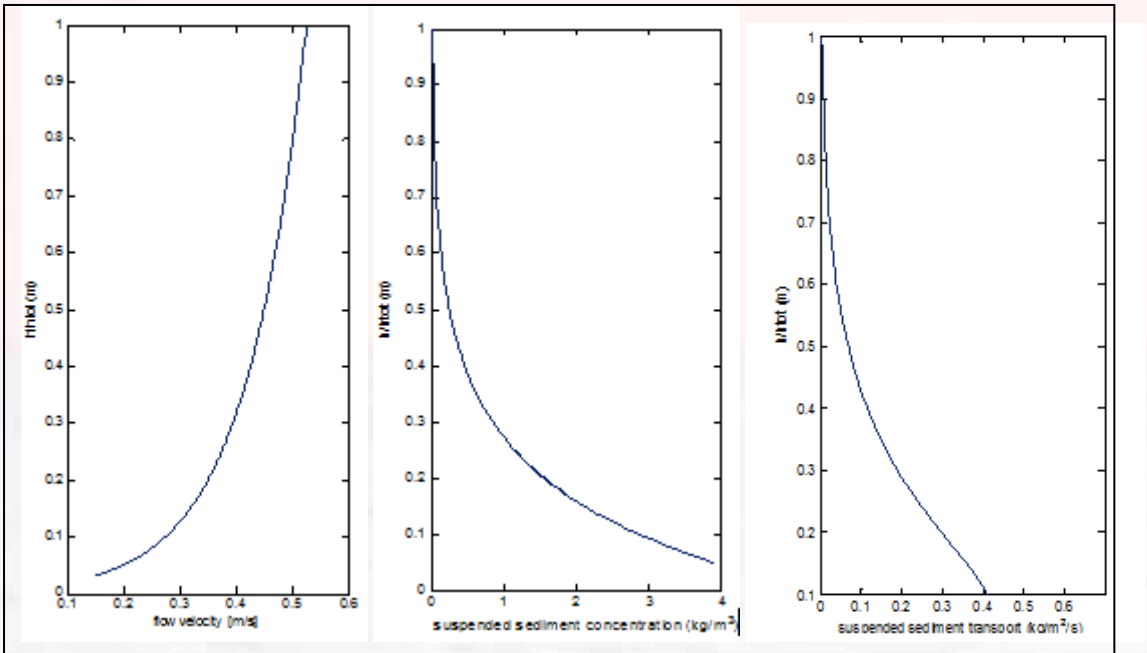

Figure 2-3 A) Logarithmic vertical velocity profile B) SSC profile C) Vertical suspended sediment transport profile

Sediment concentration profiles generally follow an exponential shape, where concentrations are highest in the near-bottom zone and strongly diminish with depth. The sediment concentration profile shape is fitted to:.

$$c_z = c_0 \exp(-\frac{w_s}{\varepsilon_s}) \qquad [3\text{-}9]$$

where c_z is the concentration at height z above the bed, c_0 is a reference concentration at bed level, w_s is the particle fall velocity and ε_s denotes an eddy diffusion coefficient. The concentration profiles are obtained through linear regression of $ln(c_z)$ and z:

$$\ln(c_z) = az + b \qquad [3\text{-}10]$$

which can re-written:

$$c_z = b\exp(az) \qquad [3\text{-}11]$$

Where a is $-w_s/\varepsilon_s$ and b is c_0. As stated before, concentration results often show high temporal and spatial variability in the signal. Therefore best reliable data is used i.e. data sequence that fits the proposed concentration distribution (equation 3-11). This implies that some data of OBS-instruments is not included in calculations. Also to optimize the concentration fit, an additional constant is set at water surface (dependable water height) with value 0.05 kg/m^3. Consequently, the products of velocity and concentration profiles result in a vertical suspended transport profile (fig 2-3 C).

2.5 Dune Tracking

Bed-load transport is calculated based on 2-D dune tracking of the Slufters channels bed. A set of 5 two-dimensional longitudinal profiles of approximately 36 meters were constructed out of survey leveling data with a spacing of about 3 meters. Dunes were measured at LW on three successive days, with an approximate 25 h. interval i.e. two tidal cycles respectively on 25, 26 and 27 September 2008. The positions of the 5 fixed measuring lines were determined by marked signs at a string stretched over the channel width at both far ends. Out of longitudinal profiles dune forms are recognized and dune tracking software DT2D (of Ten Brinke et al., 1999, modified by Roy Frings) is used to calculate longitudinal dune surface. Out of slight changes in form and position a daily net specific bed-load transport is calculated:

$$qb = (\frac{1}{2}\Delta \cdot \lambda \cdot c \cdot F) \qquad [3\text{-}16]$$

Where q_b is the specific bedload transport (m^3 m^{-1} day^{-1}), Δ is dune height (m), λ denotes dune length (m), c is dune migration rate (m day^{-1}) and F is the shape factor (-) which is a correction parameter

equal to the ratio between the cross-sectional area of the actual dune and the cross-sectional area of a triangular dune with the same length and height (Frings and Kleinhans, 2008).

2.6 Morphological Changes

From visual observation a scour hole was notable that developed at the location of the main frame. Parts of the measurement instruments were located above the hole. Instruments were initially installed at a relative distance from bottom level and due to the sudden reduction of the bottom level the spacing between sensors and bottom level had increased. Initially, to account for an additional 30 centimeters, calculations were adapted to the new situation. However, results of sediment fluxes became unsatisfactory large as concentrations were constructed with an exponential fit which reached unreliable large values in the near-bottom range due to the increased distance from instruments to bottom. Furthermore, the scour hole had a strong dynamic character particularly under spring tidal conditions but vanished completely during the storm event. Complications arise to account for the continually changing distance between instruments and bottom. Therefore, the presence of the scour hole is ignored in calculations of water and sediment transport. For this, the initial relative position is used.

The combined effect of a storm event which occurred from 30 September to 5 October 2008 and spring tidal condition was a total inundation of the Slufters basin. Effects were strong currents and substantial sediment transports which have resulted in a significant relocation of the Slufters meandering channel at the measuring site. The main channel has moved approximately 10-15 meters to the north in roughly 3 days and the cross sectional profile had increased substantially (figure 2-4). Due to the sudden channel migration, the main instrument frame needed to be re-installed at a new location. This resulted in a total data loss of almost 4 days (Appendix 1).

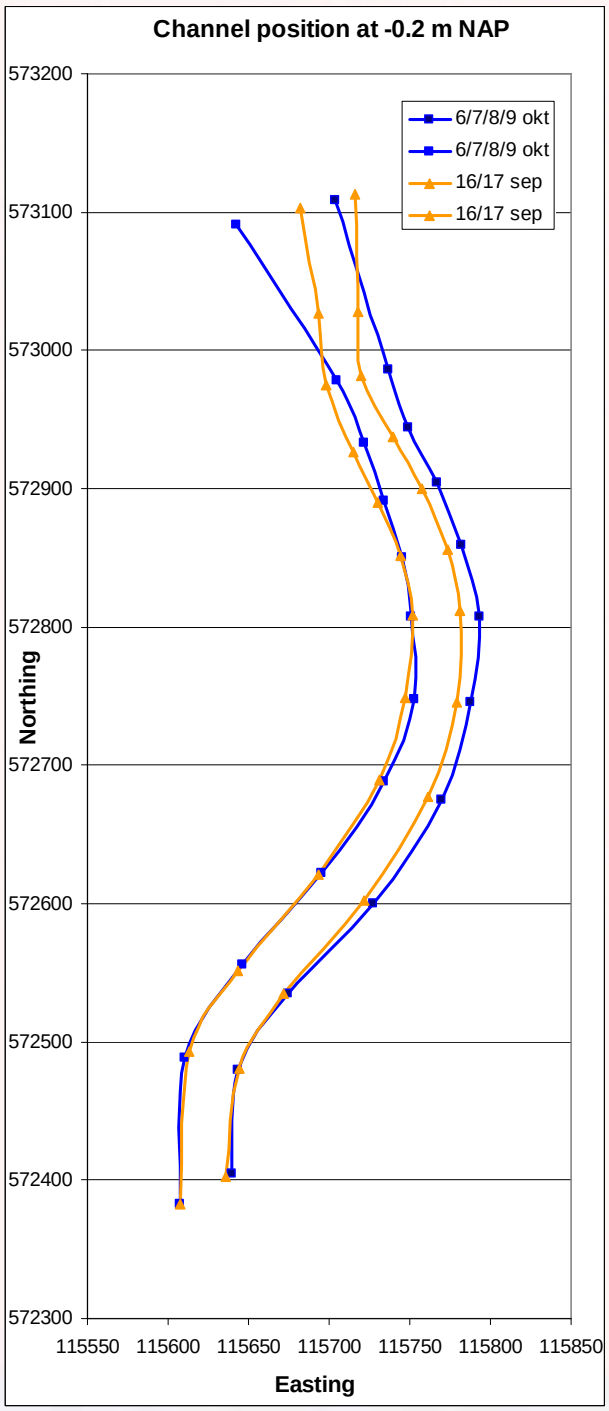

Figure 2-4 Overview of the channel position at -0.2 m NAP for 16/17 September (pre-storm) and for 06/07/08/09 October (post-storm). From: van Puivelde (2010).

3 HYDRODYNAMIC RESULTS

3.1 Introduction

In this chapter an analysis is made of the hydrodynamic conditions in the Slufter inlet. Using the hypothesis that water transport characteristics vary under different energetic conditions, a distinction is made between *non-flooding* (max HW < 1.1 m. + NAP) and *flooding* circumstances (max HW > 1.1 m. + NAP). During non-flooding circumstances, when tidal exchange is restricted to the main channel, the hydrodynamics are studied for different tidal regimes. For hydrodynamic analysis two neap and two spring tidal cycles are selected.

This chapter completes with an analysis of the measured current velocities, water elevations and wave dynamics in the Slufters inlet during a flooding event (high energetic conditions). Within the flooding cycle three stages are recognized: inflow, high water and outflow. For all three situations the current velocities in both x and y-direction are analyzed. For the analysis under high-energetic conditions no subdivision is made between neap and spring tidal conditions due to the overruling processes that occur during flooding conditions.

3.2 External conditions

The time of year during which the fieldwork was carried out can is generally characterized as a period of seasonal transition from summer to autumn. In fact, during the field campaign a continuous calm, dry period was experienced succeeded by a period with high energetic conditions. This external factor partly determined the boundary condition for hydrodynamics, sediment transport processes and morphological changes for the fieldwork in the Slufter.

Wind characteristics for the fieldwork period at de Koog, Texel demonstrate a high variability in wind magnitude and direction (figure 3-1). Generally eastern and southwestern winds dominate and strongest winds blow from the SW peaking to values over 20 m/s in the night between 4 and 5 October. Wind speeds in the class 5.0 -7.5 m/s were most frequently observed. The offshore wave height distribution shows two peaks events, being observed between 30/09 – 03/10 and 04/10 – 05/10. The first event coincided with spring tidal conditions (table 3-1 and figure 3-1) leading to high maximum water levels. After the two storm events, the weather became calm again but less calm than the period before the storm, as can be derived from the set-up in figure 3-1.

Storm event	$H_{s,\ off\ max}$ (cm)	Period (Julian days)	Wind dir (°)	Tidal range (m)	Set-up (m)
event 1	450	274.0 - 276.5	270	2.0	0.60
event 2	478	277.8 – 295.5	270	1.3	0.55

Table 3-1 Several characteristics of the two main storm event during the fieldwork period.

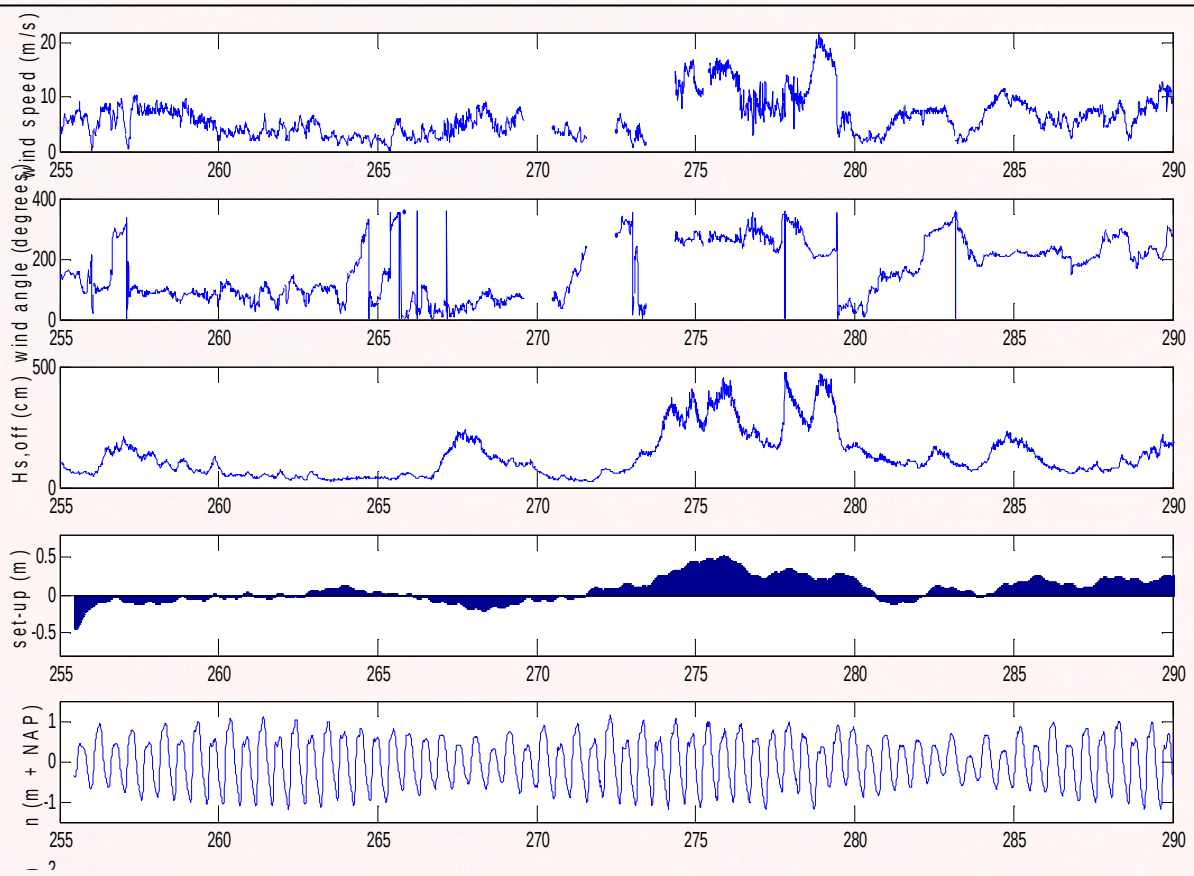

Figure 3-1 Boundary conditions during the fieldwork period from September 11, 2008 (255 Julian Day) to October 16, 2008 (290 Julian Day). A) Wind speeds distribution at de Koog, Texel. B) Wind direction distribution at de Koog, Texel. C) Offshore significant wave height distribution measured on the North Sea buoy in proximity of de Koog, Texel. D) Meteorological tide (set-up) as a result of wind-stress based on the difference between actual and predicted tide.

Figure 3-2 demonstrates the astronomical-, measured-, and meteorological tide at Texel during the fieldwork period. Tides are semi-diurnal implying that water levels rise and fall twice a day. Tidal amplitude ranged from 0.8 m for neap- to approximately 2.3 m for spring tidal conditions. During the fieldwork approximately 3 spring-neap cycles were experienced. The largest differences between astronomical- and measured tide lead to highest set-up which is particularly experienced during the storm period.

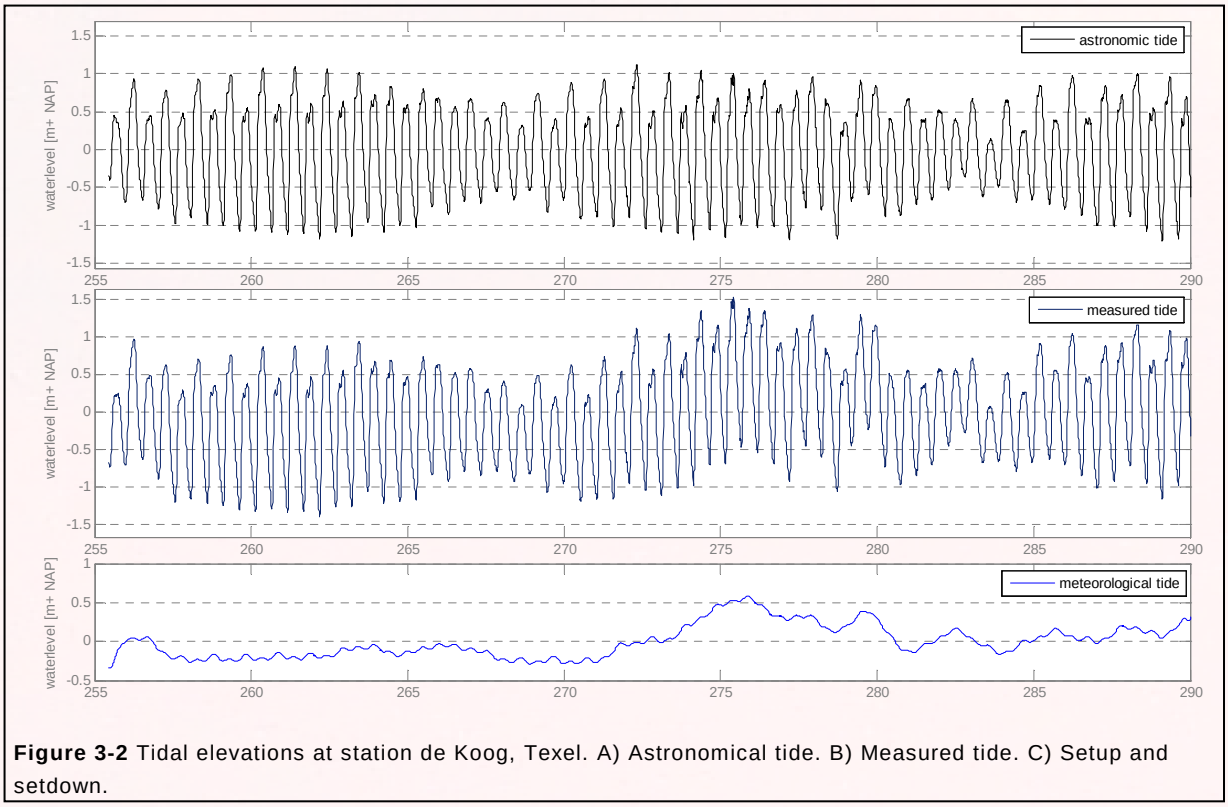

Figure 3-2 Tidal elevations at station de Koog, Texel. A) Astronomical tide. B) Measured tide. C) Setup and setdown.

3.3 Truncation

Figure 3-3 shows the tidal curve for September 13, 2008 at four different locations in and around the mouth of the Slufter. The curves measured seaward from the mouth differ substantially from the curves measured in the Slufters' inlet. Over a distance of about 200 meters – between breaker zone and Slufter channel – differences between both water levels of approximately 0.6-07 m appear. This effect is seen in the trough of the tidal curve. As the falling tide proceeds offshore, the fall of water level in the main channel clearly decelerates and reaches its minimum level far above the lowest levels measured offshore. Subsequently it rises almost simultaneously again in comparison to the measuring station offshore.

Truncation of the tide, as is demonstrated above, is caused by the relative high situated bed level of the Slufters channel which is above MLWL (Mean Low Water Level). The effect is a reduction of the tidal amplitudes inside the Slufter and a change in tidal asymmetry. The amplitudes of M2 and M4 and the M4/M2-ratio all decrease compared to the North Sea. According to van Puijvelde, compared to the North Sea (where the tide is already slightly deformed), the ebb-duration in the Slufter increases with 53.5 minutes on average (table 3-2).

	North Sea (Jul. day)	Slufter (Jul day)	difference (minutes)
mean ebb duration	0.28005	0.31737	+ 53.73
mean flood duration	0.23694	0.19983	- 53.43

Table 3-2 Mean ebb and flood durations and duration differences between North Sea and main frame. After van Puivelde (2010).

Figure 3-4 demonstrates truncation during the total fieldwork campaign, illustrating truncation on both neap and spring tides. Since tidal amplitudes during neap are relative small, less of the tidal through is

truncated in comparison with the larger spring tidal curve. Therefore the change in asymmetry of the tidal curve due to truncation is greater for spring than for neap tides. Truncation also leads to somewhat equal minimum water levels for both neap and spring tidal conditions.

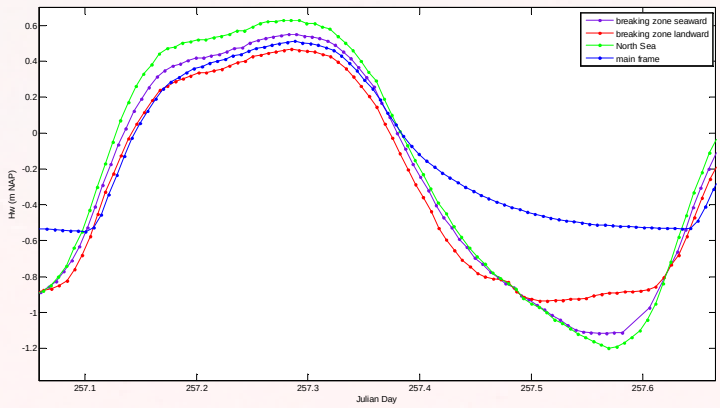

Figure 3-3 Truncation of the tide, September 13 measured at various locations in and out the Slufter mouth simultaneously, respectively: the North in proximity of de Koog, breaker zone Slufter (miniframe 15&16) and main channel Slufter.

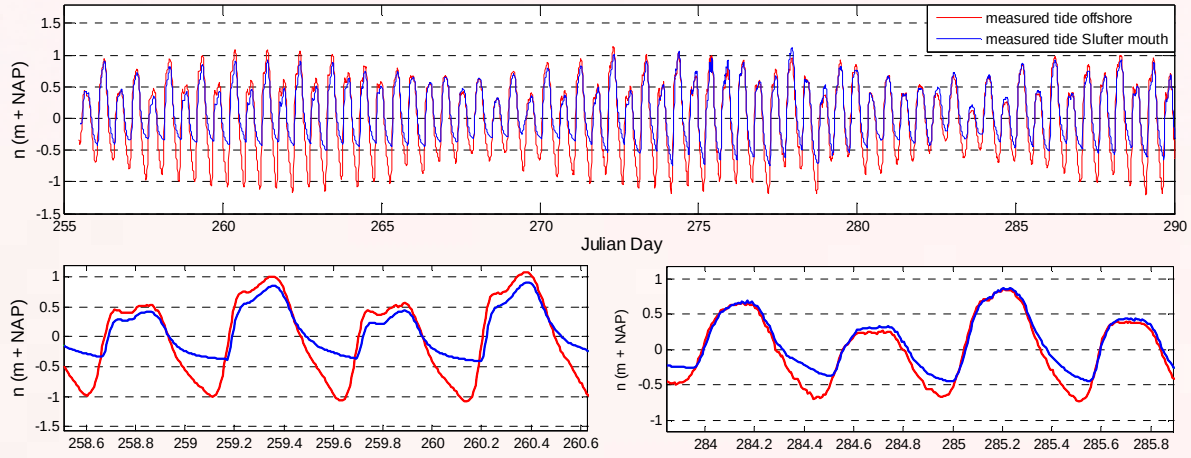

Figure 3-4 Truncation of the tide during the fieldwork period. Upper figure: combined measured tide offshore (de Koog) and measured tide in mouth Slufter. Detailed reproduction of truncation for a spring (bottom left) and neap (bottom right) tide.

3.4 Non Flooding Situations

In the following section several hydrodynamical characteristics under non flooding conditions measured (or derived from measurements) in the Slufter will be discussed. As mentioned in paragraph 3.1, for non-flooding situations two neap (neap 1 and 2) - and spring (spring 1 and 2) tidal cycles have been selected as representatives for the different tidal conditions. The tidal cycles that are used for analysis are marked in figure 3-5. Table 3-3 shows the four selected cycles with different hydrodynamic characteristics. Remarkable is the relative large difference of maximum water level between spring tide 1 (106 cm + NAP) and spring tide 2 (86 cm + NAP), which is caused by differences in set-up. Another aspect which becomes clear from table 3-3 is that maximum flows

during neap tidal conditions are larger for the landward than for the seaward directed component, whereas for spring tidal conditions maximum seaward directed flows exceed landward directed flows.

Plots of velocity and elevation against time are given, providing a good impression of the hydraulics in the Slufters inlet under different tidal conditions, These plots illustrate the degree of asymmetry, relative duration, rates of change and the phase relationship between elevation and flow. Also, velocity stage plots are presented which give an indication of flood/ebb dominance and highlight the magnitude of velocities at different elevations. A circle or oval represents a symmetric tide and increasing asymmetry produces distorted balloon shapes, where the area of the shape, relative to the axes, indicates flood or ebb dominance (Walton, 2002). Plots for spring- and neap tide 2 are presented in appendix A. Hydrodynamic analysis is completed with results of van Puijvelde (2010) who related different hydrodynamic parameters to both neap- and spring tidal conditions. The variation of water level with time (*dh/dt*) is the most relevant parameter for this research.

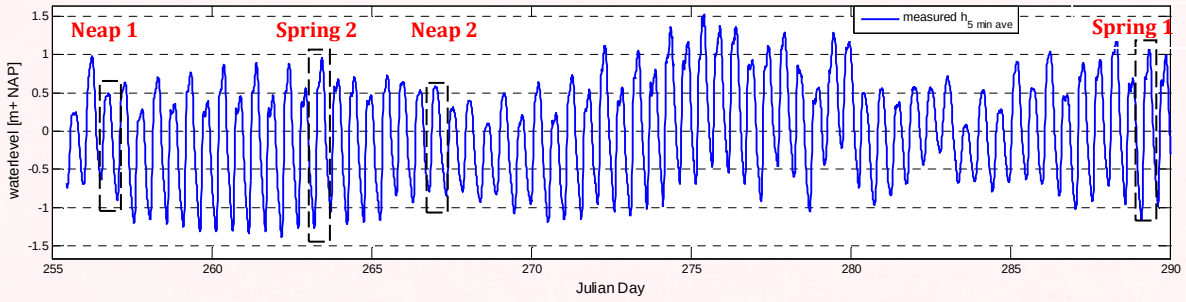

Figure 3-5 Measured tide as a function of time. Selected tidal cycles for analysis are marked with a dotted box.

Date & Time	Tide	Tidal Amplitude (cm)	HW (cm + N.A.P.)	D [-]	$U_{max,ebb}$ (m/s)	$U_{max,flood}$ (m/s)
12-09-08 14:30-02:00	Neap1	44	35	6	0,39	0,47
23-09-08 10:00-22:15	Neap2	42	25	-16	0,26	0,32
12-10-08 3:30-16:00	Spring1	75	106	18	1,15	0,85
19-09-08 7:00-19:30	Spring2	69	86	- 6	0,71	0,65

Table 3-3 Tidal amplitudes, maximum water level, setup and peak inflow- and outflow velocities for four selected tidal cycles

3.4.1 Neap Tide

Figure 3-6 shows that during neap tide measured flow velocities are rather low (less than 0.5 m/s) and also the differences between flood and ebb are small. Water levels and flow velocities during neap tide indicate that the vertical tide is already asymmetric before it enters the Slufter-channel. The asymmetric shape is visible in the short flood-phase succeeded by a relative long ebb phase. The initial rise of the tide results in the highest current velocities; after that the flood current decelerates and finally reaches somewhat smaller peak velocities. As for the ebb phase, flow velocities rapidly reach maximum values whereas due to a gradual decrease of vertical tide acceleration, flow current velocities consequently reduce. Figure 7-1 A and B in appendix A shows a neap tidal curve with similar results. Figure 3-6 B and 7-1 B in appendix A indicate that flow velocities during flood

generally exceed flow velocities during ebb. The stage-velocity plots therefore clearly point to flood dominance. Flood/ebb tidal asymmetry will be further discussed in paragraph 3.4.3.

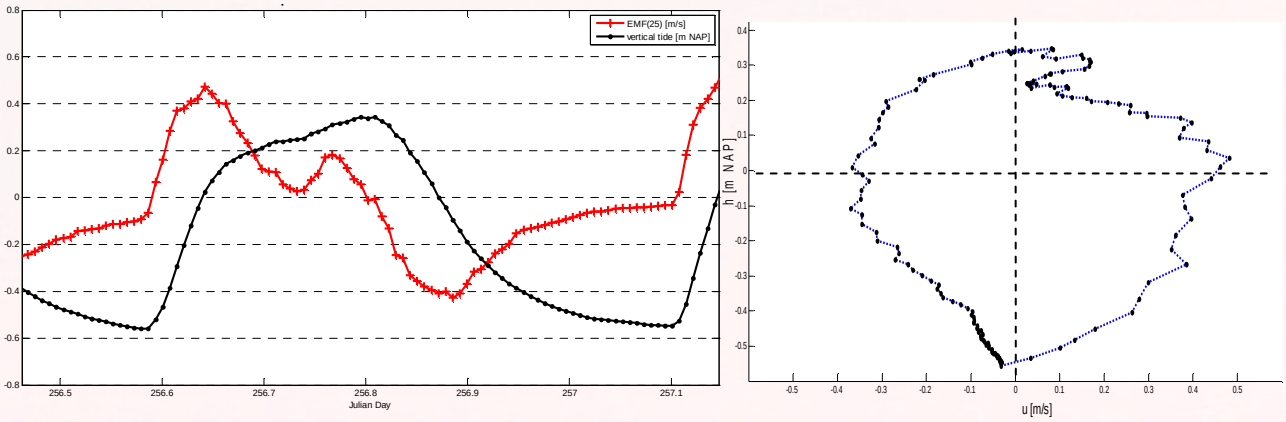

Figure 3-6 A) Vertical and horizontal tide during a neap tide (1), September 12 14:30-02:00. **B**) Stage velocity of neap tide 1

Starting at LW, it can be seen in figure 3-7 that both flow velocity and the variation of water level with time (*dh/dt*) start to increase rapidly. Maximum values of *dh/dt* are reached earlier than maximum measured flow velocities. The delay with maximum values of *dh/dt* is 27 minutes (van Puijvelde, 2010). Maximum values of *dh/dt* are remarkably higher than maximum flow velocities. After HW *dh/dt* and flow velocities decrease almost simultaneously. During the ebb phase values of *dh/dt* are much smaller, but are also much more in phase with maximum ebb velocities compared to the flood phase.

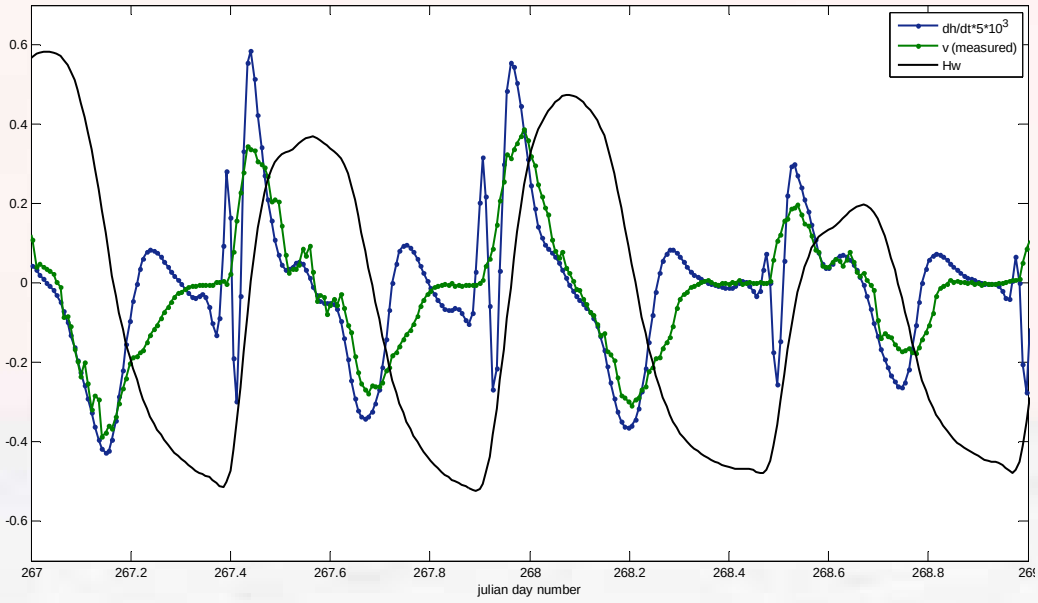

Figure 3-7 Different hydrodynamic parameters for neap tidal conditions including Hw (m NAP), dh/dt (m/s) and measured velocities (m/s). After van Puijvelde (2010).

3.4.2 Spring Tide

Figure 3-8 A and 7-2 A (appendix A) show that the shape of the tidal curve is steeper compared to neap tide situation, which lead to higher velocities in both directions. Particularly outflow velocities

are much larger, exceeding the maximum inflow velocities. This is also seen in the stage velocity plot (figure 3-8 B) which clearly indicates ebb-dominance.
The differences between maximum landward and seaward flow are also larger compared to neap tides. Spring tide 1 (fig 3-8 A) is the best example, where the maximum landward flow reaches 0.85 m/s versus 1.15 m/s for the seaward flow. The asymmetry of the tidal form is also larger compared to the neap tide.

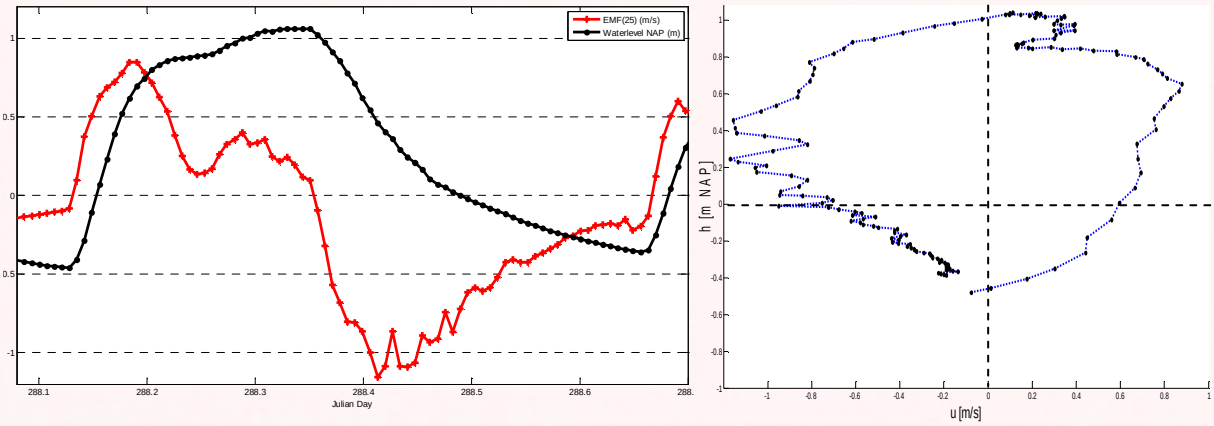

Figure 3-8 A) Vertical and horizontal tide during a spring tide (1), October 12 03:30-16:00. **B**) Stage velocity of spring tide 1

Figure 3-9 demonstrates several hydrodynamic parameters for spring tidal conditions. During the flood phase differences between values of *dh/dt* and maximum flow velocities are higher compared to neap tidal conditions. As for the ebb phase, maximum flow becomes significantly larger than values of *dh/dt* and this effect increases with increasing maximum water level (262.45-262.6 and 263.5-263.7). Figure 3-7 and 3-9 suggest that *dh/dt* values indicate higher flood velocities than are actually measured. Also *dh/dt* values underestimate ebb directed flows during spring tidal conditions.

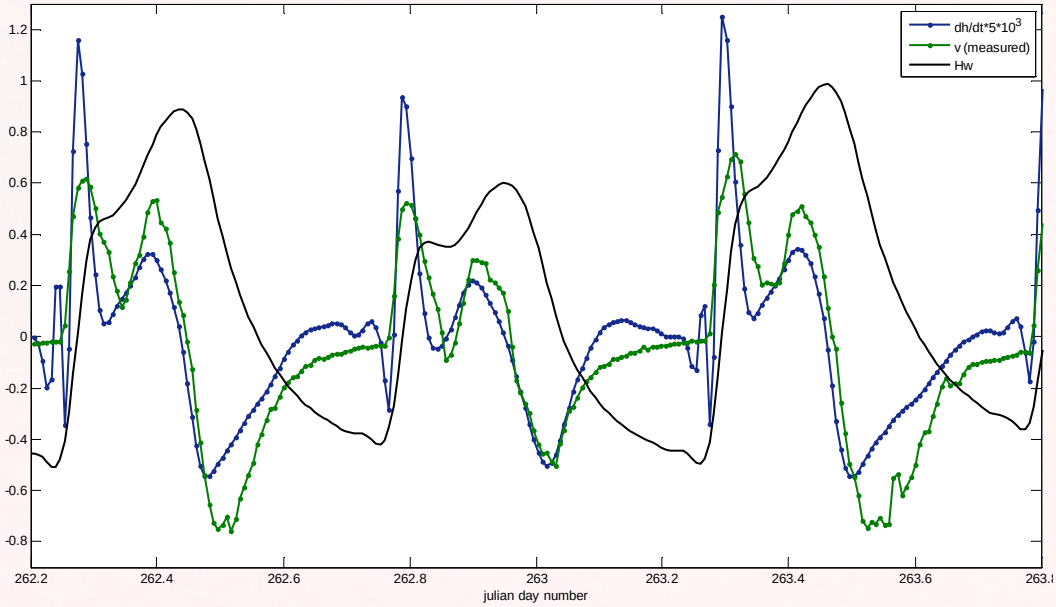

Figure 3-9 Different hydrodynamic parameters for spring tidal conditions including Hw (m NAP), dh/dt (m/s) and measured velocities (m/s). After van Puijvelde (2010).

3.4.3 Tidal asymmetry

The simplest representation of asymmetry is to note the difference between the duration of the flood and ebb. It is expected that an unequal duration of flood and ebb phase causes a difference between maximum flow velocities during the rise and fall of the tide. The asymmetry of the surface elevation over time can be expressed with a non-dimensional parameter D (Lincoln and Fitzgerald, 1988):

$$D = [(d_{rise} - d_{fall}) / (d_{rise} + d_{fall})] * 100$$

Where d_{rise} and d_{fall} represent the duration of respectively the rising (from LW to HW) and falling tide (from HW to LW). For a symmetric tide D is zero. D is negative when the duration of the falling tide exceeds the rising tide duration and can be defined as flood dominant. Flood dominance indicates to higher flood currents than ebb currents. The calculated parameter D (table 3-3) for each tidal cycle shows negative values. In fact, this applies for the whole fieldwork period (Appendix E), which indicates a continuous flood dominance. However from the velocity measurements (paragraph 3.4, 3.4.2, table 3-3 and appendix E) can be derived that ebb directed currents are often much stronger than flood currents. Therefore, the relation between asymmetry as a result of differences in tidal durations and maximum flow asymmetry is indistinct.

As indicated in paragraph 3.4, 3.4.1 and 3.4.2 the variation of maximum flow asymmetry is most likely related to the tidal amplitude. An easy representation of maximum flow asymmetry is to note the ratio of maximum flood velocity, measured for each tidal cycle, to its maximum ebb velocity ($U_{max,flood}/U_{max,ebb}$). For a symmetric tide, the ratio of peak flood and peak ebb current magnitudes is one. Values greater than one indicate flood dominance, subsequently values smaller than zero point to

ebb-dominance. Following, the results are plot together with HW-level in figure 3-9, including storm results.

Figure 3-9 indicates that the ratio of peak flood and peak ebb current magnitudes is reversely related to the tidal amplitude, which corresponds to the findings in paragraph 3.4.1 and 3.4.2. When tidal amplitudes are small (neap tide), inflow velocities are greater than outflow velocities. On the other hand, when amplitudes are high (spring tide) ebb-directed flows are generally stronger than flood-directed flows. From the intersection of the linear fit with x = 1 turns out that the reversal from flood- to ebb-dominance is found at 0.64 m + NAP.

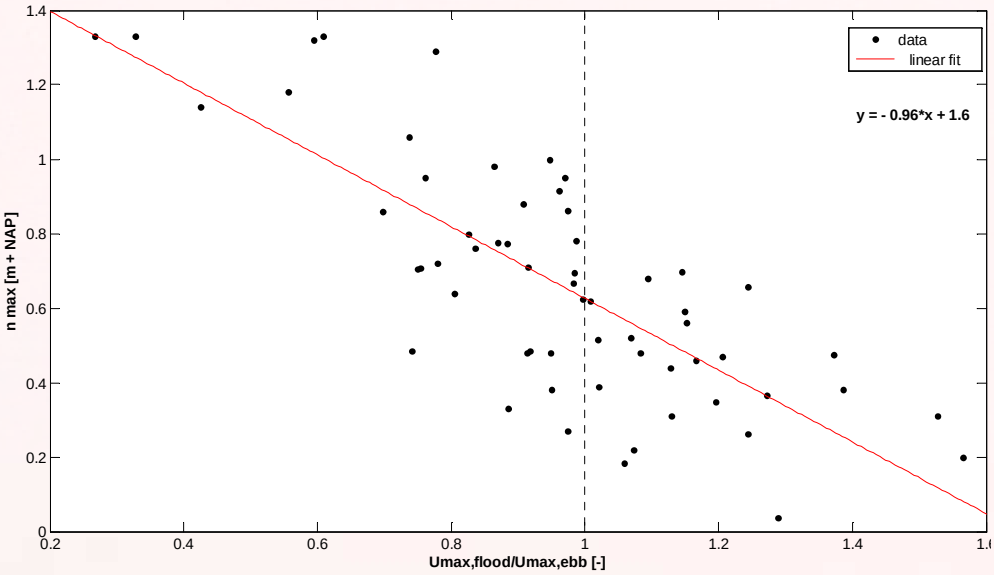

Figure 3-10 Umax,flood-Umax,ebb ratios against maximum water height, measured in the main channel of the Slufter.

Using Dronkers tidal asymmetry ratio (equation 1-2) an indication is given of ebb/flood dominance for different tidal conditions. Values of total basins surface water at low water (S_{lw}) and high water (S_{hw}) are obtained using the hypsometric curve (both surface and volume), derived from GIS-analysis and performed by Stijn van Puijvelde. Van Puijvelde (2009) created a DTM based on laser altimetry data. The applicability of laser altimetry is limited at lower terrain levels (below 0 m N.A.P) when water bodies are involved. Therefore the minimum level in the hypsometric- and volume is set at 0 m + N.A.P. Through linear extrapolation, values between -0.6 – 0 m + N.A.P. have been obtained, to determine the total basin area during low water (S_{lw}).

The results (table 3-4) show a reasonable correlation between the degrees of ebb dominance as measured by the ratio of peak flood and peak ebb current magnitudes and as calculated by the Dronkers parameter, γ. Both the ratio of peak flood to ebb current and Dronkers parameter for the neap tide situation are greater than one, indicating flood dominance. During spring tidal conditions

both parameters are smaller than one indicating ebb dominance. The results suggest that the Slufter shifts from flood to ebb-dominance from neap to spring tide at respectively 0.64 m + NAP.

The form ratio γ is also proportional to the ratio of the time between high water and the high water slack ($t_{HW,slack}$- t_{HW}) and the time between low water and the low water slack($t_{LW,slack}$- t_{LW}) (Dronkers, 1986). Thus with γ decreasing, ebb tides reduce in duration with respect to flood tides.

Date & Time	**Tide**	**Tidal Amplitude** (cm)	**HW** (cm + N.A.P.)	**D** [-]	$U_{max,ebb}$ (m/s)	$U_{max,flood}$ (m/s)	$U_{max,flood}$/ $U_{max,ebb}$	**Dronkers Parameter** γ (–)
12-09-08 14:30-02:00	Neap1	44	35	-19.2	0.39	0.47	1.21	4.87
23-09-08 10:00-22:15	Neap2	42	25	-28.9	0.26	0.32	1.23	3.35
12-10-08 3:30-16:00	Spring1	75	106	-17.8	1.15	0.85	0.74	0.60
19-09-08 7:00-19:30	Spring2	71	86	-22.4	0.71	0.69	0.78	0.78

Table 3-4 Different hydrodynamic characteristics (tidal amplitude, maximum water level, duration asymmetry D, peak flood- and ebb currents, ratio of peak flood to ebb currents and Dronkers parameter) for two neap and spring tidal situations

3.5 Flooding situation

A low pressure system reached the Netherlands at 30 September 2008 carrying considerable amounts of precipitation, accompanied by strong winds (up to 22 m/s). The latter is for this research of great importance. Onshore winds are the fundamental mechanism for the development of a wind set-up. Set-up during this period was approximately 0.4 m, reaching a maximum of more than 0.5 m. (figure 3-1 and 3-2). The storm more or less coincided with spring tide and resulted in significant overwash on top of the beach plain. Based on the inlets morphology it can be stated that the adjacent beach flat is flooded when water levels exceed 1.1 m + N.A.P. Since at least seven flooding events have been measured, tidal flows during high energetic conditions can be compared with that during low energetic conditions. Two examples of tidal cycles under high energetic conditions are presented in table 3-5, the first is studied in more detail. Tripods that were installed on the beach flat during flooding conditions, gathered additional data regarding flow velocities and sediment concentrations.

Date & Time	**Tide**	**HW** (cm + N.A.P.)	**Dominant wind dir. (°)**	$H_{s,off}$ (m)	**Setup** (cm)	U_{max} **,flood** (m/s)	U_{max} **ebb** (m/s)
01-10-08 05:00-16:00	Spring	131	268 (W)	3.15	46	0.79	2.16
16-10-08 04:25-15:55	Spring	111	291 (WNW)	2.24	26	1.22	2.01

Table 3-5 storm-events during the field campaign, including the duration of the event and the offshore significant wave height, wind direction, tidal range and set-up during the peak of the events. After Klein-Breteler (2009)

The impact of surges on current intensities in the Slufters main channel is tested taking maximum water level (HW) as conditional parameter for both tidal and meteorological conditions. Based on 5 minutes average peak velocities in both ebb and flood direction, the hydraulic situation in the main channel is demonstrated (fig 3-11). A distinction is made in flooding and non-flooding circumstances

on the one hand and flow direction on the other hand. From figure 3-11 becomes clear that the highest flow velocities are measured during high energetic (-flooding) condition, particular for the ebb phase. Maximum flow velocities during flood amount to 1.6 m, whereas ebb directed flow reach values of 2.16 m/s (see example above). Under non-flooding circumstances flow velocities are substantially smaller, since for calm weather conditions hydraulics in the main channel are principally tidal driven.

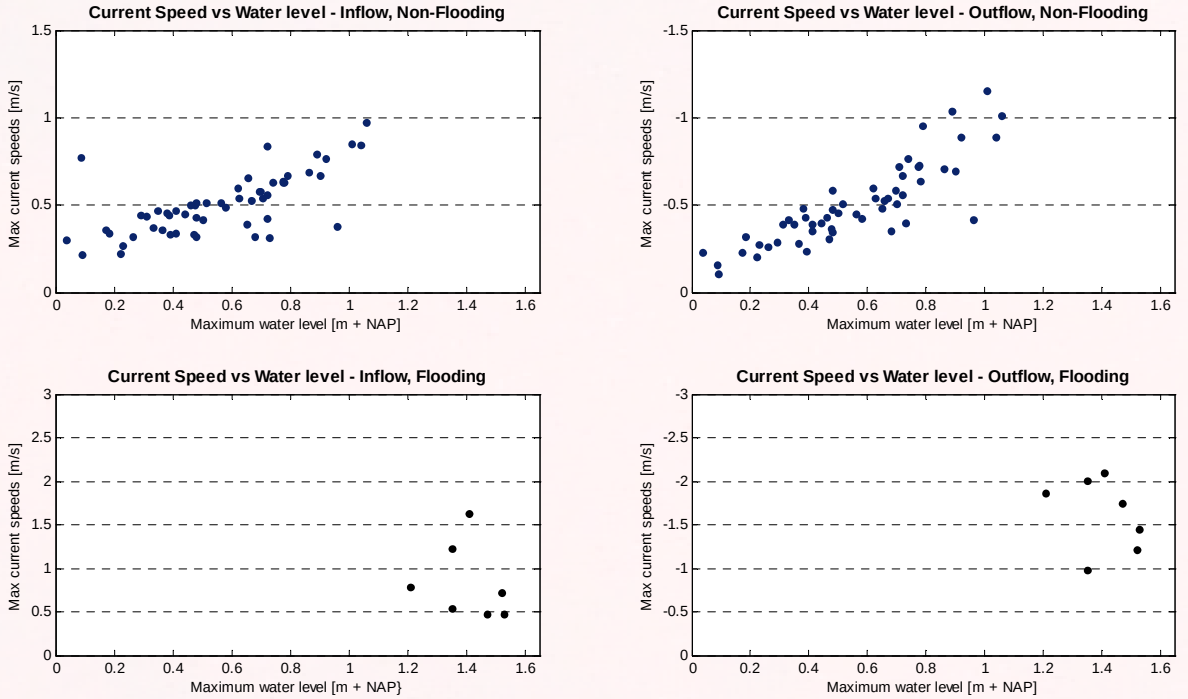

Figure 3-5 Maximum flow velocity versus waterlevel for both inflow, outflow and non-flooding and flooding conditions.

3.5.1 Hydrodynamics in the main channel

Flows and water levels

Flow conditions measured in the main channel during energetic conditions are considerably larger compared to tidally driven flows during calm conditions. Water levels for this particular flood event reach a maximum level of 1.5 m. above Dutch ordnance (fig 3-11). Since at this level, the exchange of water occurs on a much greater spatial scale, the flow patterns in the main channel are strongly affected. This can be seen in the short duration of peak flood velocities which is succeeded by a relatively long period with rather low channel flow velocities. In contrast to regular flood events the inflow of water is apparently delayed at a certain water level. This phenomenon is most likely related to flow patterns on the beach flat and will be discussed in paragraph 3.5.2.

Flow velocities can be decomposed into longitudinal and cross flows, respectively *x*- and *y* direction. Figure 3-12 indicates that especially flow velocities in *x*-direction differ significantly over time. The rising tide is associated with maximum flood velocities of 0.76 m/s, whereas during the ebb phase, maximum flow velocities are a factor 2-3 higher. This agrees with the hypotheses that the main channel is strongly ebb-dominated during flooding conditions. Just after HW, water levels drop

rapidly as large amounts of water have to be transported seaward through the confined mouth of the Slufter. Maximum flow velocities reached values over 2 m/s.
Cross flows reach approximately 0.1 m/s during high energetic conditions. Figure 3-12 indicates that during inflow the lateral-flow is very small, whereas for the ebb phase lateral flow velocities are higher and slightly directed to the north, especially during the begin stage of the outflow when water levels decrease rapidly.

Figure 7-3 to 7-5 in Appendix B provide a detailed image of the instantaneous velocities in both cross- (EMFx) and longitudinal (EMFy) direction during three stage of the tidal cycle: inflow, HW and outflow. From the beginning of the rise of the tide, the EMFx velocities are still negative. This indicates that an amount of water is still leaving the Slufter even when the water levels are rising. The EMFx velocities briefly respond to the rising tide and reach maximum values of 1 m/s, indicating that the instantaneously measured values were not as low as the averaged velocities. EMFy velocities are generally negative but very small. Negative EMFy velocities point to a very small southern directed component. A clear difference between the instantaneous signals during inflow and that of high water or outflow is the little variation in both flows and pressure signals. Apparently, water movement during inflow occurs rather smooth in comparison with high water or outflow situations.

During high water, both instantaneous flow and pressure signals show more variation. Longitudinal flow velocities, which are obviously small, respond well to changes in water elevation. Instantaneous longitudinal flows of +0.5 to -0.5 m/s are found. Cross flows range between -0.2 – 0.2 m/s. The relative high variation is a result of wave dynamics.

During falling tide, instantaneous outflow velocities in longitudinal direction of 2.5 m/s are found. EMFy velocities range between -0.2 to 0.5 m/s indicating a general northern directed component.

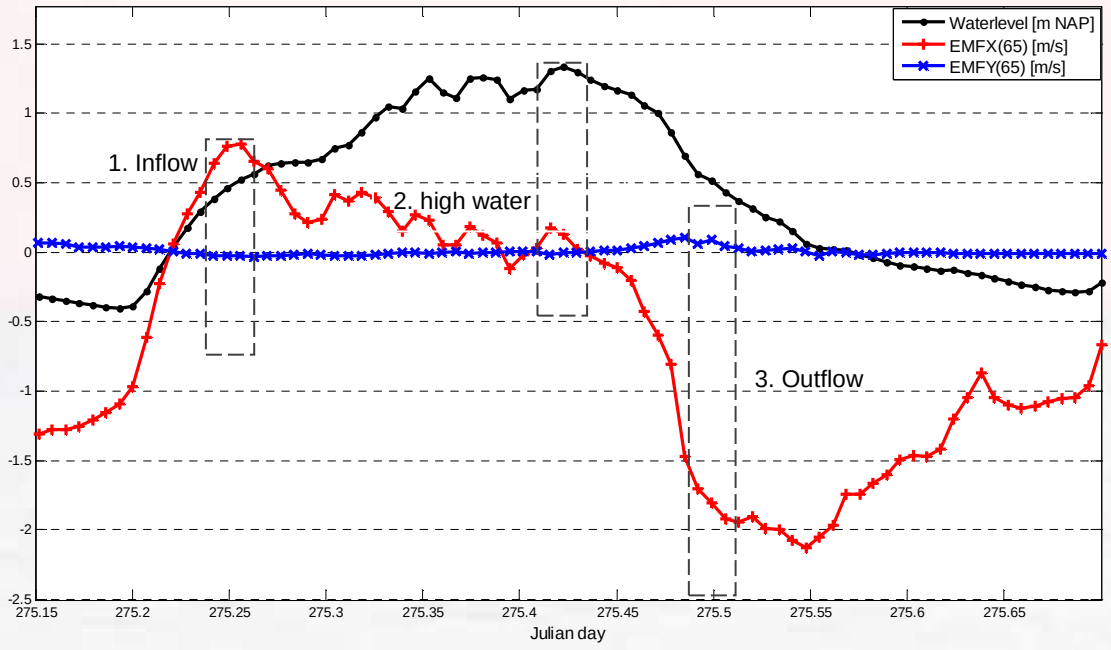

Figure 3-6 Water level and flows (in two directions) in the Slufters mouth during a flooding event at 1 October 2008 04:45-16:15

Wave dynamics

Wave dynamics in the main channel are derived from the vertical oscillating term of wave height, using least square technique. As can be seen in figure 3-13, wave heights clearly depend on the water level as maximum wave heights are found during HW stages. Consequently the lowest values are encountered around LW. During HW, when bottom friction is minimized, less seaward wave breaking occurs so that waves have a better change to develop. It is also assumed that winds have more influence on the water surface when water is not sheltered by the channel banks. Wave heights reach approximately 0.45 m during HW, simultaneously the significant wave height peaks to 0.31 m.

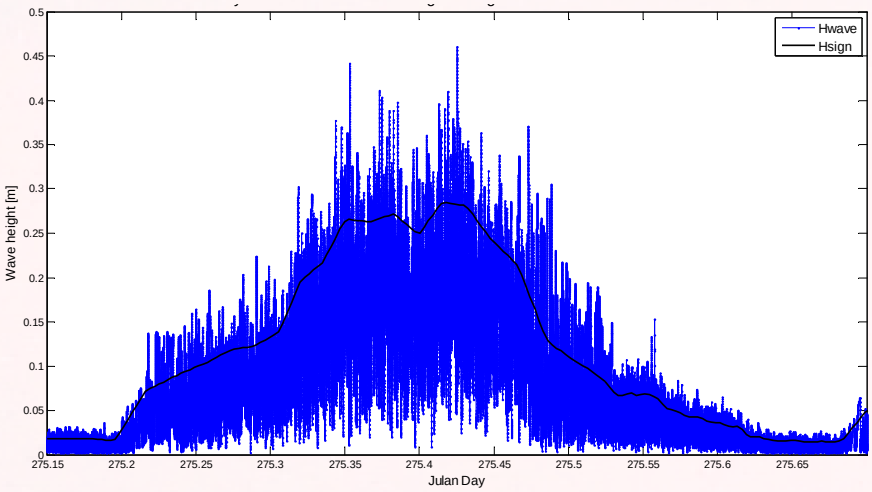

Figure 3-7 Wave dynamics in the main channel at 1 October 2008 04:45-16:15 derived from the vertical oscillating term of wave height using least square technique. Significant wave height (Hsign) given in black are computed for each 32 seconds.

To illustrate wave energy in the main channel during high energetic conditions, power spectral density plots are established (figure 7-6 in Appendix C). The plots indicate that wave energy in the main channel is very small and most likely has an insignificant effect on sediment transport processes. As is stated above, the largest waves are encountered during the high water stage. Since flows are weak during high water, sediment transports are therefore also small.

3.5.2 Hydrodynamics at the beach flat

The flows and water heights on the beach flat during several flooding events were analyzed by Klein Breteler (2009), who computed significant wave height and flow velocities in both cross- and longshore direction (fig 3-14). For optimal reliability a minimum water level of 0.2 m above the instruments is required, therefore only data is used in analysis for which $h_w > 0.2$. Flows, water levels and wave heights are most clearly visible in the first two flooding events.

Figure 3-14 shows mean flows decomposed into flows into the basin (U_{mean}) and parallel to the coast (V_{mean}). During the initial stage of the flooding, when water depths rapidly rise from 0.45 to 0.85 m, mean onshore velocities range between 0.5 - 0.6 m/s. After high water, velocities reverse into the offshore direction and reach magnitudes of 0.2 - 0.3 m/s. The along basin velocity remains positive (northern directed) ranging between 0.2-0.3 m/s. This coincides with a positive peak in the along basin

velocity (0.25 m/s) at d=275.95, indicating that part of the drainage of the system occurs from the beach flat to the main channel (Klein Breteler, 2009).
Inflow velocities across the beach are stronger than outflow velocities. The opposite applies for the main channel. Water exchange across the beach flat occurs on a much greater spatial scale than the size of the inlet. Therefore it is assumed that the majority of the water enters the Slufter across the beach but most of the water leaves the inlet through the mouth.

Both inflow and outflows are slightly directed toward the channel. Presumably the main flow direction is affected by the beaches topography. This leads to a continuous drainage from beach flat towards the main channel. This process correlates with the findings in the main channel. Flood flows are seemingly delayed due to a conservation of mass.

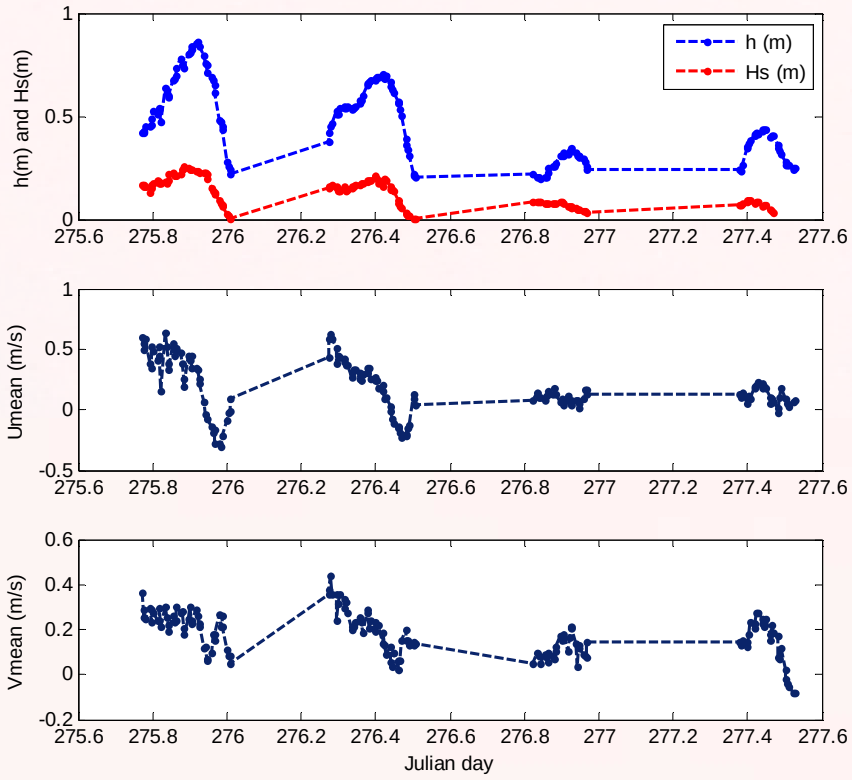

Figure 3-8 First period of the beach flat inundation; plotted are the water depth (h), the significant wave height and the cross-shore and long-shore velocity. The black dashed line denotes the h=0.2 m boundary. After Klein Breteler (2009).

3.6 Hydrodynamics during bed load transport measurements

Dune form measurements performed at 25,26 and 27 September 2008 have brought information on bed-load transport in the Slufters mouth. In this paragraph the hydraulic situation is sketched for the short time span when the bed form measurements were done. As can been seen in figure 3-15 the moments of leveling were separated by 2 tidal cycles. Daily tides basically consist of one low and one high tide. The period in which the development of dunes was followed can be characterized as neap

tide with increasing tidal amplitude over time towards spring tide. Flow velocities yield values ranging from 0 to approximately 0.5 m/s in both directions.

It is generally believed demonstrated that the third-power velocity moment is a good predictor for bed-load transport direction (van Rijn, 1994), which is therefore calculated and included in figure 3-15. Parts of data of the first flood event are missing and estimated amounts are added. Third-power velocities corresponding to the high tide situation are approximately a factor 8 to 10 higher compared to the low tide situation. Integrated third-power velocities of the ebb situations are approximately 2 to 3 factors larger (table 3-6), therefore a seaward directed net transport direction is expected.

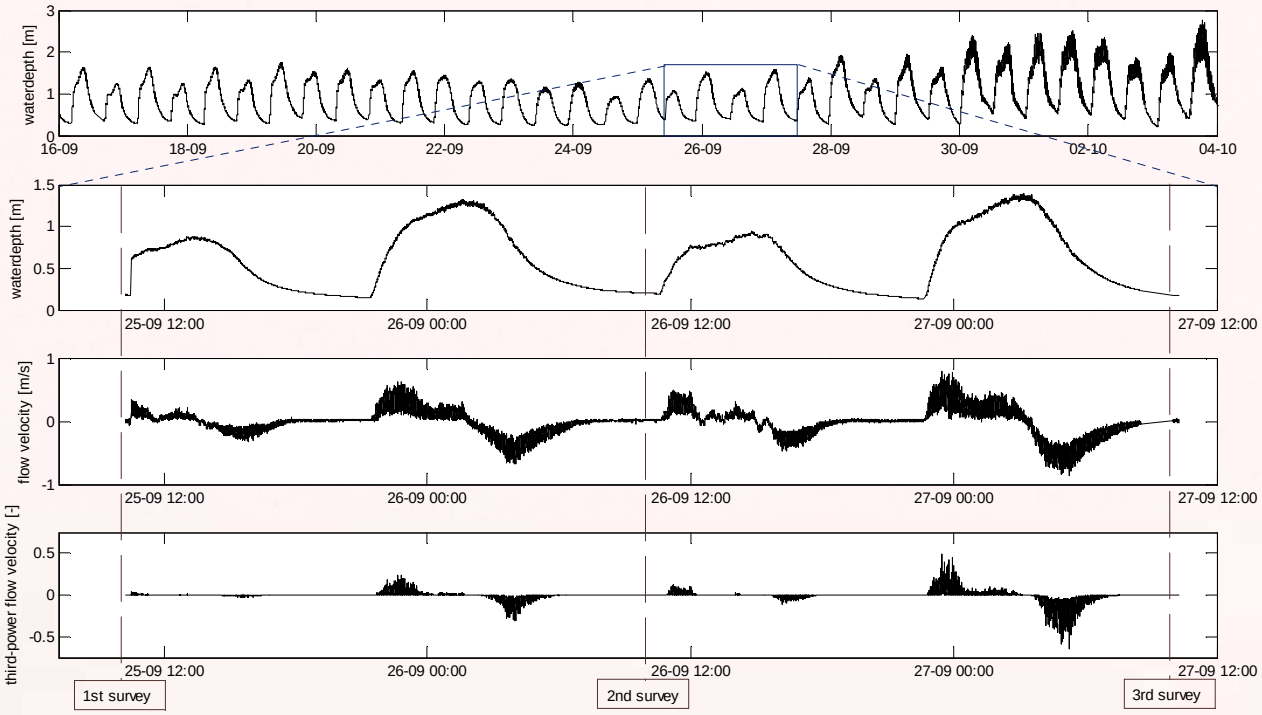

Figure 3-9 Hydraulic situation in the Slufters main channel during the period of dune measurements. **A)** Water level fluctuation over a large time scale, indicating that the survey period concerns the transition from neap to spring **B)** Water level fluctuation at the specific period. **C)** Flow velocity distribution based on EMF-25 cm **D**) Third power flow velocities based on EMF-25 cm. The brown dotted line correspond to moments of survey.

		Flood 1	**Ebb 1**	**Flood 2**	**Ebb 2**
25/09 - 26/09	U_{max} (m/s)	0,24	0,225	0,425	0,51
	$U^3_{integrated}$ (-)	106,39	126,86	891,75	1698,1
26/09 - 27/09	U_{max} (m/s)	0,270	0,277	0,421	0,562
	$U^3_{integrated}$ (-)	355,32	440,24	1892,6	4588,8

Table 3-6 Hydrodynamic characteristics for the bed-load measurement period in the Slufters main channel. Maximum flows are found for each stage, third power velocities are integrated over time.

3.7 Main conclusions concerning hydrodynamics

Based on flow measurements in the Slufters mouth and adjacent beach flat, water transport patterns during different tidal and energetic conditions are identified. Even though the clearness and reliability of these patterns, especially during flooding conditions, are debatable, an general impression concerning the hydrodynamics of the Slufter is given:

- The effect of tidal truncation emerges in a reduction of the tidal amplitudes inside the Slufter and a change in tidal asymmetry. The length of the ebb phase is extended by roughly 54 minutes. Truncation is caused by the relative high position of channels bed level in respect to the tidal wave.
- Flow magnitudes during neap tide are rather low (less than 0.5 m/s) and also the differences between flood and ebb are small. Maximum flood flows exceed maximum ebb flows ($U_{flood} > U_{ebb}$), resulting in a hydraulic flood dominance
- Spring tide velocities are much higher in comparison with neap tide (up to 1.2 m/s). Maximum ebb flows are larger than maximum flood flows ($U_{flood} < U_{ebb}$). The difference between maximum inflow and outflow velocities are also larger during spring tide in comparison with neap tidal conditions. This results in a hydraulic ebb dominance during spring tide,
- Maximum tidal flow asymmetry is related to the maximum water level (HW), rather than the differentiation between duration of the ebb and flood currents. From neap to spring tide the Slufters main channel shifts from flood-dominance to ebb-dominance generally at 0.64 m + NAP. Based on the Slufters basin hypsometry a Dronkers parameter is calculated for both spring and neap tidal conditions. The results show a similar trend as stated above.
- Under flooding conditions the maximum outflow velocities in the Slufters mouth exceed the maximum inflow velocities by far ($U_{flood} << U_{ebb}$). Maximum instantaneous outflow velocities measure 2.5 m/s. Also, the mean flows during the initial stage of tidal fall are slightly directed to the North.
- Wave energy in the main channel, even under high energetic conditions, is small.
- Landward mean flows across the beach flat measure up to 0.5 m/s. Presumably, the majority of water that enters the Slufter during flooding conditions travels over the beach, since this process occurs on a much greater spatial scale than the size of the inlet. Based on the high outflow velocities encountered in the main channel, it is assumed that the majority of the water leaves the Slufter through the mouth.
- Flows across the beach are slightly directed towards the channel.
- Changes in flow velocities are associated with strong differences in tidal exchange, which under normal conditions is restricted to the main channel but during storm and/or spring tide conditions is observed over the entire entrance over spit like platforms (here the platform is termed beach flat).

Figure 3-15 demonstrates an overview of inflow and outflow patterns during both non-flooding and flooding situations.

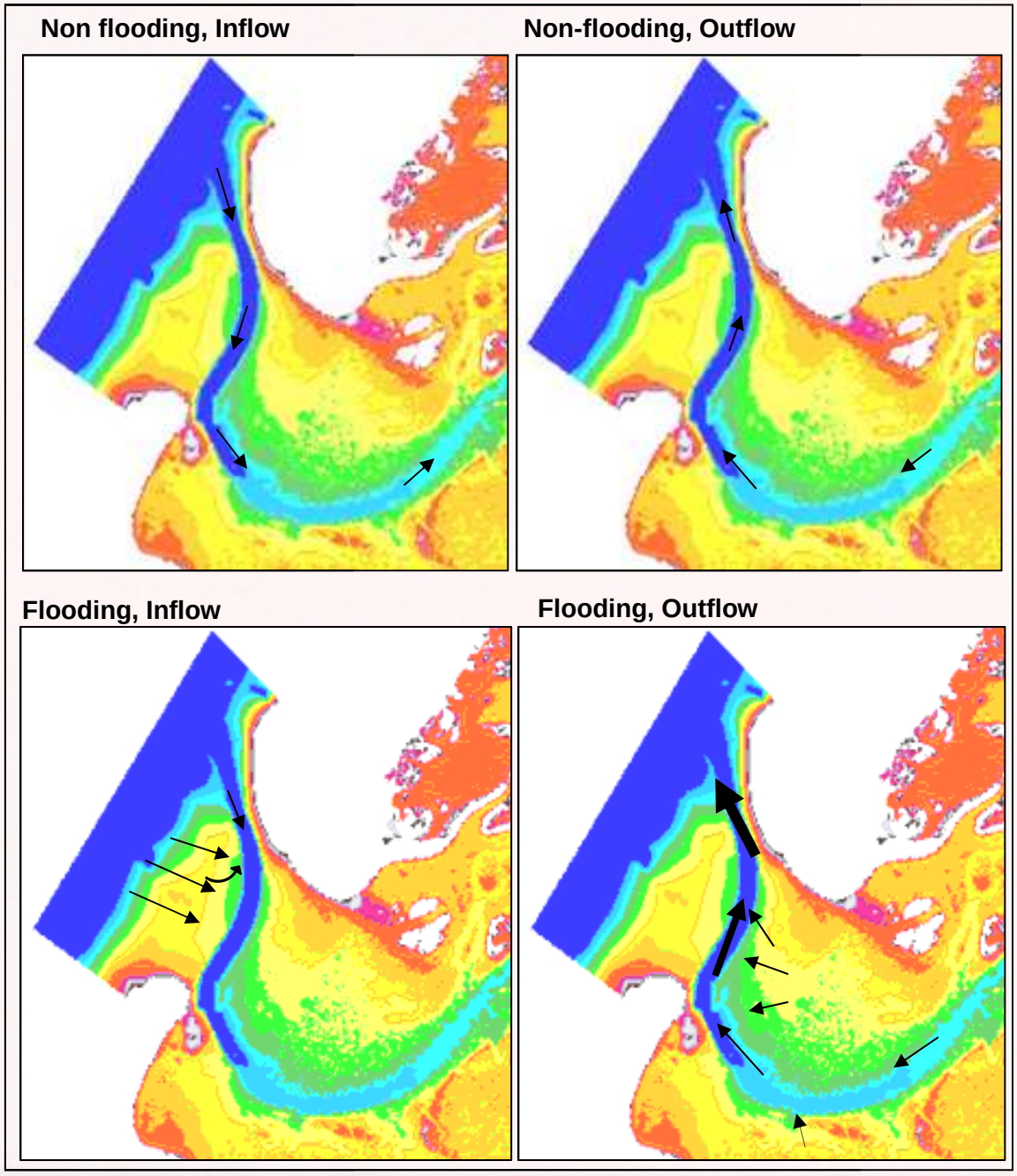

and flooding

4 SEDIMENT TRANSPORT RESULTS

4.1 Introduction

In this chapter the sediment transport in the Slufter will be analyzed. This will be done based on the water transport patterns as described in the previous chapter, sediment concentration measurements, dune migration measurements and Baillard transport models. As mentioned in paragraph 2.3, results depicted by the OBS-devices are uncertain. Consequently, it is difficult to perform a quantitative analysis based on the measurements. Therefore a more qualitative impression of the sediment transports is given.

Based on measured sediment concentrations and measured flow velocities, instantaneous sediment fluxes are calculated. Together with modeled sediment fluxes, based on Bailards transport model, the sediment fluxes act as indicators for net sediment transport in the main channel.

4.2 Sediment Characteristics

Sediment samples were collected at various measuring locations in the Slufter system. Sediment particle size distribution were used for OBS-calibration and applied in the sediment transport models. Sampling was done at October 13, 2008. Determination of grain size distribution is done at the FG-laboratory with selective sieving technique. Results are presented in table 4-1.

Sediments at the main frame location basically consists of well-sorted, fine to medium grained quartz sand with some marine-shell debris and gravel. After the storm drapes of clay/peat was found particularly in dune troughs, originating from eroded hinterland. These coating and drapes were less conspicuous prior to the semi-storm and water was much clearer.

Grain size	Main frame	Breaker zone	Beach flat (µm)	Upstream (µm)
d10	231	250	196	210
d50	275	390	275	231
d90	390	790	370	380

Table 4-1 D10, D50 and D90 grain size distribution at the Slufter system at October 13, 2008

4.3 Sediment Concentration

Sediment concentration as depicted from the OBS instruments between September 12 and September 14 2008 are shown in figure 4-1. Additionally, the tidal curve is added that indicates the water height above the pressure sensor. The results as displayed in figure 4-1 were measured during a neap tide period with low energetic conditions. The degree of inconsistency in the concentration signal is clearly noticeable, especially when the water heights in the main channel are low. During such condition less or no water stands above the instruments. In general, reliable data is found when water levels are substantial enough; at least 20 cm above each instrument. The SSC distribution shows that concentrations are relatively high considering the calm hydrodynamic environment in the main channel. Concentration decrease with height above the depth and correlates with the theoretical concentration profile. Furthermore SSC during the flood phase are seemingly higher compared to the ebb phase (between date 257.1 - 257.5).

High SSC during flood in comparison with ebb may be related to differences between the current fields during the ebb and flood phase. Another physical explanation may be the effect of suspended sediment advection by the tidal current. Sediments are more easily put into suspension in a higher energetic environment, for instance the wave breaker zone. Once sediment are in suspension they are transported by the tidal current (paragraph 1.2.3). It can be expected that flood current contain a larger amount of sediment in comparison with the ebb current. In figure 4-2 offshore significant wave height and suspended sediment concentration in the main channel over time are given. The offshore wave height distribution shows much resemblance with the SSC distribution. Increased offshore wave heights enhance sediment entrainment in the breaker zone resulting in higher sediment concentration. Sediments are transported by the tidal current leading to an increased sediment concentration in the main channel primarily for the flood phase. This effect is best seen for the highest OBS-sensor.

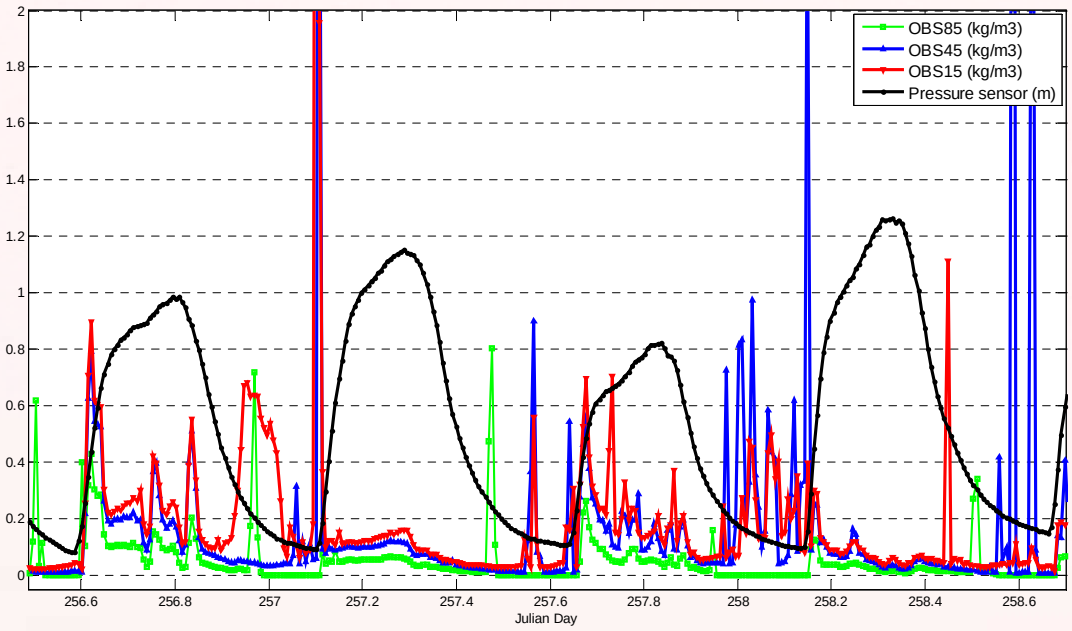

Figure 4-1 Time series of SSC in the main channel of the Slufter as depicted from OBS-15,45 and 85 in the period September 12-14 2008

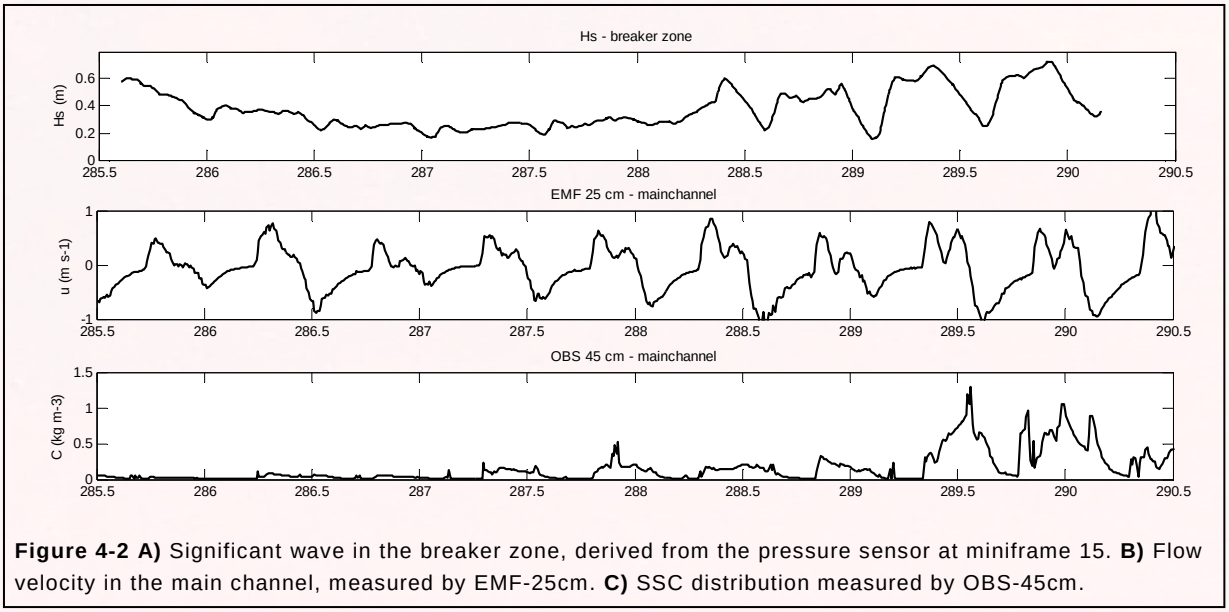

Figure 4-2 A) Significant wave in the breaker zone, derived from the pressure sensor at miniframe 15. **B)** Flow velocity in the main channel, measured by EMF-25cm. **C)** SSC distribution measured by OBS-45cm.

4.4 Suspended sediment transport for non flooding situations

For sediment transport analysis the same tidal cycles are used as described in the previous chapter. Theoretical sediment transport fluxes are computed with a model of Bailard (out of van Helvert, 2006). The Bailard model is a reliable and robust sediment transport model and is used in many coastal and/or nearshore zone applications (van Rijn, 1994). Bailard suspended transport formulation is expressed as follows:

$$q_s = \rho_s (f_c \varepsilon_s) / (g(s-1)w_s) \left| U_{inst} \right|^3 u \qquad [4\text{-}1]$$

Where q_s is the depth-integrated suspended transport (kg/ms), ρ_s is the absolute sediment density 2650 (kg/m^3), f_c is the friction factor (-), ε_s is a efficiency factor for suspended-load transport 0.01-0.02 (-) g is the acceleration of gravity 9.81 (m/s^2), s is the relative density (-), w_s the settling velocity (-), U_{inst} is the instantaneous current velocity (m/s) and u is the time-averaged velocity (m/s).

U_{inst} in the formulation is a velocity vector directly obtained from the EMF25-instrument. EMF25 has provided the most average and consistent results. For the time averaged velocity u, 5 minutes- and depth-averaged velocities are used. For low energetic conditions a current related friction factor f_c is determined for sediment transport computation. Its formulation is expressed as follows:

$$f_c = 0.24 \left(\log \left(\frac{12h}{k_{s,c}} \right) \right)^{-2} \qquad [4\text{-}2]$$

where h is the water depth and $k_{s,c}$ is the current related roughness height (3d90). The current related friction factor used in the calculation is given an averaged value for each 5 minutes. Table 4-2 shows the values of the parameters and factors used in the transport calculation.

d50 (μm)	d90 (μm)	s (-)	ε_s (-)	w_s (m/s)
275	390	2.65	0.01	0.05

Table 4-2 Used constants for suspended sediment transport calculations

4.4.1 Neap and Spring Tide

Figure 4-3 and 4-4 contain multiple graphs of hydrodynamic results along with computed and measured sediment fluxes for both neap and spring tidal situations. As is demonstrated in the previous chapter a slight hydraulic flood dominance is present during neap tide. This is expressed as small differences between flood and ebb currents. Since suspended sediment transport in the Bailard formulation (1981) is proportional to the flow velocity power 4, computed sediment fluxes during the flood phase are higher compared to the ebb phase (fig 4-3) and a net landward flux can be identified (table 4-3). As for the measured sediment fluxes, which are significantly larger (factor 40), this trend is even more pronounced. Both computed and measured sediment fluxes therefore indicate an import of sediment during neap tidal conditions.

In paragraph 3.4 it is demonstrated that when water levels reach higher elevations, during spring tidal conditions, the Slufter channel is hydraulic ebb dominant. Time series of computed sediment fluxes show a similar result (fig 4-4). Also, measured net sediment fluxes during the ebb phase are greater than net sediment fluxes during the flood phase. The fraction suspended sediment export for computed fluxes are much higher than the export fraction for measured fluxes. This indicates that modeled suspended transport results show a higher degree of ebb-dominance during spring tidal conditions than measured suspended transport results. This may be related to the higher sediment concentrations during inflow stage, which are more or less compensated by stronger measured outflow velocities. Nevertheless both computed and measured transport results indicate an export of suspended sediment during spring tidal conditions.

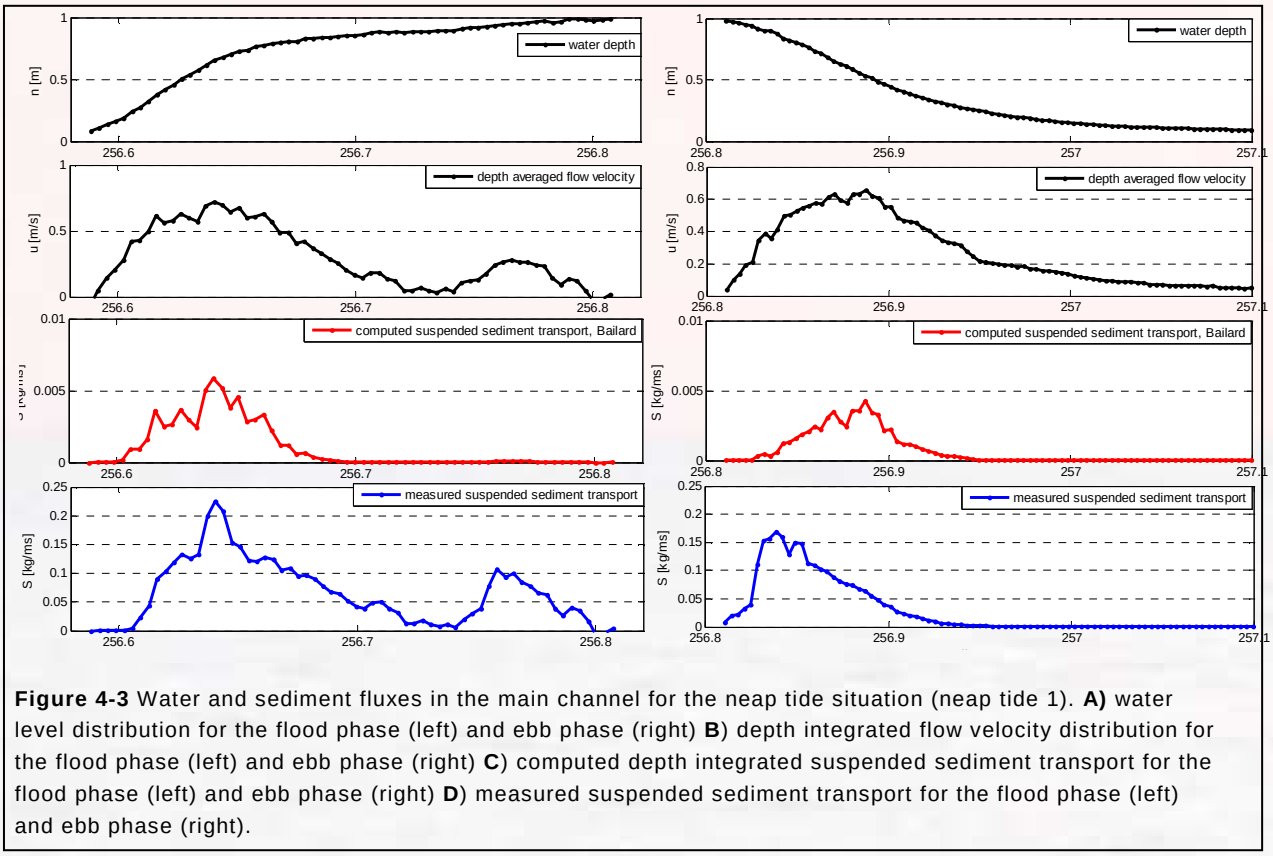

Figure 4-3 Water and sediment fluxes in the main channel for the neap tide situation (neap tide 1). **A)** water level distribution for the flood phase (left) and ebb phase (right) **B**) depth integrated flow velocity distribution for the flood phase (left) and ebb phase (right) **C**) computed depth integrated suspended sediment transport for the flood phase (left) and ebb phase (right) **D**) measured suspended sediment transport for the flood phase (left) and ebb phase (right).

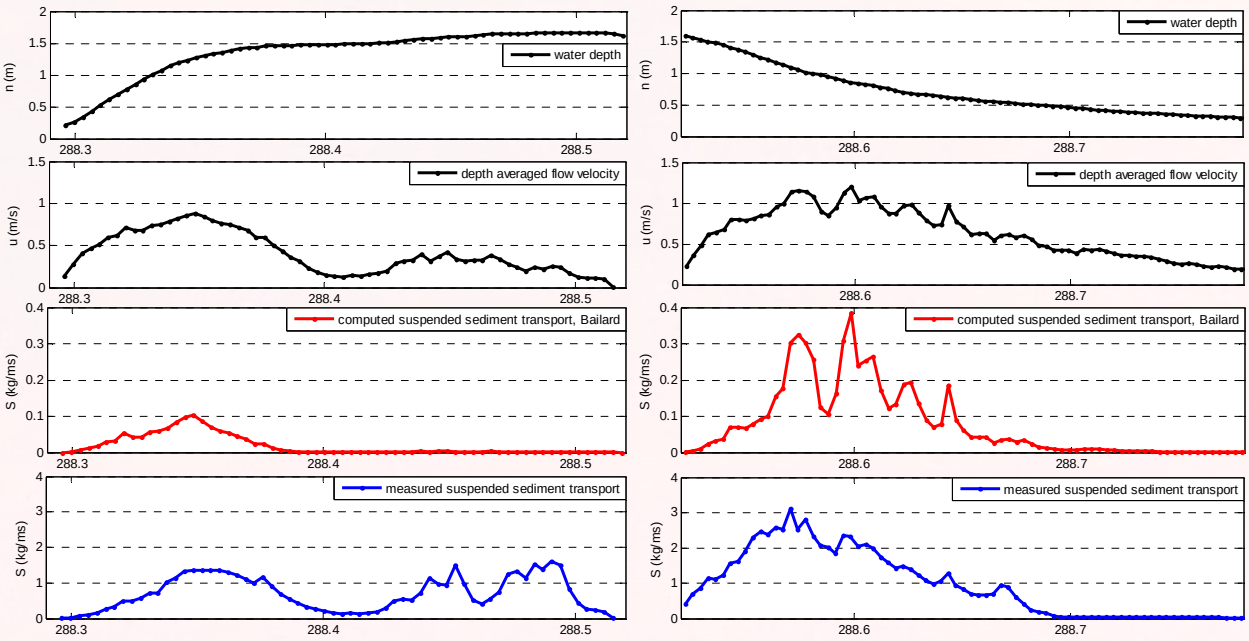

Figure 4-4 Water and sediment fluxes in the main channel for the spring tide situation (spring tide 1). **A)** water level distribution for the flood phase (left) and ebb phase (right) **B**) depth integrated flow velocity distribution for the flood phase (left) and ebb phase (right) **C**) computed depth integrated suspended sediment transport for the flood phase (left) and ebb phase (right) **D**) measured suspended sediment transport for the flood phase (left) and ebb phase (right).

Fraction of suspended sediment transport	Computed		Measured	
	Import	**Export**	**Import**	**Export**
Neap1	0,5203	0,4796	0,6244	0,3755
Neap2	0,6429	0,3570	0,6589	0,3410
Average	**0,5816**	**0,4139**	**0,6416**	**0,3583**
Spring1	0,1645	0,8354	0,3155	0,6844
Spring2	0,3403	0,6596	0,4535	0,5464
Average	**0,2524**	**0,7476**	**0,3845**	**0,6154**

Table 4-3 Fraction of calculated and measured import and export of suspended sediment transport through the main channel of the Slufter as a percentage of total suspended sediment transport during both neap and spring tidal conditions.

4.5 Suspended sediment transport for flooding situations

This paragraph will discuss suspended sediment transport both in the main channel and across the beach flat during flooding conditions. Chapter 3.5.3 demonstrated the presence of wave dynamics in the main channel during such an event. The effect of waves on suspended sediment transport is included in the sediment transport formulation (equation 4-3) by a friction coefficient for currents and waves following van Rijn (1993, out of Grasmeijer & van Rijn, 2002):

$$f_{cw} = \alpha f_c + (1-\alpha) f_w \qquad [4\text{-}3]$$

$$\alpha = \frac{v_{r,\delta}}{v_{r,\delta} + u_{w,\delta}} \qquad [4\text{-}4]$$

where f_{cw} is the friction coefficient for currents and waves, α is a weight factor , $v_{r,\delta}$ is the mean near-bed velocity at top of the wave boundary layer, f_c is the current-related friction factor (equation 4-2) and $u_{w,\delta}$ is the peak near-bed orbital velocity without mean current. $u_{w,\delta}$ is calculated with linear theory which is valid for small amplitude progressive waves in homogeneous fluid of a constant depth (Soulsby, 1997):

$$u_{w,\delta} = \frac{\pi H}{T \sinh(kh)} \qquad [4\text{-}5]$$

where H is significant wave height, T is significant wave period. *sinh* is the hyperbolic sine, k is the wave number and is obtained through iterative calculation and h is waterdepth. Values of T and H have been obtained using the wave orbital velocity spectrum. The wave-related friction factor is calculated according to Swart (1974):

$$f_w = \exp\left(-6 + 5.2\left(\frac{A}{k_{s,w}}\right)^{-0.19}\right) \qquad [4\text{-}6]$$

$$A = \frac{u_{w,\delta} T}{2\pi} \qquad [4\text{-}7]$$

$$k_{s,w} = D_{50} \qquad [4\text{-}8]$$

Where f_w is the wave-related friction factor, A is the semi-orbital excursion, T is the significant wave period and $k_{s,w}$ is the wave related roughness height which is equivalent to the medium grain size. Table 4-4 shows the values of the parameters and factors for the flooding cycle in the main channel at October 1, 2008 between 04:45-16:15 h.

T	H	$u_{w,\delta}$	D_{50}	f_w
3.04 (s)	0.13 (m)	0.14 (m/s)	0.275 (mm)	0.0099 (-)

Table 4-4 Used constants for suspended sediment transport calculations under flooding conditions

4.5.1 Suspended sediment transport in main channel

The time series of suspended sediment fluxes in the main channel during flooding conditions show that fluxes are significantly larger in comparison with sediment fluxes during low energetic, non-flooding conditions. Computed fluxes are calculated to be around 0.2 kg/m^2/s for the flood phase and nearly 10 kg/m^2/s for the ebb phase. Table 4-5 shows that 99.4% of the total calculated suspended sediment transport rate occurs during ebb. This significant difference between sediment import and export rate can be directly derived from difference between inflow and outflow velocities. Remarkable is the significant differences between measured and computed sediment fluxes, especially during the

flood phase. Here, the measured fluxes show much higher values compared to the modeled fluxes. Subsequently, the differences between fraction of sediment during ebb and flood are much smaller, 0.59 for ebb, 0.41 for flood (table 4-5). The much higher measured sediment import/export ratio is particularly due to much greater measured SSC during the flood phase. In general it can be concluded that the main channel during a flooding event is strongly ebb-dominant.

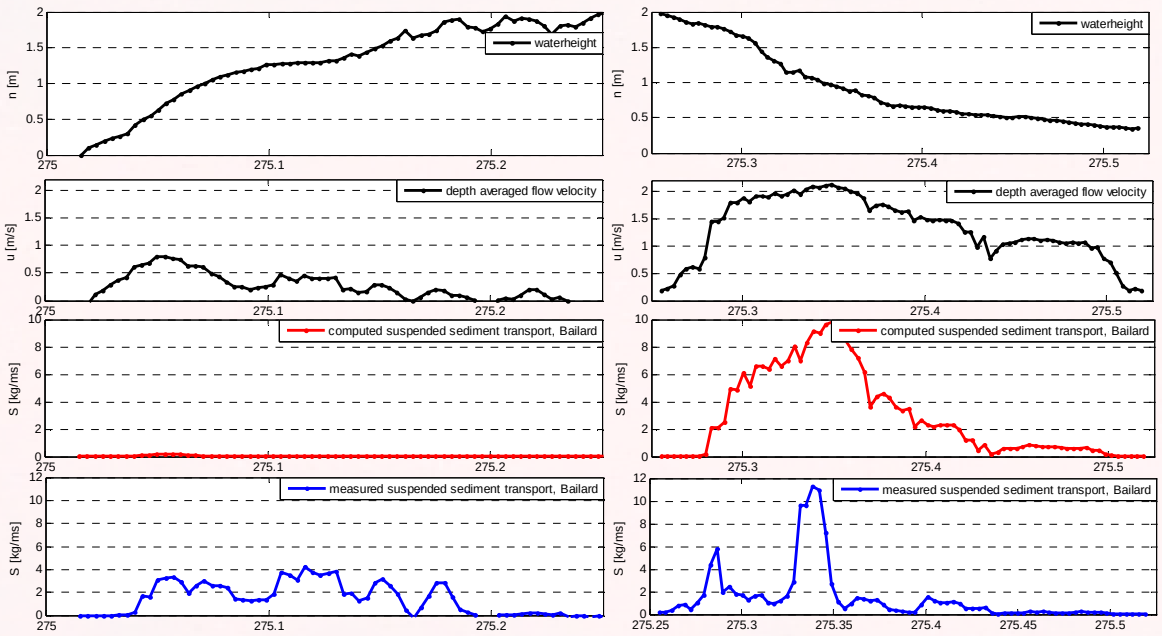

Figure 4-5 Water and sediment fluxes in the main channel for the storm situation. **A)** water level distribution for the flood phase (left) and ebb phase (right) **B**) depth integrated flow velocity distribution for the flood phase (left) and ebb phase (right) **C**) computed depth integrated suspended sediment transport for the flood phase (left) and ebb phase (right) **D**) measured suspended sediment transport for the flood phase (left) and ebb phase (right).

Fraction of suspended sediment transport	**Calculated**	**Measured**
Import	0.006	0.41
Export	0.994	0.59

Table 4-5 fraction of calculated and measured import and export of suspended sediment transport through the main channel of the Slufter as a percentage of total suspended sediment transport during the storm event at October 1 2008.

4.5.2 Suspended sediment transport at the beach flat

The time series of averaged sediment concentrations on the beach flat show that concentrations are large during the initial flooding and during ebb (figure 4-6). 5-Min averaged measured sediment fluxes at the beach flat are calculated to 0.6 kg/m^2/s and 0.3 kg/m^2/s for the upper sensor (Klein Breteler, 2009). During the major part of the inundation, cross-shore mean fluxes are positive and thus directed into the basin. Mean current fluxes contribute most strongly to sediment import into the system, rather than wave oscillatory velocity.

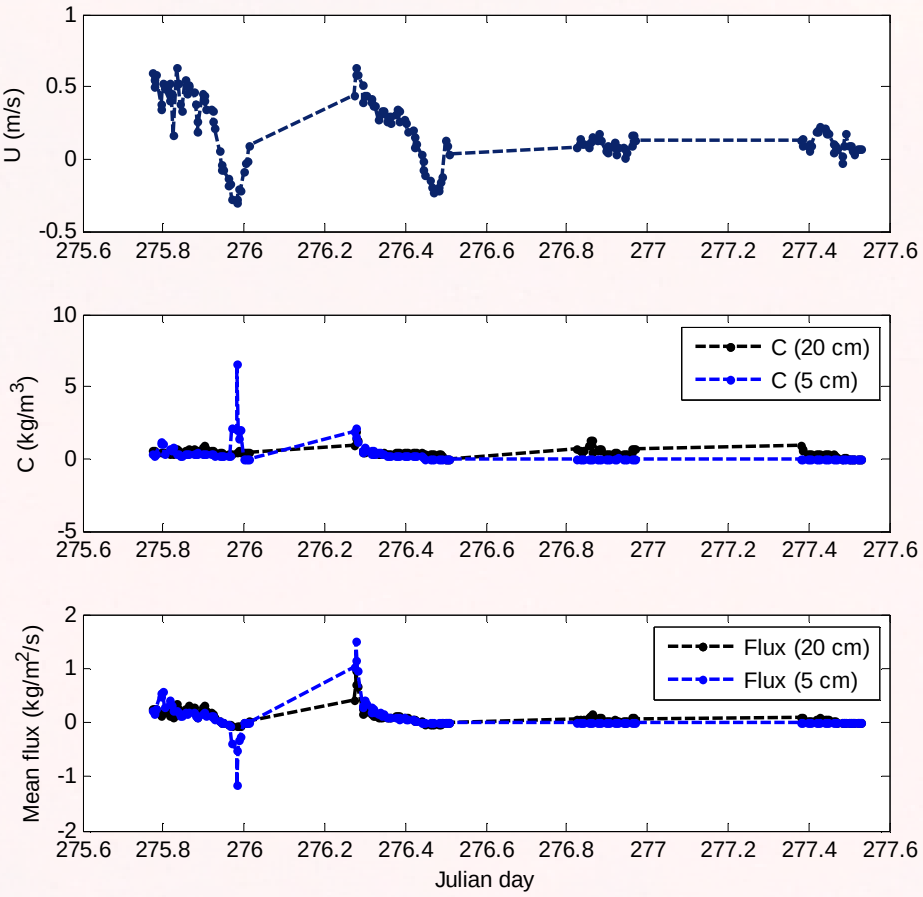

Figure 4-6 Cross-shore mean velocities over the beach flat and measured concentrations to obtain the mean fluxes during the flooding events. After Klein Breteler (2009).

4.6 Bed load transport

4.6.1 Measured results

The temporal and spatial developments of bed-forms in the Slufters main channel are displayed in figure 4-7. From top to bottom the profiles respectively represent the most northward line of measurements to the most southern line, separated by roughly 3 meters.

Generally the common trend of all profiles is a steady offshore migration (figure 4-7). It can be demonstrated that the most distinct dunes are present in the centre of the channel, whereas the most sideward dunes are more difficult to interpret due to their irregular shape. Consequently, analysis is done on the centre three longitudinal profiles. In each profile (36 meter in length) four dunes are clearly noticeable. A lateral variation of dune form is visible when comparing the relative positions of the dunes tops. This indicates that the dune tops follow a point shaped line, where the middle dune top is situated at the most seaward end (clearly visible in picture 4-1). Furthermore, at the most seaward end of the profiles, bottom level decreases dramatically, indicating the position of the measuring main frame and its scour hole. Also, just at the landward side of the scour hole the bottom level is somewhat higher indicating on accumulation of sand. From a visual perspective this is displayed as in photograph 4-1. Parts of the dunes summits in front of the mainframe even stand clear of the water,

whereas level of the bottom drops rapidly in seaward direction. This accumulation of sand is induced by the presence of the mainframe and is therefore excluded from analysis.

Picture 4-1 Dune formations in the Slufters main channel. **A)** Lateral distribution of dune crest following a point shaped line, picture was taken on September 25, 2008 at 11:02**. B)** Sharp transition of bed level near the measuring frame.

Height of the dunes in the middle dune profile range from 0.146 – 0.219 meter (table 4-6). The dunes length range from 5.09 to 9.08 m both spatially and temporally. A temporal change of the dunes' shape is recognized. Out of figure 4-7 and table 4-6 an increase in both the height and length of the dunes can be observed. This implies that the dimensions of the dunes grow over time.

Bed-load transport is calculated based on dune migration (table 4-6) using dunetracking software DT2D. The two most seaward dunes are not included due to their unreliable volumes, indirectly as a consequence of the presence of the measuring frame. On the other hand, the most landward dune is not detected by DT2D, consequently three dunes remain for bed-load transport calculations. Transport rates vary from 0.045 to 0.105 $m^2 day^{-1}$. Since one of the three dunes have shown a temporal decrease in transport rate (dune 1, table 4-6) the temporal and spatial variation of transport rate is not consistent. Nevertheless on average, one can argue that bed-load transport rates increase over time, thereupon transport rates can be related to the hydraulic conditions.

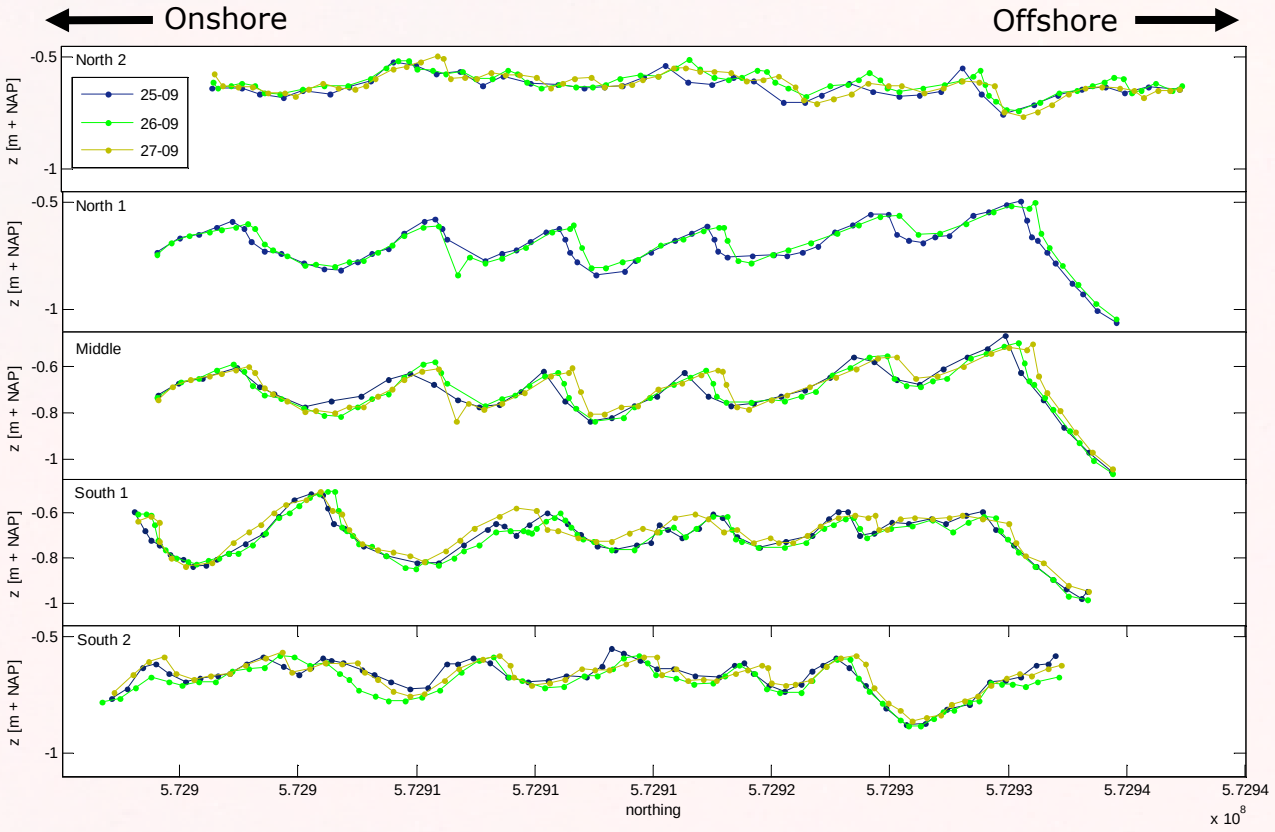

Figure 4-7 Temporal and spatial change of dune forms in the main channel of the Slufters. Measurements were done at successive 3 days at fixed lines (36 meter in length), respectively 25, 26 and 27 September, 2008. From top to bottom the profiles respectively correspond to the most northern measuring to the most southern line separated by approximately 3 meters. Data from profile north-1 of 27 September is missing.

Dune nr.	Date	Length [m]	Height [m]	Volume [m^2m]	c [m^2/day]	F-factor [-]	qb [m^2mday^{-1}]
1	*25-sep*	8.075	0.146	0.517	-	0.877	**-**
1	*26-sep*	6.635	0.205	0.641	1.068	0.943	**0.088**
1	*27-sep*	5.954	0.219	0.654	0.425	1.003	**0.045**
2	*25-sep*	5.100	0.193	0.401	-	0.815	**-**
2	*26-sep*	5.097	0.190	0.436	0.625	0.900	**0.054**
2	*27-sep*	6.103	0.203	0.648	1.018	1.046	**0.105**
3	*25-sep*	6.531	0.167	0.395	-	0.724	**-**
3	*26-sep*	6.169	0.154	0.398	0.942	0.838	**0.063**
3	*27-sep*	7.455	0.172	0.552	0.952	0.861	**0.067**

Table 4-6. Net daily specific bed load transport q_b (m^2/day) for three separate dunes between 25, 26 and 27 September, 2008, including dune length (m), height (m), volume (m^3) and migration rates c (m^2/day).

4.6.2 Modeled results

Measured bed load transport results are compared with the model of Bailard for bed-load transport, which is similar to the model for suspended load transport (equation 4-1):

$$q_b = \rho_s (c_f \varepsilon_b) / (g(s-1)\tan\varphi) \left| U_{inst} \right|^2 u \qquad [4\text{-}9]$$

Where q_b is the depth-integrated bed-load transport (kg/ms), ε_b is a efficiency factor for bed-load transport (0.1-0.2) and $tan\varphi$ is a dynamic friction coefficient (-). For ε_b a constant value 0.1 is attained, for $tan\varphi$ a value of 0.6.

In table 4-7 the calculate- and measured net daily bed-load transport rates are given in $m^2 mday^{-1}$. In general the results of the transport model are smaller than the measured results, however both results show much resemblance especially for the second day (-0.0596 against -0.072).

	Calculated net daily bed-load transport ($m^2 mday^{-1}$)	Measured net daily bed-load transport ($m^2 mday^{-1}$)
25/09 – 26/09	0.0147	0.0583
26/09 – 27/09	0.0596	0.072

Table 4-7 Calculated and measured net daily bed load transport in the Slufter main channel for two successive days. All transport results are seaward directed.

4.6.3 Calculated bed load- and suspended load transport

Based on the transport model of Bailard, suspended- and bed-load transport calculations have been performed for different tidal and storm conditions. During storm conditions the fraction of suspended sediment transport as a percentage of total transport has become larger than the bed load transport fraction. As is explained in paragraph 1.2.3 suspended load- and bed load transport is proportional to respectively flow power 3 and 4. This implies that as flow velocity increases the percentage suspended load transport of total transport also increases.

Suspended- and bed-load transport haven been calculated for intermediate tidal and storm conditions (figure 4-8 and 4-9) using sediment transport calculations of Bailard (equation 4-1 and 4-9). From figure 4-8 and table 4-8 becomes clear that modeled bed load transport fluxes are significantly higher than modeled suspended sediment fluxes. This indicates that tide-induced sediment transport in the Slufter channel predominantly occurs as bed load sediment. During storms however, the suspended transport mode has become dominant (67.2 %)

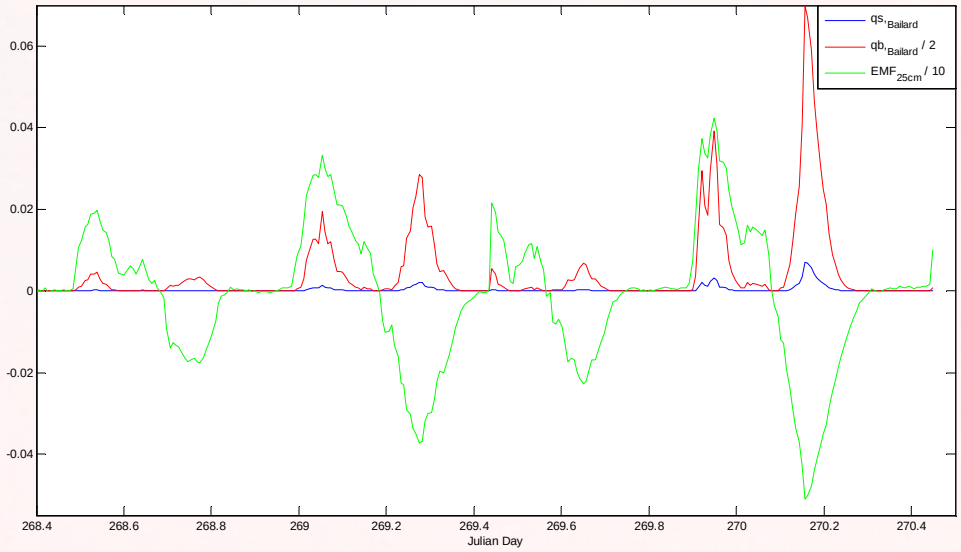

Figure 4-8. Calculated bed-load and suspended sediment transport distribution for intermediate tidal conditions, using Bailard's transport models.

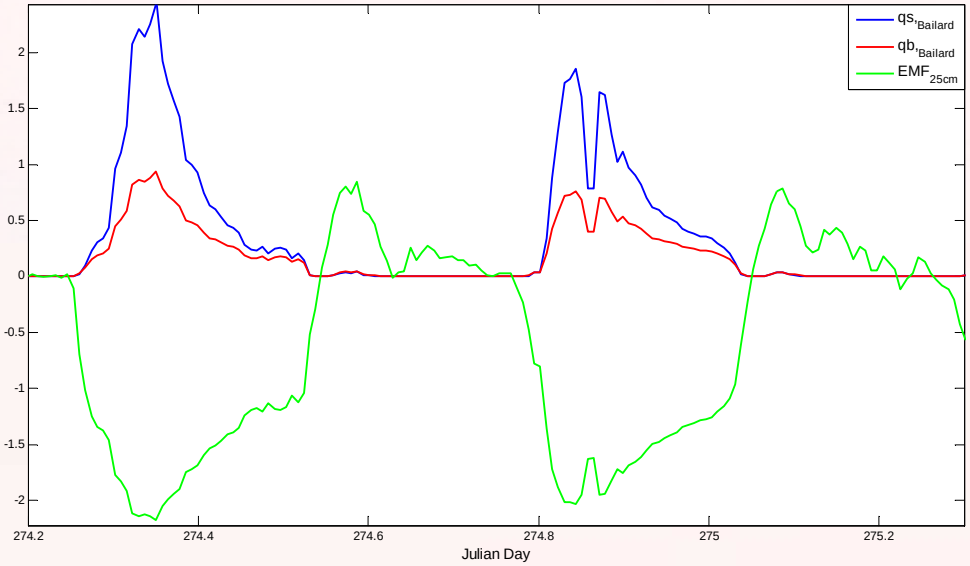

Figure 4-9 Calculated bed-load and suspended sediment transport distribution for storm conditions, using Bailard's transport models.

Fraction of calculated sediment transport	Bed load	Suspended load
Neap tide	71.2	28.8
Spring tide	57.2	42.5
Storm	32.6	67.4

Table 4-8 fraction of calculated sediment transport mode for neap tride, spring tide and storm based on Bailard transport models.

4.7 Main conclusions concerning sediment transport

Based on sediment concentration measurements and flow measurement in the Slufters mouth and adjacent beach flat, sediment transport patterns during different tidal and energetic conditions are identified. Subsequently these results were compared with transport models of Bailard (1981). Summarized, concerning the overall sediment transport under different conditions, the following impression is obtained:

- During the flood phase, the sediment concentration in the Slufters main channel is slightly higher than during the ebb phase. This may be related to the advection of sediment.
- For non-flooding conditions, a net input of fine sediment through the channel seems to occur under neap tidal conditions. Measured fluxes are hereby larger than the modeled fluxes. For spring tidal conditions, a net output of fine sediments is found where modeled fluxes show more resemblance with measured fluxed in comparison with the neap tidal situation.
- During flooding conditions, the main channel of the Slufter is strongly ebb-dominant. According to Bailiards transport model 99.4% of the total calculated suspended sediment transport rate occurs during ebb. Measured sediment fluxes for the flood phase are much higher compared to the calculated fluxes. According to the measurement 59% of the total measured suspended sediment transport rate occurs during ebb.
- The dominant transport direction of fine sediments across the beach flat mainly occurs is landwards.
- Bed load transport in the main channel of the Slufter occurs in seaward direction and correlates reasonable well with the results of Bailards bed-load transport model.
- According to Bailard’s transport models, the fraction calculated bed-load transport as function of total transport is the largest during neap tidal conditions, whereas during the storm conditions the suspended sediment is the dominant transport mode.

5 Discussion and Conclusion

The Slufter is a small tidal inlet influenced by an interaction of wave- and tide-generated processes that produces a complex of wave-dominated, mixed-energy and tide-dominated elements. The nearshore zone, as is studied by Klein Breteler (2009) is typically a wave-dominated element, whereas hydrodynamics in the main channel of the Slufter, are primarily tidal driven and therefore tide-dominated. Under calm weather conditions the main channel of the Slufter acts as a conduit for water and sediment to the intertidal salt marshes in the basin of the inlet. Under flooding conditions (HW > 1.1 m + N.A.P.), mixed energy elements are present and water and sediment exchange occurs on a much larger spatial scale.

This chapter will discuss the results of this research. It starts with the hydrodynamic results as subject for debate. Next, sediment transport results are discussed. Also morphology, stability of the Slufter and the reliability of the measurements are debated. This chapter concludes with answers to the specific (main) research questions. .

5.1 Hydrodynamics

Based on the results in chapter 3, one can state that there is a significant discrepancy between the vertical and horizontal tide in the Slufters main channel. This effect grows with increasing tidal amplitude. Under calm conditions, neap tidal flows are slightly flood dominant, whereas spring tidal currents show a higher degree of ebb dominance. During high energetic flooding conditions the main channel of the Slufter becomes strongly ebb dominant. In this research it is believed that this effect is caused by the Slufters basin hypsometry.

Basin hypsometry

Due to the relative small dimensions of the Slufter basin it is assumed that tidal wave distortion as a result of bottom friction is negligible. Also the differentiation of ebb and flood phase duration does not lead to the flow asymmetry one would expect. Flow asymmetry seems to be generated by the geometry of the Slufter. Asymmetry generated by tidal interaction with inlet channel geometry is studied by numerous authors. Boon and Byrne (1981) and Fitzgerald and Nummedal (1983) have suggested that an inlet where basin water surface area increases with tide stage moves in the direction of hydraulic ebb-dominance. DiLorenzo (1988) confirms this, based on interpretation of a nonlinear expansion of the momentum equation. Seelig and Sorenson (1978), utilizing both linear and exponential bay water surface area variation with tidal elevation in numerical model simulations and found that increasing basin water surface area with tidal elevation moves the inlet system toward ebb dominance.

Van Puijvelde (2010) already demonstrated a hypsometric curve of the Slufter indicating that the total water surface in the Slufters basin significantly increases with water elevation. Since nearly 50% of the surface are of the Slufter is elevated between 1.1 m and 1.5 m + N.A.P, this strongly affects flow

characteristics when water levels reach this window. The hypsometry of the Slufters basin determines the inundation and subsequent emergence of the intertidal flats. Inundation of the intertidal flats retards the flood phase, which lead to increasing flood duration and decreasing ebb duration. This leads to higher peak ebb velocities compared to peak flood velocities.

Reneerkens (2003) also states that the waterlevel in the Slufter is the boundary condition that determine hydraulic and sediment transport processes in the entire Slufter basin. Reneerkens suggests that reversal from flood- to ebb dominance in the Slufter is at 0.9 m + NAP, whereas results in 3.4.3 indicate a flood/ebb dominance reversal at ca. 0.64 m + NAP. This difference may be attributed due to errors or differences in measurements or due to differences in morphology between fieldwork 2003 and 2008. Also, the unit used to indicate flood/ebb dominance in the thesis of Reneerkens is peculiar (m^2/s^2).

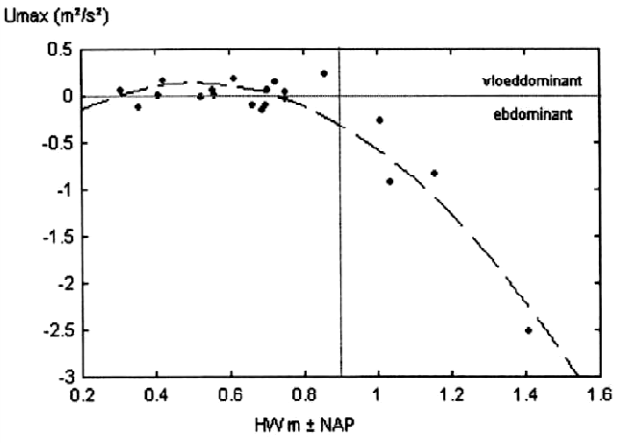

Figure 5-1 Asymmetry of the maximum flow velocity in respect to HW, threshold value is set on 0.9 m + NAP (Reneerkens, 2003).

Storm

Storm surges add an extra rise of water above the normal tide. During such conditions flooding of a significant larger area of the basin occurs, particularly when the surge coincides with a spring tide. The hydrodynamic budgets in the Slufter are particularly difficult to formulate because the paths for water movement are complex and neither well known or directly measurable. Based on measurements performed at two locations it is suggested that water moves in circular motion. During the first stage from LW to HW, the majority of the total water amount during high water slack has traveled across the beach flat. Thereby a clear flow component towards the main channel is visible. This announces the presence of a residual circular flow pattern inside the Slufter system. Inlet circulation is governed by tide range, bay geometry, inlet geometry, bottom topography, and nontidal forcing, such as wind and river inflow (Millitello and Hughes, 2000). The secondary flow in the Slufter is probably caused by the topography of the beach flat. Isolated residual eddies usually emerge at both landward- and seaward side of the inlet and dominate the current field near the inlet (Millitello and Hughes, 2000). Unfortunately no data is measured at the seaward side of the inlet, leaving this assumption unconfirmed.

The influence of waves, particularly on sediment import/export processes in the Slufter, is restricted to the offshore zone and strongly depends on surge levels. The effect of (infragravity) waves on sediment fluxes in the main channel is very small ($Q_{currents} >> Q_{waves}$). However, waves breaking in the nearshore zone in proximity of the Slufters mouth enhance sediment entrainment. This leads to higher SSC, which may enhance advective sediment transport through the Slufters channel.

5.2 Sediment Transport

It is difficult to correlate sediment transport results in the Slufter to results of other studies, due to the unique morphological characteristics of the Slufter. Fieldworks in slufterlike areas were done in "de Verdronken Zwarte Polder" and "'t Zwin". Van Helvert (2006) did not use OBS-results because measured concentrations did not show relation with bed shear stress. Beijk (2002) found SSC in 't Zwin ranging between 0-3 g/L under spring tidal conditions (u_{max} ~ 1.6 m/s). Measured concentrations also showed much spikes but generally results are quite similar to OBS-results in the Slufter.

Bailard transport results show an distinctive export of sediment, particular during storm conditions. As described in paragraph 1.2.3. time flow asymmetry, lag-effects, advection and aeolian transport have not been taken into account in the Bailard transport models. These other sediment transport mechanisms may contribute significantly to the net sediment budget of the Slufter and are further discussed.

Time flow asymmetry

Dronkers (1986) showed that if the rate of change of tidal velocity is slower at the high water slack this will provide better opportunities for fine sediments to settle down than during more rapid flow reversal at low water. In this case more suspended sediment will be deposited on the upper mudflats at high water than on the lower mudflats at low water and an import of fine sediment is favored. However it is demonstrated in chapter 3, that truncation leads to increased ebb duration and a rapid increase of flow velocity during the flood phase when the truncation sill is overtopped. According to the time-flow series (fig 3-5, 3-7, 7-1 and 7-2), during the neap-spring cycle generally stronger currents are measured during slack before ebb (SBE) than during slack before flood (SBF) suggesting that the time-flow asymmetry is ebb-dominant.

However van Puijvelde (2010) has demonstrated that tidal interaction with basin hypsometry lead to a retarded flood phase especially when water levels exceed 1.1 m + N.A.P. During spring tidal conditions and storm conditions, the ebb phase is still longer than the flood phase but differences are minimal. Figure 5-1 demonstrates the flow velocity distribution over a number of tidal cycles during the storm condition. The flow acceleration during SBF seems to be larger than during SBF. This indicates a net landward directed suspended sediment transport during storm conditions.

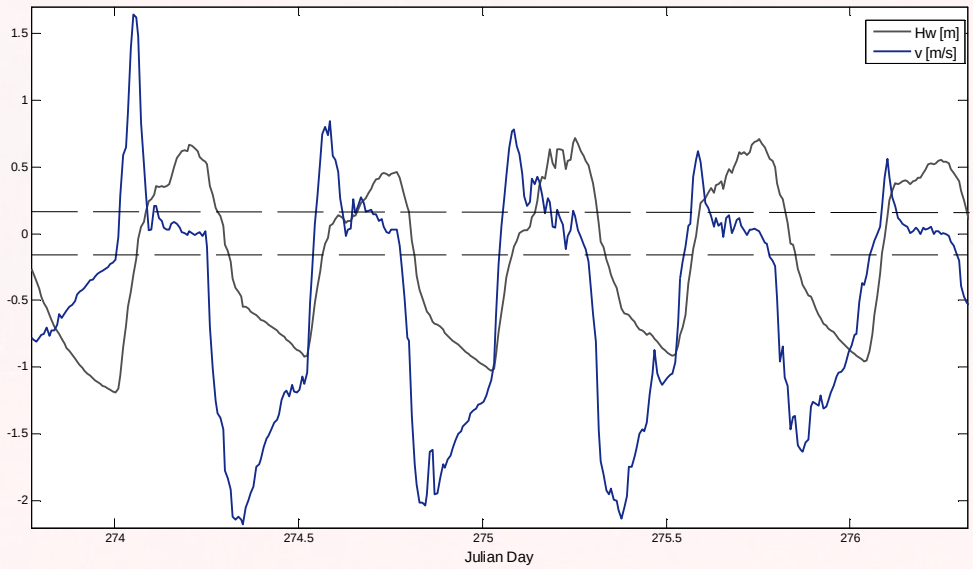

Figure 5-2 Measured velocities in the main channel of the Slufter during storm conditions.

Lag effects and advection

The simple Bailard suspended transport model used for this research has limitations. The model of Bailard only takes local processes into account without taking the critical bed shear stress into account. Also, the importance of lag-effects and residual advective sediment transport are ignored..Time lag effects occur simultaneously and are difficult to separate. Schuttelaars & de Swart (1996) demonstrated an equation which expressed dimension suspended sediment transport by including the effect of spatial lag effect. They created a model which was capable of simulating increased transport in the direction of decreasing depth, since particles in shallow waters settle down in a higher rate (Swart and Zimmerman, 2009). However, this method excluded the effect of the flow asymmetry on residual sediment transport. The relative importance of lag effects and flow asymmetry on residual transport of suspended sediment is studied by Hoitink et al. (2003), who proposed a numerical based model including appropriate parameterizations to account for lag effects. It was found that the asymmetry in flow maxima was capable of forcing a residual transport of suspended load approximately 5 times larger than that caused by a lag effect in symmetrical flow (Hoitink et al., 2003). The contribution of asymmetry in flow maxima on residual transport is more important, but the effect of lag effect is clearly significant.

Also, as is described in paragraph 1.2.3 and demonstrated in paragraph 4.2, advection may play an important role for residual suspended sediment transport. Pritchard (2005) created in a semi-analytical approach for SSC and residual sediment transport in a simple mathematical model of short tidal embayment. Main conclusions were that advective transport is crucial to investigating the variation of SSC in these embayments.

Both lag-effects and advection are favorable for sediment import of fine sediments (paragraph 1.2.3), but ignored in the Bailard sediment transport predictor. Generally, modeling sediment budgets for inlets is found to be extremely difficult since the paths for sediment movement are complex and

neither well known not directly measurable (Pacheco et al., 2007). Therefore, extra care should be taken to inspect the best applicable model for future researches on net sediment transport patterns in the Slufter.

Aeolian transport

In this research another sediment transport mechanism has not been taking into account. From visual observation, particularly during storm periods, aeolian transport was clearly noticeable. Varying winds speeds up to 20 m/s have brought vast amounts of sand into motion resulting in the development of numerous small parabolic dunes on the Slufters sandy shoals. Comprehension of aeolian transport across beaches is however complex and governed by the interaction of beach geometry, surface conditions and wind field (Bauer et al., 2009). Bauer et al. measured aeolian transport at a sandy beach on Prince Edward Island in Canada which is quite similar to the beaches at the Slufter. In this fieldwork wind speeds varied between 2-20 m/s, resulting in transport rate of up to 1.5 g/sec per meter. At normal windy days rates were approximately 0.7 g/s per meter. Considering the dominant wind direction (southwest) at the Wadden barrier islands and the orientation of the Slufter coast one can expect that aeolian transport lead to a dry import of sediment in the Slufter.

5.3 Morphology and Stability

Tidally driven ebb dominance lead to a net sediment transport towards the mouth of the Slufter. Durieux (2005) states that neap-spring averaged tidally driven ebb dominance will tend to enhance the development of a ebb shoal. In van Puijvelde (2010) the presence of a morphological threshold was demonstrated, seaward from the measuring instruments in the main channel. According to 1-D SOBEK modeling it is expected that, when conditions no not change, the inlet will eventually close.

However, the effect of frequent basin wide flooding events probably interrupts this trend. During a storm, when a great part of the Slufter basin is inundated, flow velocities in the inlet are much higher compared to low energetic tidal driven flows. The strong ebb directed currents subsequently breach a way to sea at the expense of the ebb shoal development. This process seems to play an important role in the assessment of the Slufters stability. For further information on the stability of the Slufter a referral is made to van Puijvelde (2010).

5.4 Reliability and validity measurements and analysis

Measured SSC as depicted by the OBS-sensors have shown a high degree of inconsistencies. This does not mean that OBS instruments did not function properly, but can be caused by physically; turbulence or background concentrations of fine suspended matter can disturb the signal. Puleo et al. (2006) performed a study on the effect of air bubbles on the output voltage from optical backscatter sensors (OBS). Results show voltages increase caused by bubbles in the presence of sediment particles to be in order of 25%. Another deviation is the calibration of the OBS instruments. Calibration is done on one bulk sample of sediment from one location. The variability of the particle sizes in time and space is not taken into account in the calibration.

5.5 Conclusions

What is the influence of tides on the import and export patterns in the Slufters main channel?

During non-flooding conditions (HW < 1.1 m + N.A.P.), tides are the fundamental transport mechanisms for water and sediment, inducing inflow and outflow of seawater at the Slufter twice daily in response to a semi-diurnal regime. During neap tide, both computed and measured sediment fluxes indicate an import of sediment. The flood dominance is a direct result of tidal asymmetry, which emerges in longer ebb durations resulting in higher maximum landward directed flow velocities. During spring tide, tidal interaction with the Slufters' basin hypsometry enhances flow asymmetry which becomes ebb dominant. The ebb dominance is not caused by the tidal asymmetry. Measured and calculated sediment fluxes clearly indicate an export of sediment during spring tidal conditions.
During flooding conditions (HW > 1.1 m + N.A.P), inundation of the basin occurs on a much greater scale. During these conditions transport patterns of water and sediments are more determined by the basin hypsometry / morphology of the Slufter, rather than tides or tidal asymmetry.

Does the tidal current field contribute to a net, tidally-averaged, transport of sediments in or out of the tidal inlet: what is the contribution of tidal asymmetries

Measurement and calculations indicate that the current field in the Slufter contributes to a net tidally averaged export of sediment transport. The specific contribution of tidal asymmetry when referred to as vertical tide, is however small. According to duration asymmetry one would expect flood dominance. The basin hypsometry seems to govern the current field as the discrepancy between horizontal and vertical tidal asymmetry grows with tidal elevation. As a result, flow asymmetry moves the Slufter towards ebb-dominance.

What is the (quantitative) role of storm events for the import/export of sediment in the main tidal channel? What is the contribution of incoming waves?

Since paths for water movement during storms are complex and neither well known and directly measured it is difficult to recognize a dominant transport direction. A circulation pattern which has been identified during the storm illustrates the complexity of the flow patterns. During the inflow stage, import of water and sediment mainly happens at lower rates but occurs over a much larger area than during the outflow stage. Export is mainly restricted to the relative narrow tidal channel, but occurs at much higher transport rates. Therefore a very clear ebb dominance is recognized in the Slufters main channel. The influence of waves is restricted to the nearshore zone and is very small in the Slufter channel, even during storm conditions.

What is the dominant mode of sand transport: bed-load or suspended load and how does this vary with offshore hydrodynamic conditions?

Based on a 3 day dune measuring campaign and Bailard's transport model it can be said that during the neap-spring cycle bed-load seem to be the dominant transport mode. However, as measured sediment concentration indicated, Bailard's transport may underestimate suspended sediment transport due to the lag-effects and advection. According to the Bailaird sediment transport predictor bed-load transport is the dominant mode of sediment during the neap-spring cycle. During storm conditions suspended sediment becomes the dominant transport mode.

6 REFERENCES

Arens, S.M., Bakker, Th. W.M. & C. ten Haaf, 2005. Natuurontwikkeling Ameland. Arens Bureau voor Strand en Duinonderzoek, Amsterdam. By order of Rijkswaterstaat, Directie Noord-Nederland.

Bauer, B.O., Davidson-Arnott, R.G.D. Hesp, P.A. Namikas, S.L. Ollerhead J. Walker I.J., 2009. Aeolian sediment transport on a beach: Surface moisture, wind fetch, and mean transport. Geomorphology 105 (2009) 106–116

Beijk., V., 2002. Tidal hydrodynamics and sediment transport processes in the Zwin tidal inlet, the Netherlands. Msc-thesis for Utrecht University.

Boon, J.D., Byrne, R.J., 1981. On Basin Hypsometry and the Morphodynamic Response of Coastal Inlet Systems. Mar. Geol. 40, 27-48

Bruun, P., 1978. Stability of Tidal Inlets – theory and engineering. Elsevier. Amsterdam. 510 p.

Bruun, P., Gerritsen, F., 1960. Stability of Coastal Inlets. Coastal Engineering Laboratory, University of Florida, Gainesvilles, 274 p.

Camenen, B. and Larson., M., 2003 A bed-load sediment transport formula for the near shore, Journal of Coastal Engineering.

DiLorenzo, J. L., 1988. "The overtide and filtering response of small inlet/bay systems," Hydrodynamics and sediment dynamics of tidal inlets. D. G. Aubrey and L. Weishar, eds., 24-53, Springer Verlag, New York, NY.

Dronkers, J., 1985. Tide-induced residual transport of fine sediment. Netherlands Journal of Sea Research, 20(2/3), 117 – 131.

Durieux, M.X., 2003. De stabiliteit van the Slufter op Texel. Msc Graduation research Delft University. Delft. 79 p.

Escoffier,, 1940. In: **Kreeke, J. van de., 2004.** Equilibrium and cross-sectional stability of tidal inlets: application to the Frisian Inlet before and after basin reduction. Coastal engineering 51, 337-350.

FitzGerald, D. M., and Nummedal, D., 1983. "Response characteristics of an ebb-dominated tidal inlet channel," Journal of Sedimentary Petrology 53, 833-845.

Fortunato, A.B. and Oliveira, A., 2003. Influence of intertidal flats on tidal asymmetry. Journal of Coastal Research 21(5) 1062-1067.

Friedrichs, C.T. and Aubrey, D.G., 1988. Non-linear tidal distortion in shallow well-mixed estuaries: a synthesis, Estuarine Coastal and Shelf Science, 27, 521-545.

Frings, R.M., Kleinhans, M.G., 2008. Complex variations in sediment transport at three large river bifurcations during discharge waves in the river Rhine. Sedimentology (2008) 55, 1145–1171.

Grasmeijer, B.G.; van Rijn, L.C., **2002**. Basic features of sand transport in the surf zone of Egmond: field data and model results, **in**: van Rijn, L.C.; Ruessink, B.G. et al. (Ed.) (2002). The behaviour of a straight sandy coast on the time scale of storms and seasons: process knowledge and guidelines for coastal management: end document March 2002. EC MAST Project, MAS3-CT97-0086: pp. F1-F18

Grasmeijer, B., 2005. Preparation MSc fieldwork Physical Geography Data acquisition and processing in Coastal research April 2005

Helvert van, M., 2006. Tidal asymmetry and sediment transport in the 'Slufter' of the Verdronken Zwarte Polder. MSc graduation research, University of Utrecht. 87 p.

Hoitink, A.J.F., Hoekstra, P., van Maren, D.S., 2005. Flow asymmetry associated with astronomical tides: Implications for the residual transport of sediment. Journal of Geophysical research, Vol 108, 3315.

Klein Breteler, R., 2009. Wave-induced sediment transport at the small tidal inlet 'Slufter' of Texel, the Netherlands. Msc graduation research Utrecht University. 102 p.

Kreeke van de, J., 1984. Stability of tidal inlet, Pass Cavallo, Texas. Estuarine, Coastal and Shelf Science (1985), 21, 33-4

Kreeke van de, J., 2004. Equilibrium and cross-sectional stability of tidal inlets: application to the Frisian Inlet before and after basin reduction. Coastal engineering 51, 337-350.

Keulegan, G. H., 1967. "Tidal flow in entrances: Water level fluctuations of basins in communication with seas," Technical Bulletin No. 14, Committee on Tidal Hydraulics, U.S. Army Corps of Engineers, Washington, DC.

Lincoln, J.M., FitzGerald, D.M., 1988. Tidal distortions and flood tidal dominance at five small tidal inlets in southern Maine. Marine Geology. 82: 133-148.

Maren, D.S. van., Hoekstra, P., Hoitink, A.J.F., 2004. Tidal flow asymmetry in the diurnal regime: bed load transport and morphologic changes around the Red River Delta. Ocean Dynamics 3–4, 424–434

Militello, A. and Hughes, S.A., 2000 Circulation Patterns at Tidal Inlets with Jetties US Army corps of engineers. ERDC/CHL CETN-IV-29.10 p.

Nichols, M.N., Boon, J.D., 1991. Sediment transport processes in coastal lagoons. In: Coastal Lagoon Preocesses, Elsevier, Amsterdam, pp 177-185

Oliveira, I. B., 1970. Natural flushing ability in tidal inlets," Proceedings, 12th Coastal Engineering Conference, ASCE, 1827-1845.

Pacheco, A., Vila-Concejo, A., Ferreira, O., Dias, J.A., 2006. Assessment of tidal inlet evolution and stability using sedimentbudget computations and hydraulic parameter analysis. Marine Geology 247 (2008) 104–127

Pritchard, D., 2005. Suspended sediment transport along an idealised tidal embayment: settling lag, residual transport and the interpretation of tidal signals. Ocean Dynamics (2005) p. 124–136

Puijvelde van, S., 2010. Morphodynamics of The Slufter. Morfodynamical processes in a small tidal inlet in the Netherlands. Msc-thesis, Utrecht University. 93 p.

Puleo, J.A. Johnson, R.V.,Timothy, T.B., Kooney, N. Holland, K.T., 2006. The effect of air bubbles on optical backscatter sensors. Marine Geology Volume 230, Issues 1-2, 2, Pages 87 97

Reneerkens, M.J.J., 2003. Factors controlling the stability of the Slufter inlet throat, Texel. MSc graduation thesis, Utrecht University, pp. 38

Rijn van, L.C., 1993. Principles of sediment transport in river, estuaries and coastal seas. Aqua publication, Amsterdam. ISBN 90-800356-1-0. second edition. 335 p.

Rijn van, L.C., 1994. Principles of fluid flows and surface flows in rivers, estuaries, seas and oceans. Aqua publication, second edition. 345 p.

Straaten van, L., and Kuenen, P.H., 1957. Accumulation of fine grained sediments in the Dutch Wadden Sea. Biological Research Ems-Dollard Estuary, Netherlands Institute for Sea esearch, Texel, The Netherlands. 16 p

Seelig, W. H., and Sorenson, R. M., 1978. Numerical model investigation of selected tidal inlet-bay system characteristics. Proceedings 14th Coastal Engineering Conference, ASCE, 1302-315.

Soulsby, R., 1997. Dynamics of marine sands: a manual for practical application. Thomas Telford, London, 249p.

Speer P.E., Aubrey D.G., 1985. A study of non-linear propagation in shallow inlet/estuarine systems, Part II: Theory. Eastern Coast Shelf Science. 21: 207–224

Swart de, H.E., Zimmerman, 2008. J.T.F.Supplemental Appendix B: Net Sediment Transport by Tidal Currents. Main paper: Morphodynamics of Tidal Inlet Systems. Annual review of fluid mechanics

Wang, Z.B., Jeuken, M. C. J. L., Gerritsen, H., Vriend, H. J. de, Kornman, B. A., 2002. Morphology and asymmetry of the vertical tide in the Westerschelde estuary. Continental Shelf Research Volume 22, Issue 17, p. 2599-2609.

Zantinge A.M., 2007. Stability if an artificial tidal channel in the Zwarte Polder at the Dutch Western Scheldt. Msc research thesis, University of Utrecht, 98 p.

7 APPENDICES

Appendix A. Flows, waterlevels and stage velocity plots

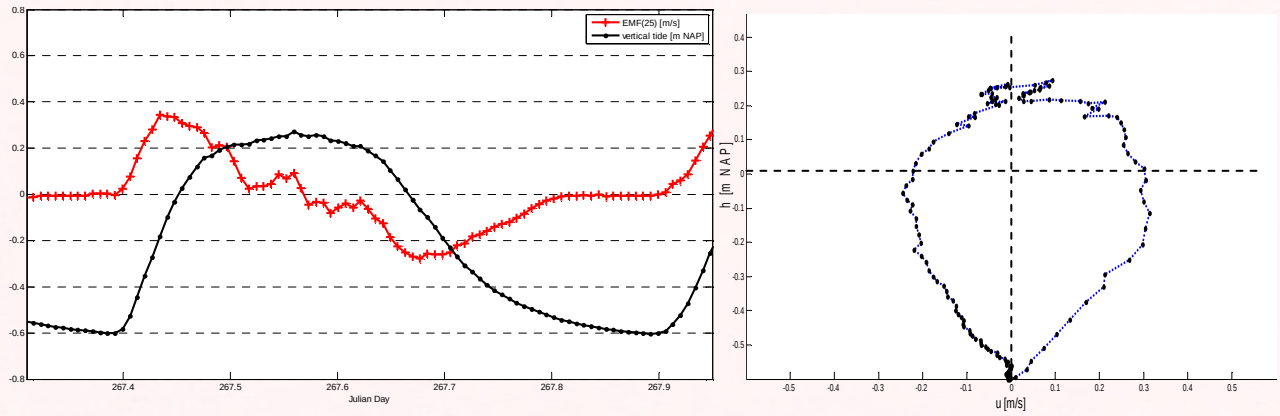

Figure 7-1 A) Vertical and horizontal tide during a neap tide (2), 23-09-08 10:00-22:15. **B**) Stage velocity of neap tide 2

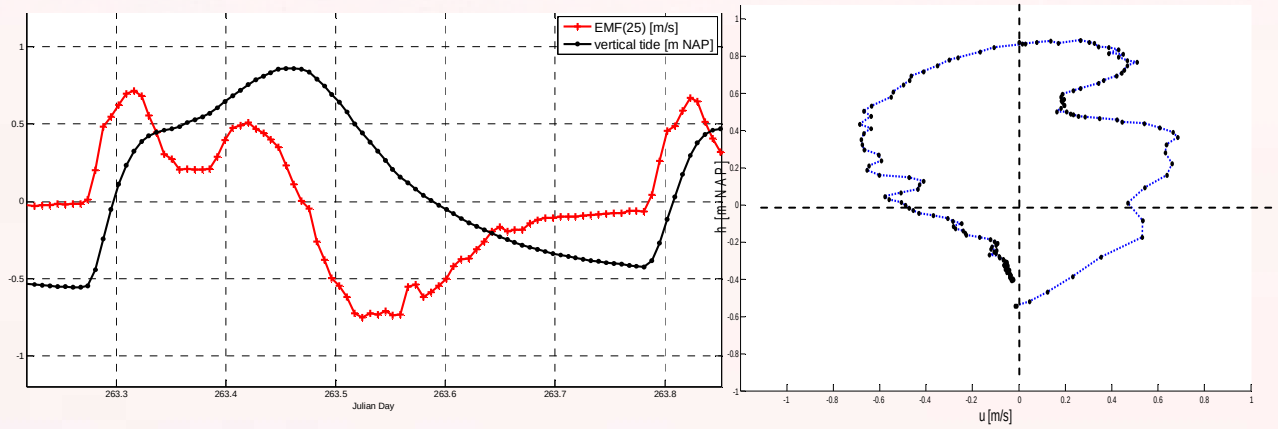

Figure 7-2 A) Vertical and horizontal tide during a spring tide (2), 19-09-08 7:00-19:30. **B**) Stage velocity of spring tide 2

Appendix B. Instantaneous measuered flow velocities

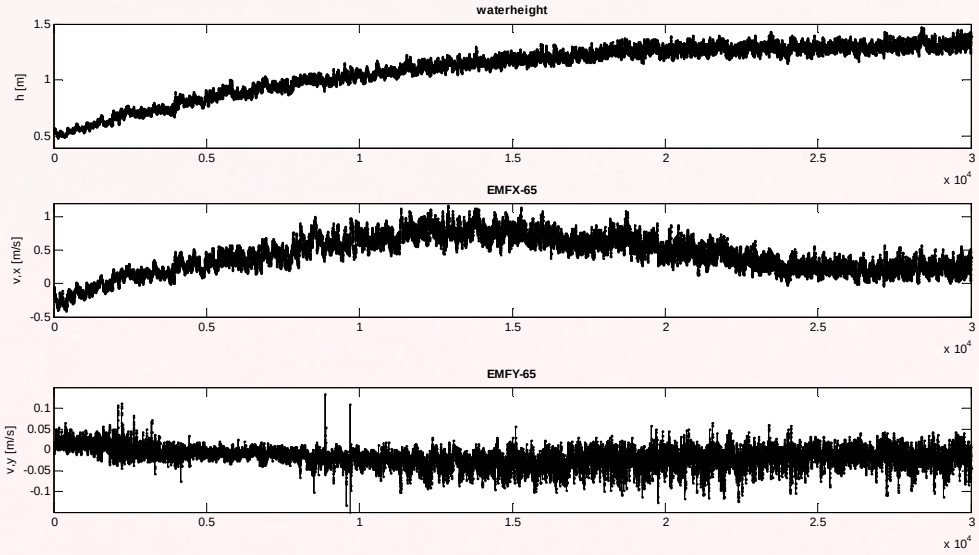

Figure 7-3 Instantaneous measured velocities in two direction during the inflow stage (main channel, the Slufter at 01-10-08)

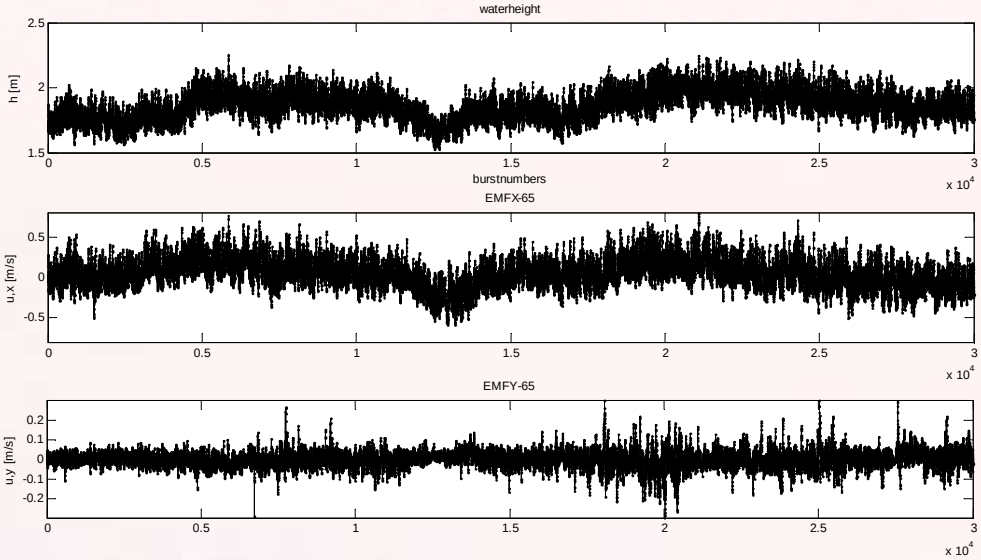

Figure 7-4 Instantaneous measured velocities in two direction at HW (main channel, the Slufter at 01-10-08)

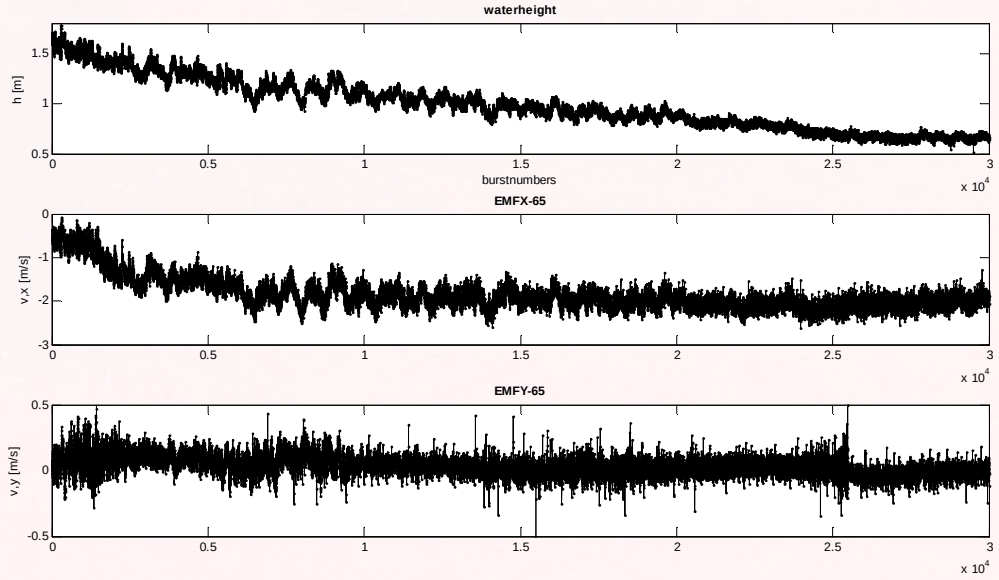

Figure 7-5 Instantaneous measured velocities in two direction during the outflow stage (main channel, the Slufter at 01-10-08)

Appendix C. Power spectral density of waves

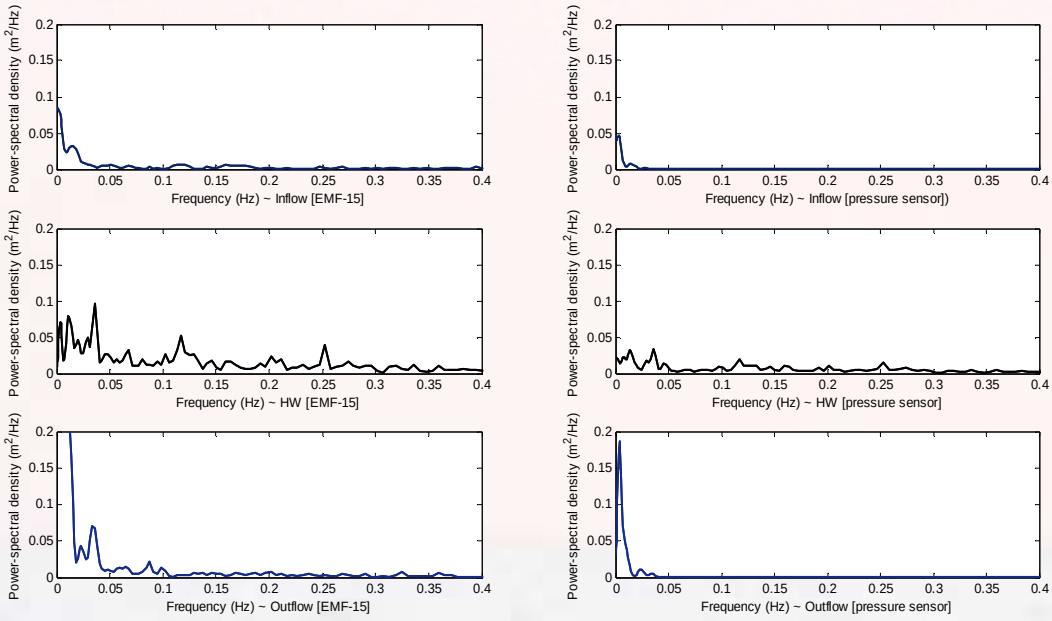

Figure 7-6 Power spectral density of waves derived from the oscillating- and vertical term of orbital motion for A-B) inflow C-D) High water and E-F) Outflow based upon 240 seconds 8 halfway overlapping 512-points Fourier transform

Appendix D. Measuring protocol

day	date	julian	Main	Frame	Breaking	zone	Upstream		Beach flat	
Mon	08/09/2008	252	Truc Vert	Frame 16	landward	seaward	seaward	landward	landward	seaward
Tue	09/09/2008	253			17:00	17:00				
Wed	10/09/2008	254		11:00						
Thur	11/09/2008	255	11:00							
Fri	12/09/2008	256								
Sat	13/09/2008	257								
Sun	14/09/2008	258								
Mon	15/09/2008	259								
Tue	16/09/2008	260								
Wed	17/09/2008	261			21:00	08:00				
Thur	18/09/2008	262								
Fri	19/09/2008	263		12:00						
Sat	20/09/2008	264								
Sun	21/09/2008	265					16:00	16:00		
Mon	22/09/2008	266					16:00/18:00	18:00/20:00		
Tue	23/09/2008	267								
Wed	24/09/2008	268					10:00/13:00	09:00/11:00	change	program
Thur	25/09/2008	269								
Fri	26/09/2008	270					13:00/15:30	11:00/13:30		
Sat	27/09/2008	271		15:00				13:30/23:00		
Sun	28/09/2008	272								
Mon	29/09/2008	273					12:30			
Tue	30/09/2008	274								
Wed	01/10/2008	275							16:00	18:00
Thur	02/10/2008	276								
Fri	03/10/2008	277							13:00/15:00	13:00
Sat	04/10/2008	278		16:00						22:30
Sun	05/10/2008	279								
Mon	06/10/2008	280	11:00/ 18:00		16:30	16:30			16:00	16:00
Tue	07/10/2008	281			16:30/19:30	15:30/19:00				
Wed	08/10/2008	282								

Thur	09/10/2008	283							
Fri	10/10/2008	284	8:30/ 11:00		08:30				
Sat	11/10/2008	285			14:30	10:30			
Sun	12/10/2008	286		13:30					
Mon	13/10/2008	287		13:30					
Tue	14/10/2008	288							
Wed	15/10/2008	289							
Thur	16/10/2008	290	17:00		15:30				
Fri	17/10/2008	291				15:00			

Appendix E. Hydraulic characteristics in the main channel for each tidal phase

	start	end	period	avgU (EMF-25)	Umax (EMF-25)	Hs,off	wind dir	amplitude	HW
	[Jul date]	[Jul date]	[h]	[m/s]	[m/s]	[m]	(deg)	[m]	[m]
flood	255,55	255,77	5,28	0,120601	0,2977	0,591875	138	0,63	0,036
ebb	255,77	256,04	-6,48	-0,1104	-0,231	0,576944	138	0,68	
flood	256,04	256,28	5,76	0,300743	0,541	1,384833	119	1,34	0,707
ebb	256,28	256,59	-7,44	-0,33323	-0,718	1,329388	119	1,22	
flood	256,59	256,8	5,04	0,202962	0,47	1,52625	119	0,98	0,348
ebb	256,8	257,11	-7,44	-0,15219	-0,393	1,737174	119	0,87	
flood	257,11	257,29	4,32	0,266377	0,515	1,667308	93	1,15	0,515
ebb	257,29	257,635	-8,28	-0,16799	-0,505	1,383137	93	1,08	
flood	257,635	257,836	4,824	0,129658	0,341	1,32931	93	0,71	0,183
ebb	257,836	258,14	-7,296	-0,10456	-0,322	1,229778	81	0,73	
flood	258,14	258,333	4,632	0,276182	0,54	0,984138	81	1,15	0,625
ebb	258,333	258,666	-7,992	-0,20371	-0,542	0,87551	81	1,13	
flood	258,666	258,868	4,848	0,151607	0,438	0,983226	81	0,8	0,31
ebb	258,868	259,172	-7,296	-0,12721	-0,388	0,939778	83	0,85	
flood	259,172	259,367	4,68	0,273537	0,578	0,688276	83	1,24	0,698
ebb	259,367	259,695	-7,872	-0,1207	-0,505	0,62878	83	1,19	
flood	259,695	259,892	4,728	0,144709	0,372	0,965455	83	0,826	0,331
ebb	259,892	260,199	-7,368	-0,12979	-0,42	0,777045	83	0,88	
flood	260,199	260,396	4,728	0,335895	0,636	0,488667	83	1,34	0,774
ebb	260,396	260,72	-7,776	-0,1261	-0,72	0,5042	83	1,26	
flood	260,72	260,914	4,656	0,178535	0,442	0,515357	83	0,766	0,388
ebb	260,914	261,223	-7,416	-0,12933	-0,433	0,478478	83	0,76	
flood	261,223	261,414	4,584	0,345469	0,631	0,4475	83	1,33	0,78
ebb	261,414	261,745	-7,944	-0,27012	-0,639	0,511224	83	1,28	
flood	261,745	261,938	4,632	0,17831	0,456	0,499333	83	0,88	0,38
ebb	261,938	262,248	-7,44	-0,1342	-0,48	0,471778	88	0,93	
flood	262,248	262,447	4,776	0,338354	0,63	0,379	88	1,23	0,775
ebb	262,447	262,765	-7,632	-0,2553	-0,725	0,390213	88	1,25	
flood	262,765	262,96	4,68	0,211778	0,512	0,549655	88	0,96	0,48
ebb	262,96	263,271	-7,464	-0,14585	-0,473	0,456591	69	1,03	
flood	263,271	263,47	4,776	0,359414	0,687	0,318333	69	1,41	0,863
ebb	263,47	263,784	-7,536	-0,29801	-0,705	0,308444	69	1,28	
flood	263,784	263,974	4,56	0,238967	0,658	0,312414	69	1,08	0,657
ebb	263,974	264,303	-7,896	-0,16947	-0,529	0,381633	74	1,13	
flood	264,303	264,49	4,488	0,264506	0,578	0,389259	74	1,18	0,6945
ebb	264,49	264,817	-7,848	-0,19661	-0,587	0,384545	74	1,16	
flood	264,817	265,006	4,536	0,192629	0,498	0,397143	74	0,93	0,46
ebb	265,006	265,33	-7,776	-0,11977	-0,427	0,385745	1	0,99	
flood	265,33	265,517	4,488	0,277536	0,528	0,357857	1	1,18	0,668
ebb	265,517	265,832	-7,56	-0,19582	-0,537	0,448372	1	1,19	
flood	265,832	266,011	4,296	0,23507	0,516	0,57	1	1,09	0,562
ebb	266,011	266,36	-8,376	-0,15405	-0,448	0,460408	45	1,13	
flood	266,36	266,538	4,272	0,212272	0,448	0,440769	45	1,02	0,44
ebb	266,538	266,854	-7,584	-0,13752	-0,397	0,464255	45	1,02	
flood	266,854	267,055	4,824	0,205879	0,498	0,81375	45	1,06	0,475
ebb	267,055	267,385	-7,92	-0,13158	-0,363	1,488571	41	1,08	
flood	267,385	267,569	4,416	0,150229	0,322	2,028148	41	0,87	0,262
ebb	267,569	267,903	-8,016	-0,08998	-0,259	2,119388	41	0,87	
flood	267,903	268,089	4,464	0,178884	0,36	1,972963	41	0,97	0,365
ebb	268,089	268,45	-8,664	-0,09324	-0,283	1,680755	67	0,95	
flood	268,45	268,683	5,592	0,07118	0,77	1,243429	67	0,66	0,088

ebb	268,683	268,838	-3,72	-0,10186	-0,157	1,24375	67	0,63	
flood	268,838	269,184	8,304	0,094739	0,318	1,037	67	1,03	0,48
ebb	269,184	269,413	-5,496	-0,16042	-0,348	1,054242	72	0,94	
flood	269,413	269,565	3,648	0,076015	0,22	0,947391	72	0,68	0,22
ebb	269,565	269,74	-4,2	-0,10608	-0,205	0,939615	72	0,71	
flood	269,74	270,08	8,16	0,114687	0,389	0,881731	72	1,14	
ebb	270,08	270,312	-5,568	-0,20257	-0,483	0,575714	69	1,1	
flood	270,312	270,625	7,512	0,070085	0,270	0,39413	69	0,71	
ebb	270,625	270,786	-3,864	-0,13306	-0,277	0,373333	69	0,77	
flood	270,786	271,14	8,496	0,131056	0,421	0,397692	69	1,21	
ebb	271,14	271,417	-6,648	-0,2484	-0,562	0,298889	233	1,2	
flood	271,417	271,674	6,168	0,149384	0,420	0,276842	233	0,97	
ebb	271,674	271,92	-5,904	-0,16853	-0,458	0,310526	233	1,04	
flood	271,92	272,18	6,24	0,308362	0,843	0,640769	233	1,56	
ebb	272,18	272,496	-7,584	-0,41931	-0,89	0,692826	290	1,39	
flood	272,495	272,704	5,016	0,170028	0,432	0,610645	290	0,87	
ebb	272,704	272,93	-5,424	-0,22528	-0,583	0,698824	290	1,04	
flood	272,93	273,207	6,648	0,276267	0,970	0,9865	262	1,49	
ebb	273,207	273,52	-7,512	-0,56174	-1,009	1,405319	262	1,38	
flood	273,52	273,742	5,328	0,30854	0,840	1,445758	262	1,33	
ebb	273,742	274,01	-6,432	-0,47097	0,768	2,044	262	1,25	
flood	274,01	274,182	4,128	0,439967	1,630	3,049167	264	1,84	
ebb	274,182	274,545	-8,712	-1,08612	-2,1	3,132222	264	1,57	
flood	274,545	274,76	5,16	0,242156	0,790	2,846774	264	1,35	
ebb	274,76	275,051	-6,984	-1,16034	-1,86	3,4375	264	1,48	
flood	275,051	275,24	4,536	0,185546	0,468	2,716786	268	1,74	
ebb	275,24	275,54	-7,2	-0,78785	-1,75	3,15	268	1,62	
flood	275,54	275,74	4,8	0,096241	0,475	2,196552	268	1,51	
ebb	275,74	276,07	-7,92	-0,74003	-1,45	4,0018	268	1,66	
flood	276,07	276,255	4,44	0,152	0,545	3,625357	274	1,5	
ebb	276,255	276,584	-7,896	-0,697	-0,98	2,545319	274	1,62	
flood	276,584	276,768	4,416	0,138	0,312	2,167778	274	1,18	
ebb	276,768	277,09	-7,728	-0,134	-0,4	2,18625	274	1,15	
flood	277,09	277,292	4,848	0,123	0,381	1,842333	275	1,47	
ebb	277,292	277,577	-6,84	-0,1289	-0,42	1,690732	275	1,3	
flood	277,577	277,702	3	0,186	0,72	1,817368	275	1,78	
ebb	277,82	278,12	-7,2	-0,8123	-1,21	3,945111	275	1,67	
flood	280,83	280,96	3,12	0,105571	0,337	1,22	76	0,99	
ebb	280,96	281,338	-9,072	-0,14454	0,355	1,036111	158	1,05	
flood	281,338	281,544	4,944	0,130839	0,36	0,976875	158	0,76	
ebb	281,544	281,824	-6,72	-0,11918	0,23	1,04575	158	0,79	
flood	281,824	282,06	5,664	0,158224	0,44	0,959143	158	0,94	
ebb	282,06	282,326	-6,384	-0,14614	0,288	0,966	282	0,87	
flood	282,326	282,567	5,784	0,154674	0,33	1,442973	282	1,02	
ebb	282,567	282,847	-6,72	-0,146	0,309	1,434634	282	0,74	
flood	282,847	283,048	4,824	0,212776	0,32	1,266897	282	0,94	
ebb	283,048	283,46	-9,888	-0,14867	0,35	0,950667	225	1,1	
flood	283,46	283,645	4,44	0,086531	0,219	0,806429	225	0,55	
ebb	283,645	283,88	-5,64	-0,06522	0,105	0,730571	225	0,55	
flood	284,51	284,71	4,8	0,020678	0,33	1,86444	219	0,78	
ebb	284,71	284,975	-6,36	-0,07699	-0,238	2,089744	209	0,8	
flood	284,975	285,243	6,432	0,042273	0,671	1,899091	219	1,37	
ebb	285,243	285,564	-7,704	-0,3378	-0,692	1,708958	219	1,28	
flood	285,564	285,72	3,744	0,022076	0,485	1,399091	219	0,93	
ebb	285,72	286,065	-8,28	-0,13076	-0,422	1,0788	219	0,92	
flood	286,065	286,273	4,992	0,058087	0,767	0,840645	211	1,41	
ebb	286,273	286,61	-8,088	-0,37264	-0,888	0,7686	211	1,33	
flood	286,61	286,785	4,2	0,020653	0,47	0,6436	211	0,78	
ebb	286,785	287,11	-7,8	-0,11647	-0,39	0,675208	211	0,93	
flood	287,11	287,318	4,992	0,077899	0,558	0,728065	222	1,26	
ebb	287,318	287,63	-7,488	-0,25352	-0,668	0,857755	222	1,26	
flood	287,63	287,844	5,136	0,08844	0,632	0,755313	222	1,31	
ebb	287,844	288,133	-6,936	-0,33917	-0,765	0,722162	222	1,26	
flood	288,133	288,352	5,256	0,075226	0,85	0,818387	251	1,52	
ebb	288,352	288,666	-7,536	-0,54716	-1,153	1,111111	251	1,42	
flood	288,666	288,855	4,536	0,215565	0,6	0,923571	251	0,99	
ebb	288,855	289,169	-7,536	-0,15097	-0,595	1,256304	251	1,19	
flood	289,169	289,3847	5,1768	0,377006	0,7908	1,411786	237	1,52	
ebb	289,3847	289,685	-7,2072	-0,51989	-1,04	1,544651	237	1,47	
flood	289,685	289,902	5,208	0,328995	0,666	1,806364	237	1,37	
ebb	289,902	290,183	-6,744	-0,54133	-0,955	1,7876	291	1,37	
flood	290,183	290,415	5,568	0,48376	1,224	2,063793	291	1,87	
ebb	290,415	290,666	-6,024	-1,00284	-2,01	2,401034	291	1,57	